UNIVERSITY OF CALIFORNIA SAN DIEGO

Engineer Multi-dimensional Cell Membrane-coated Nanomaterials to Combat Bacterial Infection

A dissertation submitted in partial satisfaction of the
requirements for the degree
Doctor of Philosophy

in

NanoEngineering

by

Yue Zhang

Committee in charge:

Professor Liangfang Zhang, Chair
Professor Shaochen Chen
Professor Lars Eckmann
Professor David Gonzalez
Professor Jesse Jokerst

2019

The Dissertation of Yue Zhang is approved, and it is acceptable in quality and form for publication on microfilm and electronically:

_____

_____

_____

_____

_____

Chair

University of California San Diego

2019

DEDICATION

This dissertation is dedicated to my beloved parents, Shuling Zhang and Nengzhi Liang, who gave me all the riches that life could offer and without you, none of my achievement could be possible; And to my husband, Pengrui Wang, who offers me unconditional love and support. You are my life-long partner and my best friend ever; To the rest of my family for nursing me with love and patience.

I am truly blessed to have them in my life.

EPIGRAPH

The unexamined life is not worth living.

Socrates

TABLE OF CONTENTS

LIST OF FIGURES

ACKNOWLEDGEMENTS

First and foremost, I would like to thank my PhD advisor, Professor Liangfang Zhang. He kindly offered me the invaluable chance to join the team and freely pursue the knowledge in the field of nanomedicine. From him, I learned all of the good characters that a scientist should have, that is rigorous, diligent and kind. I deeply appreciate those insightful discussions we had about career development and personal growth. His guidance and support during those difficult times make my whole PhD training extremely remarkable. I am forever grateful to have him as my advisor.

Next, I would like to give the most credit to my mentor Dr. Weiwei Gao, without him, non-of my work will be possible. He is the person who generously offered me the guidance from the beginning to the end of my PhD training. Under his guidance, I learned how to formulate the projects, integrate resource, convey the ideas and polish the manuscript. Those skills make me graduate as a better and independent scientist.

I sincerely thank my doctoral defense committee members for the time and efforts on building the project and polishing my dissertation. I thank Professor Lars Eckmann and the team, especially the countless effort from Dr. Yukiko Mayamoto and Justin Yang, who play critical roles in expanding the application of the nanoparticle-hydrogel composite to localized *T. vaginalis* infection. The discussion we have really pushed the study to a higher level. I thank Professor Shaochen Chen, who has been my committee member since my first literature review exam. The photo-initiator synthesized and kindly offered by his team basically lay the foundation for my first two projects. Meanwhile, I want to give him a special thank because of the mentorship and

support he gave to my husband, Pengrui Wang. Thank you for letting him freely pursue the projects he like. I thank Professor David Gonzalez and Jesse Jokerst, whose passion and diligence to research have been a great influence on my academic and personal life.

In the meantime, I would like to thank all of the members in Zhang research group for creating a warm and supportive research environment. I thank Professor Jianhua Zhang for the mentorship at the beginning of my PhD study. He is the smartest and most experience chemist I have ever met. He offered me essential knowledge in chemical synthesis, purification and characterization. Those experience is critical not only for the project purpose, but also for jump-starting my academic career. I thank Ronnie Fang, Pavimol Angsantikul, Brian Luk and Soracha Thamphiwatana for establishing great role models for junior members to follow. I deeply appreciate the time and effort you spend in addressing every single question I have. Your encouragement and support make everything smoother. Meanwhile, I highly acknowledge the friendship and collaborative efforts from everyone in Zhang lab: Hua Gong, Jia Zhuang, Joo Hee Lee, Yijie Chen and Qiangzhe Zhang, Shuyan Wang, Jiarong Zhou, Diana Dehaini, Ashely Kroll, Yao Jiang, Xiaoli Wei, Maya Holay and Joon Ho Park.

I would like to thank Chinese Scholarship Council (CSC) for the generous financial support during the first four years of my PhD training. I also thank Institute of Engineering in Medicine for the scholarship in the third year of my docteral study.

I sincerely appreciate the friendship from San Diego Chinese student community. I will remember the happiness we had together, as well as the difficulty we overcame.

I want to thank Tabatha baker and her family for the help throughout my study in the US. I want to let you know you are the best host family ever. I still remember the first day you picked me up from the airport. The warm welcome made me feel at home. I hope our friendship will last forever.

Last, but not least, I would like to thank UC San Diego for the great student service. I have received tremendous help from career center for my job hunting. I appreciate the advice and resource I learned from each appointment, which helped me understand my career interests and improved the competency by perfecting the application documents.

Chapter 1, in full, is a reprint of the material as it appears in Annals of Biomedical Engineering, 2016, Weiwei Gao, Yue Zhang, Qiangzhe Zhang and Liangfang Zhang. The dissertation author was a major contributor and co-author of this paper.

The first portion of chapter 2 contains the material as it appears in Journal of Controlled Release. Yue Zhang, Jihua Zhang, Wansong Chen, Pavimol Angsantikul, Kevin, Spiekermann, Ronnie, Fang, Weiwei Gao and Liangfang Zhang. The dissertation author was the primary investigator and author of this material.

The second portion of chapter 2 is the reprint of the material being submitted. Yue Zhang; Yijie Chen; Christopher Lo; Jia Zhuang; Pavimol Angsantikul; Qiangzhe Zhang; Xiaoli Wei; Zhidong Zhou; Marygorret Obonyo; Ronnie Fang; Weiwei Gao; Liangfang Zhang. The dissertation author is the primary investigator and author of this material.

Chapter 3, in full, is a reprint of the material as it appears in ACS Nano, 2017, Yue Zhang, Weiwei Gao, Yijie Chen, Tamara Escajadillo, Jessica Ungerleider, Ronnie Fang, Karen Christman, Victor Nizet and Liangfang Zhang. The dissertation author was the primary investigator and author of this paper.

VITA

2014 B.S. in Pharmacy, Huazhong University of Science and Technology, China

2015 M.S. in NanoEngineering, University of California San Diego, USA

2019 Ph.D. in NanoEngineering, University of California San Diego, USA

PUBLICATIONS

1. Chen, Y.; Zhang, Y.; Zhuang, J.; Lee, J. H.; Wang, L.; Fang, R.; Gao, W.; Zhang, L.* "Cell membrane-cloaked oil nanosponges enable dual-modal detoxification", ACS Nano 2019, in press.
2. Chai, Z.; Ran, D.; Lu, L.; Zhan, C.; Ruan, H.; Hu, X.; Xie, C.; Jiang, K.; Li, J.; Zhou, J.; Wang, J.; Zhang, Y.; Fang, R.; Zhang, L.*, Lu, W. "Ligand-modified cell membrane enables targeted delivery of drug nanocrystals to glioma", ACS Nano 2019, in press.
3. Gong, H.; Chen, F.; Huang, Z.; Gu, Y.; Zhang, Q.; Chen, Y.; Zhang, Y.; Zhuang, J.; Cho, Y.; Fang, R.; Gao, W.; Xu, S.; Zhang, L.* "Biomembrane-modified field effect transistors for sensitive and quantitative detection of biological toxins and pathogens", ***ACS Nano*** 2019, in press.
4. Chen, Y.; Zhang, Y.; Chen, M.; Zhuang, J.; Fang, R.; Gao, W.; Zhang, L. "Biomimetic nanosponges suppress the in vivo lethality induced by the whole secreted proteins of pathogenic bacteria", ***Small*** 2019, 2019, 15, 1804994.
5. Zhuang, J.; Ying, M.; Spiekermann, K.; Holay, M.; Zhang, Y.; Chen, F.; Gong, H.; Lee, J-H.; Gao, W.; Fang, R.; Zhang, L. "Biomimetic nanoemulsions for oxygen delivery in vivo", ***Advanced Materials*** 2018, 2018, 30, 1804693.
6. Zhang, Q.; Dehaini, D.; Zhang, Y.; Zhou, J.; Chen, X.; Zhang, L.; Fang, R.; Gao, W.; Zhang, L. "Neutrophil membrane-coated nanoparticles inhibit synovial inflammation and alleviate joint damage in inflammatory arthritis", ***Nature Nanotechnology*** 2018, 13, 1182-1190.
7. Ying, M.; Zhuang, J.; Wei, X.; Zhang, X.; Zhang, Y.; Jiang, Y.; Dehaini, D.; Chen, M.; Gu, S.; Gao, W.; Lu, W.; Fang, R.; Zhang, L. "Remote-loaded platelet vesicles for disease-targeted delivery of therapeutics", ***Advanced Functional Materials*** 2018, *28*, 1801032.
8. Chen, Y.; Chen, M.; Zhang, Y.; Lee, J. H.; Escajadillo, T.; Gong, H.; Fang, R.; Gao, W.; Nizet, V.; Zhang, L. "Broad-spectrum neutralization of pore-forming toxins with human erythrocyte membrane-coated nanosponges", ***Advanced Healthcare Materials*** 2018, *7*, 1701366.
9. Gao, W.; Chen, Y.; Zhang, Y.; Zhang, Q.; Zhang, L. "Nanoparticle-based local antimicrobial drug delivery", ***Advanced Drug Delivery Reviews*** 2018, *127*, 46-57.
10. Li, J.; Angsantikul, P.; Liu, W.; Esteban-Fernandez de Avila, B.; Chang, X.; Sandraz, E.; Liang, Y.; Zhu, S.; Zhang, Y.; Chen, C.; Gao, W.; Zhang, L., Wang, J.

"Biomimetic platelet-camouflaged nanorobots for binding and isolation of biological threats", ***Advanced Materials*** 2018, *30*, 1704800.

11. Zhang, Y.; Gao, W.; Chen, Y.; Escajadillo, T.; Ungerleider, J.; Fang, R.; Christman, K.; Nizet, V.; Zhang, L. "Self-assembled colloidal gel using cell membrane-coated nanosponges as building blocks", ***ACS Nano*** 2017, *11*, 11923-11930.
12. Zhang, X.; Angsantikul, P.; Ying, M.; Zhuang, J.; Zhang, Q.; Wei, X.; Jiang, Y.; Zhang, Y.; Dehaini, D.; Chen, M.; Chen, Y.; Gao, W.; Fang, R.; Zhang, L. "Remote loading of small molecule therapeutics into cholesterol-enriched cell membrane-derived vesicles", ***Angewandte Chemie International Edition*** 2017, *56*, 14075-14079.
13. Chen, M.; Zhang, Y.; Zhang, L. "Fabrication and characterization of a 3D bioprinted nanoparticle-hydrogel hybrid device for biomimetic detoxification", ***Nanoscale*** 2017, *9*, 14506-14511.
14. Zhang, Y.; Zhang, J.; Chen, W.; Angsantikul, P.; Spiekermann, K.; Fang, R.; Gao, W.; Zhang, L. "Erythrocyte membrane-coated nanogel for combinatorial antivirulence and responsive antimicrobial delivery against Staphylococcus aureus infection", ***Journal of Controlled Release*** 2017, *263*, 185-191.
15. Dehaini, D.; Wei, X.; Fang, R.; Masson, S.; Angsantikul, P.; Luk, B.; Zhang, Y.; Ying, M.; Jiang, Y.; Kroll, A.; Gao, W.; Zhang, L. "Erythrocyte-platelet hybrid membrane coating for enhanced nanoparticle functionalization", ***Advanced Materials*** 2017, *29*, 1606209.
16. Zhang, Y.; Zhang, J.; Chen, M.; Gong, H.; Thamphiwatana, S.; Eckmann, L.; Gao, W.; Zhang, L. "A bioadhesive nanoparticle-hydrogel hybrid system for localized antimicrobial drug delivery", ***ACS Applied Materials & Interfaces*** 2016, *8*, 18367-18374.
17. Gao, W.; Zhang, Y.; Zhang, Q.; Zhang, L. "Nanoparticle-hydrogel: A hybrid biomaterial system for localized drug delivery", ***Annals of Biomedical Engineering*** 2016, *44*, 2049-2061.

ABSTRACT OF THE DISSERTATION

Engineer Multi-dimensional Cell Membrane-coated Nanomaterials to Combat Bacterial Infection

by

Yue Zhang

Doctor of Philosophy in NanoEngineering

University of California San Diego, 2019

Professor Liangfang Zhang, Chair

Designing a biomimetic nanoparticle is a challenging topic. Despite the advances in surface chemistry and material science, it's still impossible to fully replicate the complex interface that presents in nature. Besides, the bottom-up method fails to prevent the exposure of foreign material when administrated in vivo. To solve this

challenge, we directly fuse the natural cell membrane onto the synthetic core. This top-down method quickly generates natural stealth for the synthetic material and preserves the biofunction from the resource cell. Due to its unique properties, cell membrane coating technology displays great potential in the field of drug delivery, detoxification, vaccination and biosensing.

In my dissertation, I work on engineering multi-dimensional cell-membrane coated nanoparticles (also known as “nanosponge”) to treat bacterial infection. Instead of direct inhibiting the bacteria growth, nanosponge targets the virulence factors that bacteria secrete to subvert immune surveillance, which is known to place less evolutionary pressure to induce the antibiotic resistance. In the first thrust, antivirulence efficacy is carried out solely by biomimetic nanosponges. Two types of cell membrane from different origins are explored in this direction. In the second thrust, nanosponges are mixed with the supporting material to form a stable composite, which in turn boosts the antivirulence efficacy of the nanosponge. Together, the cell membrane coating technology offers us a great tool to solve the clinical challenges by mimicking the biological events in the natural biointerface.

Chapter 1

Nanoparticle-Hydrogel Composite for Localized Drug Delivery

1.1. Introduction

Nanoparticle technology offers a series of advantages for drug delivery, including high loading yield, combination therapy, controlled release, prolonged circulation, and targeted delivery. As a result, a myriad of nanoparticle-based drug delivery systems have been developed to improve therapeutic index of drugs by altering their pharmacokinetics and biodistribution profiles, resulting in nanomedicines for clinical treatment of various diseases.[5-7] Advances in biotechnology and biomedicine continue to accelerate the development of novel therapeutic nanoparticles aimed at further enhancing therapeutic efficacy.[8,9] For example, recent progress in genomics and proteomics has led to new nanoparticle formulations accommodating rational drug combinations for personalized treatment.[10-12] Biological discovery on the network of interconnected pathways within a cell has also resulted in nanoparticle formulations capable of precisely modulating the tempo-spatial distribution of drug molecules to target the internal state of malignant cells for bioactivity.[13,14] Further understandings on disease pathogenesis, particularly that of cancer and infections, have triggered the development of highly responsive nanoparticles that conduct physicochemical changes, when exposed to external stimuli, to enable preferential drug release at the target site.[15,16] Moreover, biomimetic nanoparticles made of natural biomaterials have demonstrated superior biointerfacing capabilities, leading to innovative therapeutics especially for drug delivery, detoxification, and vaccination. [17-20]

Meanwhile, on the front of nanotechnology development, therapeutic nanoparticles have been increasingly combined with other biomaterials to form hybrid systems for novel applications.[21-23] In this perspective, loading nanoparticles into hydrogels has received much attention.[24-26] Hydrogels are hydrophilic 3D polymer networks with extensive uses in tissue engineering and drug delivery.[27] Nanoparticles can be embedded into the hydrogel network by mixing with monomer solution, followed by gelation (nanocomposite hydrogel, Figure 1.1A).[28] Alternatively, they can be incorporated into gel matrix after gel formation by allowing the gel network to swell and 'breath in' nanoparticles for entrapment, a method especially useful when nanoparticles interfere with the gelation process.[29] Furthermore, inorganic nanoparticles are often grown in situ within gel matrix by loading nanoparticle precursors into a gel first,

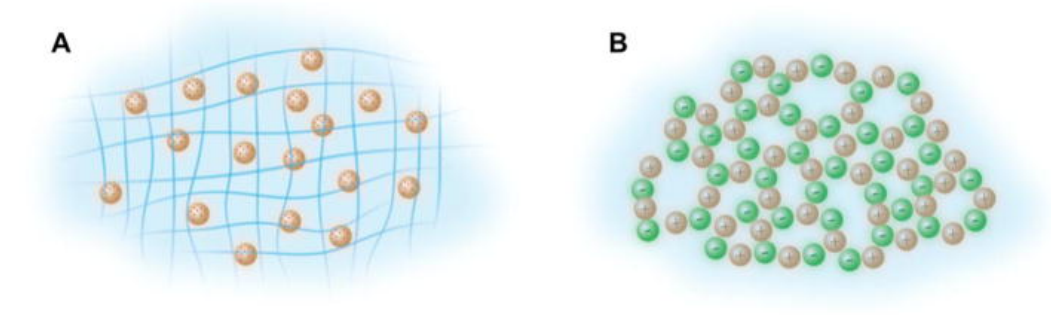

Figure 1.1: Schematic illustrations of two hybrid materials: (A) nanocomposite hydrogel, where nanoparticles are embedded into the hydrogel network, and (B) nanoparticle colloidal hydrogel, where nanoparticles are directly used as cross-linkers to construct 3D hydrogel network.

followed by reduction reactions for nanoparticle formation.[30] With appropriate compositions, hydrogels not only preserve the structural integrity and the

functionalities of the contained nanoparticles, but also offer additional engineering flexibility to improve the overall therapeutic efficacy. Besides hydrogel entrapment, directly using nanoparticles as cross-linkers to construct 3D hydrogel network offers another approach for nanoparticle assembly to acquire hydrogel-like properties (nanoparticle colloidal hydrogel, Figure 1.1B).[31-33] In this approach, nanoparticles can be linked together through strong hydrophobic interactions or by mixing nanoparticles carry opposite surface charges.[34] Alternatively, nanoparticles can be covalently linked, acting as nodes to form a hydrogel network.[35]

Overall, nanoparticle–hydrogel hybrid systems (denoted as 'NP-gels') judiciously integrate two distinct materials into one formulation with unique physicochemical and biological properties that neither one of the two building blocks can achieve independently.[25] NP-gels have demonstrated superior biointerfacing properties and attracted increasing attention to address various biological and medical challenges. In this article, we provide a review on recent advances in engineering NP-gels, with a particular emphasis on their novel applications in drug delivery. Specifically, we highlight four areas where their development and use have received the most attention, including (1) passively controlled drug release, (2) stimuli-responsive drug delivery, (3) site-specific drug targeting, and (4) detoxification. This review emphasizes nanoparticles in combination with hydrogels; however, development principles in above areas can be applied to hydrogels with other delivery platforms featuring different sizes, geometries, or dimensions such as microparticles [36] and nanofibers [37]. Overall, NP-gels have emerged as a versatile class of

biomaterials, unleashing unique synergistic properties with strong application potential to improve drug delivery.

1.2. Passively controlled drug release

Both nanoparticles and hydrogels are widely used for controlled drug release. Drug molecules encapsulated within the hydrogel network are released through diffusion, swelling, and chemically controlled mechanisms.[38] Meanwhile, nanoparticles control release kinetics through their tailored polymer structure, particle size, and fabrication conditions.[39] By integrating the two platforms, NP-gels create hierarchical matrices with remarkable versatility in modulating drug release kinetics for various delivery purposes, which are difficult for each platform to achieve alone.

Hydrogels can offer tissue-like properties but may suffer from burst release and rapid diffusion of drug molecules out of the polymer matrix.[40] In contrast, NP-gels that use nanoparticles as drug depot can overcome this drawback and significantly prolong drug release duration, which in turn can enhance drug bioavailability and patient compliance. For example, anti-inflammatory drug methylprednisolone(MP), effective in treating spinal cord injury was loaded into poly(lactic-co-glycolic acid) (PLGA) nanoparticles and then embedded within agarose hydrogels at a concentration of 2 mg/mL (based on PLGA mass); the continuous release of the fluorescence labeled MP was observed for 6 consecutive days.[41,42] These formulations extended effective drug release from a few hours up to a few days. Prolonged drug release by

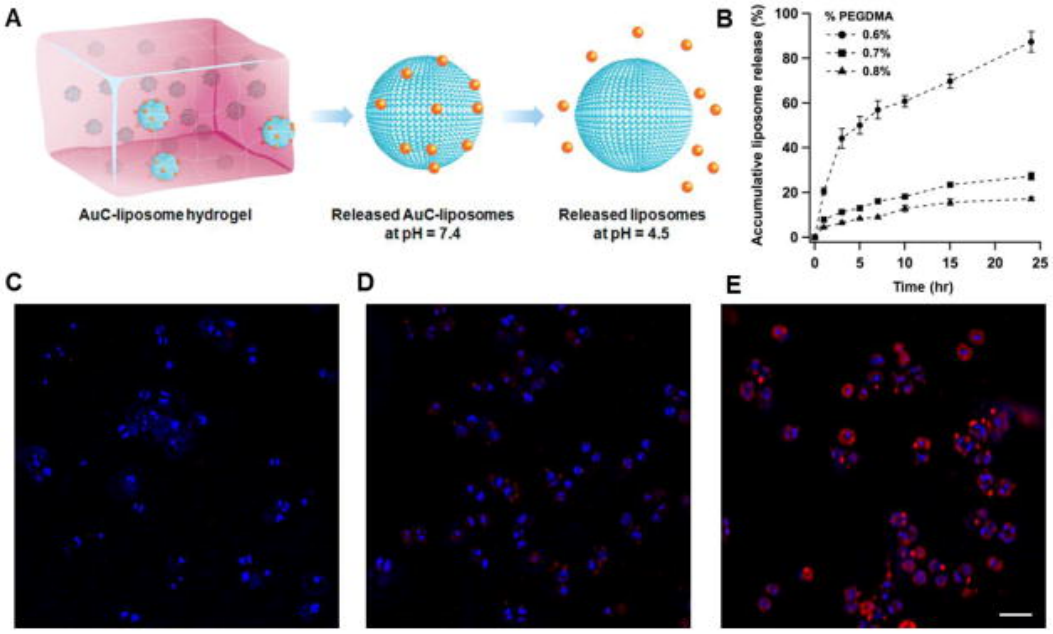

Figure 1.2: Au-liposomes encapsulated hydrogel for topic application (A) Schematic illustration of hydrogel containing nanoparticle-stabilized liposomes for topical antimicrobial delivery. Carboxyl-modified gold nanoparticles (AuC) were adsorbed onto the outer surfaces of cationic liposomes to stabilize them against fusion. The AuC-liposomes were subsequently embedded into an acrylamide-based hydrogel. At neutral pH, AuC-liposomes were released from the hydrogel in their entirety. When the pH drops below the pKa value of the carboxylic group (pKa∼5), the AuC stabilizers detached from the liposomes, resulting in the formation of bare liposomes with resumed fusion activity. (B) Accumulative liposome release profile from the hydrogel made with three different cross-linker concentrations of 0.6, 0.7, and 0.8 vol %, respectively. (C-E) Fluorescence study of the fusion interaction between hydrogel-released liposomes and S. aureus bacteria. Liposomes were labeled with fluorescent dye RhB (red) and the bacteria were stained with DAPI (blue). (C) Control bacteria without any treatment, (D) bacteria incubated with AuC-liposome-loaded hydrogel at pH = 7.4, (E) bacteria incubated with AuC-liposome-loaded hydrogel at pH = 4.5. Sscale bar, 1 μm. Reproduced with permission from Ref. 28.

NP-gel formulation is also popular in ocular drug delivery. For example, drug-loading liposomes [43], micelles [44], and polymeric nanoparticles [45] have all been incorporated into various hydrogels for the slow release of glaucoma drugs. Another area of interest is localized antibiotic release. In this perspective, metallic nanoparticles made of silver, gold, or copper, which slowly release ions to cause

strong bactericidal effects, have been widely used to formulate NP-gels and shown enhanced efficacy in treating bacterial infections including those caused by *Staphylococcus aureus*, *Escherichia coli*, and *Pseudomonas aeruginosa* bacteria. [46,47]

NP-gel formulation has also been used to directly modulate nanoparticle release with varying matrix porosity (i.e. the fraction of void space in the polymer network).[48,49] One example is the controlled release of nanoparticle-stabilized liposomes, an emerging class of antimicrobial delivery platform, for topical administration to treat bacterial infections (Figure 1.2).[28] In this formulation, carboxyl-modified gold nanoparticles were used as stabilizers for cationic liposomes consisting of L-α-phosphatidylcholine (EggPC, a zwitterionic phospholipid) and 1,2-dioleoyl-3-trimethylammonium-propane (DOTAP, a cationic phospholipid) and the stabilized liposomes were loaded into a chemically cross-linked polyacrylamide hydrogel. The hydrogel viscoeleasticity could be precisely tailored by varying the cross-linker poly (ethylene glycol) dimethacrylates (PEGDMA) concentration, which subsequently resulted in tunable release kinetics of the incorporated liposomes. Liposome release percentage correlated linearly with the square root of release time, consistent with a diffusion dominant Higuchi model characterized by weak interactions between liposomes and the gel matrix.[50,51] The hydrogel formulation preserved the structural integrity of the nanoparticle-stabilized liposomes and the released liposomes could fuse with bacterial membranes in response to acidic environment (i.e., pH = 4.5) relevant to various skin infections.[52,53] As another

example, cisplatin self-assembled nanoparticles were loaded into hydrogel composed of poly(ethylene glycol)-*b*-poly-(acrylic acid) (PEG-*b*-PAA).[54] Drug release from this NP-gel system was determined by two steps: first, nanoparticles were released from the hydrogel, which was controlled by network dissolution; second, cisplatin was released from the nanoparticles, which was controlled by ligand substitution with chloride ions in the surroundings. The two distinct release kinetics determined the overall cisplatin release profile and thus the drug's therapeutic efficacy.

Besides single drug delivery, NP-gels also combine fast diffusion-controlled release of drug molecules directly dispersed in hydrogel network with slow drug release from nanoparticle reservoirs, a unique feature useful for concurrent delivery of multiple drugs while achieving independent control of their release kinetics. This controlled release strategy is particularly suitable for the combinatorial delivery of neuroprotective and neuroregenerative agents for spinal cord injury repair. The former aims to enhance cell survival during the trauma of secondary injury and thus requires a delivery on the hours to days following the primary injury, while the latter aims to enhance axonal outgrowth and thus needs to be delivered for an extended period ranging from 7 to 28 days.[55,56] For example, an NP-gel was formulated with hyaluronan and methyl cellulose blend loaded with PLGA nanoparticles, which achieved independent delivery of neuroprotective agents such as 2,3-dihydroxy-6-nitro-7-sulfamoyl-benzo(F) quinoxaline (NBQX) and fibroblast growth factor-2 in a time span ranging from 1 to 4 days and neuroregenerative agents such as neurotrophin-3 and anti-NogoA up to 28 days.[57] In addition to loading one drug into

the hydrogel matrix and one drug into embedded nanoparticles, two or more different types of drugs can be loaded separately to different types of nanoparticles, which are then mixed as a cocktail to prepare an NP-gel. In this case, sequential drug release can be achieved by controlling the size and surface properties of the different nanoparticles. For example, cholesterol-bearing pullulan nanogel nanoparticles with a diameter of approximately 30 nm were mixed with 136 ± 4 nm liposomes (dimyristoylphosphatidylcholine: cholesterol = 3:1 mol:mol) and then loaded in a PEG hydrogel. [58] The study showed that 6% of the liposome-encapsulated dye had leaked from the nanogel-coated liposome complexes by day 40, whereas 100% of the dye had leaked by day 25 from the uncoated liposomes, implying that coating the nanogel stabilizes the lipid bilayer and strengthens the permeability barrier as an artificial cytoskeleton.

1.3. Stimuli-responsive drug delivery

Smart hydrogels that drastically change their volume in response to environmental stimuli such as temperature, pH, and chemical signals are attractive biomaterials for drug delivery.[59-61] Such responsiveness can be coupled with additional cues such as light and magnetic field via nanoparticles embedded within the matrix, creating unique NP-gels capable of remotely controlling drug release.[62] For example, nanoparticles made from melanin with an average diameter of approximately 250 nm showed UV-induced photothermal heating.[63] These nanoparticles were

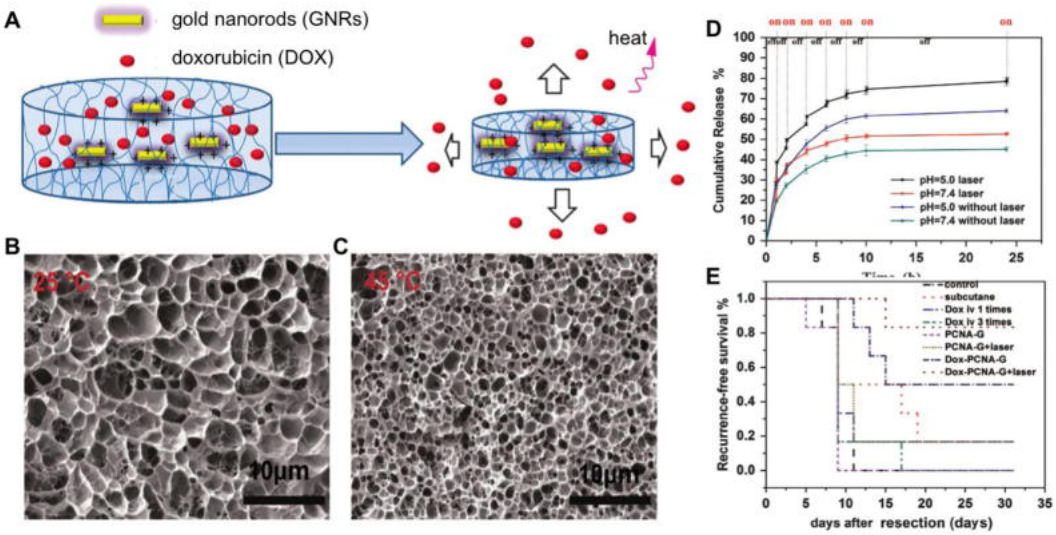

Figure 1.3: NIR triggered Doxorubicin release from GNRs-encapsulated hydrogel. (A) Schematic illustration of a hybrid hydrogel system in which gold nanorods (GNRs) were doped into a thermally responsive hydrogel. A near-infrared (NIR) laser was used to trigger the release of loaded Doxorubicin (DOX) by utilizing the photothermal effect of GNRs to induce the contraction of the thermo-responsive hydrogels. SEM images of hydrogels at (B) 25°C and (C) 45°C (C). (D) DOX-release profiles in the presence and absence of NIR laser at pH 5.0 and 7.4. (E) In vivo survival rate of mice bearing breast cancer treated by different samples. Reproduced with permission from Ref. 65.

dispersed into heat degradable hydrogel networks physically cross-linked by amphiphilic PLGA-PEG-PLGA copolymer. Under UV irradiation, the hydrogel was able to disintegrate. Compared to UV light, near-infrared (NIR) light is relatively safer and able to penetrate deeper into the soft tissues.[64] For example, gold nanorods doped into a thermally responsive hydrogel made with methoxylpoly(ethylene glycol)-poly(ε-caprolactone)-acryloyl chloride, glycidylmethacrylated chitooligosaccharide, *N*-isopropylacrylamide, and acrylamide, were able to induce the contraction of the thermo-responsive hydrogels and trigger the release of loaded doxorubicin to inhibit

breast cancer under NIR irradiation (Figure 1.3).[65] Other NIR-absorbing nanoparticles such as carbon nanotubes [66] and graphene oxide nanoparticles [67] were also incorporated into thermo-responsive polymers to harness NIR for remotely controlled drug delivery. Recently, upconversion core-shell nanoparticles made from $NaYF_4$:TmYb (core = $NaYF_4$:0.5 mol % Tm^{3+}:30 mol % Yb^{3+}; shell = $NaYF_4$, in a uniform hexagonal prism shape with an average length of 36.0 ± 1.1 nm and width of 32.0 ± 1.5 nm) capable of converting NIR light into UV light were also integrated with a photo-responsive hydrogel consisting of acrylamide monomer and the photocleavable PEG cross-linker. [68] The platform could "hide" large biomacromolecules (such as proteins) inside a polymer hydrogel, effectively "shutting down" their bioactivity, and then release them "on demand" using NIR light to enable their bioactivity.

Additionally, superparamagnetic particles that dissipate local heat upon the application of alternating magnetic field (AMF) have also been used as a trigger for remotely controlled "on-demand" drug release. [69,70] For example, superparamagnetic iron oxide (Fe_3O_4) nanoparticles (20–30 nm diameter) were incorporated into *N*-isopropylacrylamide (NIPAAm)-based matrix. Drug release was modulated by applying external AMF: continuous AMF accelerated drug release from the NP-gel, while pulse application of AMF caused pulsatile release in addition to continuous Fickian release profile.[71] Using hydrogel with a concentric-layered

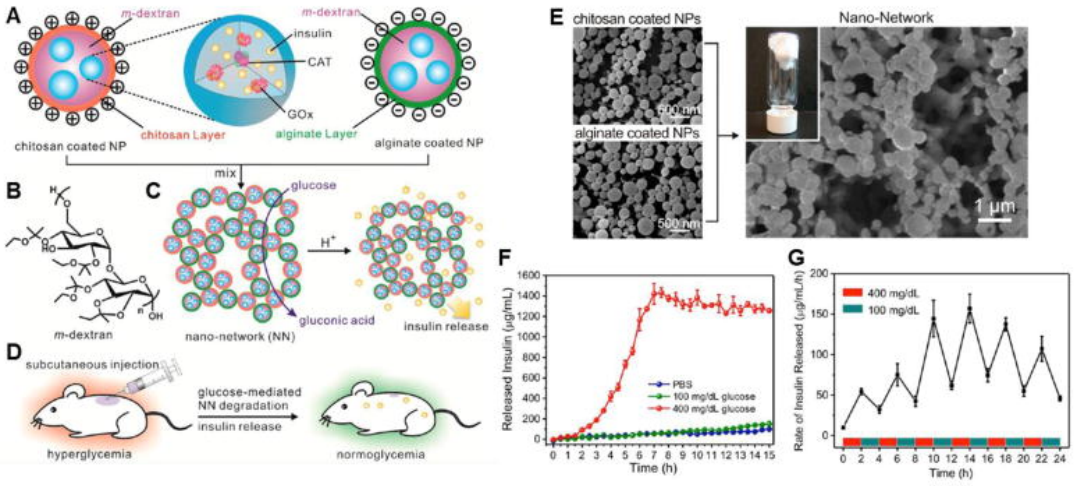

Figure 1.4: Glucose triggered insulin delivery from colloidal gel. (A) Nanoparticles encapsulating insulin and glucosespecific enzymes (GOx, glucose oxidase; CAT, catalase) are made of acidic sensitive acetal-modified dextran (B) and coated with chitosan and alginate, respectively. (C) NP-gel is formed by mixing oppositely charged nanoparticles together and efficiently degrades to release insulin upon the catalytic generation of gluconic acid under hyperglycemic conditions. (D) Schematic of glucose-mediated insulin delivery for type 1 diabetes treatment using the STZ-induced diabetic mice model. (E) SEM images of nanoparticles coated with chitosan and alginate and formation of a NP-gel. (F) In vitro accumulated insulin release of the NP-gel in different glucose concentrations at 37°C. (G) Self-regulated profile of the NP-gel presents the rate of insulin release as a function of glucose concentration. Reproduced with permission from Ref.83.

structure instead of amorphous structure further improved the responsiveness and drug release efficiency.[72] The synergy between nanoparticles and the hydrogel network has also led to NP-gels highly responsive to external pH changes. For example, silver nanoparticles were synthesized within a hydrogel containing 2-hydroxyethyl methacrylate), poly(ethylene glycol) methyl ether methacrylate, and methacrylic acid in situ.[73] Although the hydrogel itself had pH-responsive deswelling property due to the free carboxylic groups, the incorporation of silver nanoparticles significantly increased the deswelling rate. Such synergy was attributed to the presence of a large inter-phase region between the silver nanoparticles and the polymer matrix, which

likely reduced the characteristic diffusion length of water molecules and accelerated the deswelling process.

To further enhance the responsiveness, a new type of hydrogel has been made by covalently linking nanoparticles onto hydrogel matrix. [74,75] Compared to physically embedding, covalent link allows for using various hydrogel responsiveness to modulate inter-particle distances, hence offering precise control of nanoscale interactions through bulk templates.[76] Meanwhile, when nanoparticles are covalently linked, they form the nodes of the polymer network and reduce the relaxation length of hydrogel scaffolds, leading to significantly enhanced bulk response to environment stimuli.[77] Permanent linkage to the network also prevents nanoparticles from diffusing out of the gel, thereby limiting the loss of responsive materials and the potential toxic effects in biomedical applications.[78] These covalent NP-gels provide a system with better-defined coupling between nanoparticles and polymer matrix and thus open a way for better understanding of material structure-property relationship and subsequent modification for improved drug delivery properties.

Using nanoparticles as sole building blocks to form cohesive gel-like network represents an emerging class of NP-gel.[79] Combining oppositely charged nanoparticles, especially those that have already been established as drug nanocarriers such as PLGA,[34,80] gelatin,[81] and chitosan nanoparticles,[82] is a common approach to preparing this type of NP-gel. For example, positively charged chitosan-coated dextran nanoparticles (340 nm, 10.6 ± 1.9 mV) and negatively alginate-coated

dextran nanoparticles (293 nm, −11.5 ± 1.7 mV) were mixed at 20% (w/v) to form colloidal hydrogel for glucose-responsive and self-regulated insulin delivery (Figure 1.4).[83] At a macroscopic level, the construct was made with nanoparticles of small sizes and uniform distributions, which ensured sufficient cohesive strength for gelation. Such cohesive force decreased at high shear rate, resulting in low viscosities suitable for injection. At a microscopic level, the nanoparticles allowed for simultaneous loading of insulin and two glucose responsive enzymes (glucose oxidase and catalase). In a hyperglycemic state glucose was catalytically converted to gluconic acid, which caused dissociation of the gel-like network and subsequent release of insulin. This NP-gel system allowed for fast and pulsatile release of insulin in response to glucose concentrations and thus provided better glucose control in a type 1 diabetic mouse model. An alternative approach to forming colloidal gel is to use nanoparticles with responsive hydrophobic interactions. In this approach, nanoparticles are typically consisted of a core made of a hydrophobic polymer and a shell made of a thermo-responsive polymer that undergoes hydrophilic-to-hydrophobic transition in response to temperature change.[84,85] When temperature is below a critical temperature, the polymeric shell is water-soluble and stabilizes the nanoparticle; however, when temperature is above a critical temperature, the polymeric shell becomes hydrophobic, which flocculates the dispersed nanoparticles into a hydrogel network.

1.4. Site-specific drug delivery

NP-gels detain nanoparticles within 3D polymer matrices that allows for better local drug delivery. Various NP-gel formulations have been developed for targeting drugs to disease sites at the spinal cord,[41,42,55,56] the eye,[43-45] and the skin.[28,46] In these formulations, drug localization primarily relies on the properties of the hydrogel network, which allows nanoparticle design to be solely focused on modulating drug release. Such hybrid strategy offers an opportunity to decouple the spatial and temporal aspects in designing materials for drug delivery, resulting in a modular approach for highly functional drug targeting applications.

One such application is to use an anti-inflammatory tripeptide Lys-Pro-Val (KPV) loaded NP-gel for drug targeting to treat inflammatory bowel disease in the gastrointestinal (GI) tract.[86] In the study, a "double gavage" method was employed based on ion-induced polysaccharide gelation. Specifically, the first gavage was aimed to deliver 100 μL of the polysaccharides solution (alginate, 7 g/L; chitosan, 3 g/L) with homogenous suspended NPs (2 mg/mL). The polysaccharides biomaterials were in liquid phase at the time of gavage, which allows for easy administration. Then a second gavage was performed with a 50 μL solution containing 70 mmol/L calcium chloride and 30 mmol/L sodium sulfate. Once the ions and the polysaccharides solution were mixed, a hydrogel was formed. Since the cross-linking was through electrostatic interactions and sensitive to pH levels, the gel degradation could be finely controlled at different sites within the GI tract by simply varying the gel composition. Using this approach, polymeric nanoparticles loaded with KPV peptides were

encapsulated within hydrogel, forming a NP-gel formulation that was stable in gastric solutions of pH 1, 2, and 3 for 24 hours. However, when exposed to the intestinal solution with a higher pH level of 5, the hydrogel structure rapidly decomposed and the nanoparticles were released to the colonic lumen. Herein, the NP-gel formulation protected drug molecules during transit through the gastric gland and the small intestine, thereby maximizing the effective drug dosage to the site of action.

Site-specific drug targeting can also be achieved by modifying hydrogels with targeting ligands capable of specific binding to disease sites. For example, a silver-releasing antibacterial NP-gel consisting of silver nanoparticles and tissue-adhesive hydrogel has been developed.[87] In this design, the hydrogel building material PEG was modified with reactive catechol moieties to mimic the function of mussel adhesive proteins, in which the amino acid 3,4-dihydroxyphenylalanine (DOPA) that contains catechol played a critical role in enabling the mussel to adhere to various surfaces in an aqueous environment.[88] In the study, silver nitrate ($AgNO_3$, 212 mM) was used to oxidize catechol gel (Ag: catechol = 2:1 mol/mol), leading to covalent cross-linking and hydrogel formation with simultaneous reduction of Ag(I). Silver release was sustained for a period of at least two weeks in biological buffer solutions. The NP-gel was found to inhibit bacterial growth without significant cytotoxicity. Recently, gelatin hydrogel modified with DOPA showed similar bioadhesive properties and was able to withstand the shear force no less than 12.5 Pa inside the blood vessels (Figure 1.5).[89] In a mouse model of atherosclerosis, inflamed plaques treated with dexamethasone-eluting adhesive gels had reduced macrophage content

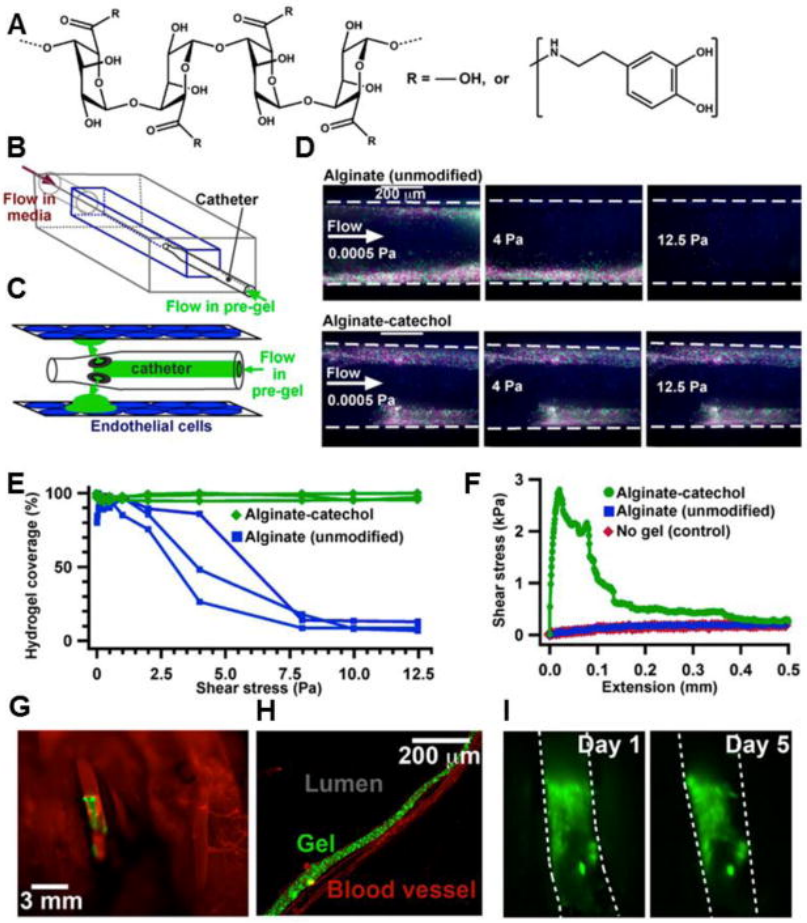

Figure 1.5: Catechol-modified hydrogel for blood vessel-targeted drug delivery. (A) Chemical structure of alginate-catechol synthesized from alginate. (B) Schematic of a microfluidic system used to compare the adhesion of alginate and alginate-catechol gels. (C) Schematic of the gel (green) being deposited on endothelial cells (blue) grown inside the device. (D) Fluorescence images of the gels containing fluorescent particles (green and purple) coated on endothelial cells in microfluidic channels (dashed lines). The unmodified alginate does not remain adhered at physiological shear stress, whereas the alginate-catechol remains adhered above physiological shear stress. (E) Quantifying the percent of gel that remained covered on the microfluidic channels at various shear stresses. (F) Quantifying the shear strength of the gels using a lap-shear tensile strain test. (G) Intravital fluorescence microscopy image of a carotid artery in a living mouse coated with the adhesive gel containing 200-nm particles (green). A fluorescent dye (red) is seen in the artery after it was injected intravenously, indicating that blood flowed through it. (H) Histological section of one wall of a carotid artery (red, elastin) coated for 28 d with the adhesive gel (green fluorescent particles). (I) Intravital microscopy images of the gel adhered to a carotid artery in a living mouse on days 1 and 5 after deposition. Reproduced with permission from Ref. 89.

and developed protective fibrous caps covering the plaque core. Treatment also lowered plasma cytokine levels and biomarkers of inflammation in the plaque. Meanwhile, the gel was shown to encapsulate both drug-loaded microparticles with diameters of 2~25 μm and fluorescently labeled nanoparticles with a diameter of 200 nm and was able to durably adhere to the inside of a carotid artery in a living mouse. These glued particles released drugs directly into the vessel wall. Currently, novel bioadhesive hydrogels with remarkable performance under various physiological conditions are rapidly emerging. [90-92] Combining drug-loaded nanoparticles with these hydrogels are expected to generate novel NP-gels with enhanced drug delivery efficiency and efficacy.

1.5. Detoxification

At first sight, it may appear a bit contradictory to dedicate a section to reviewing NP-gels for removing toxic compounds from the body, rather than delivering drugs. Upon closer inspection, these two opposing fields share many commonalities, as many new approaches in the field of detoxification rely on established drug delivery systems including nanoparticle technologies.[93] In fact, toxin-binding nanoparticles have recently attracted significant attention for detoxification applications aimed at removing both endogenous and exogenous poisonous from the body.[94] Among various detoxification platforms, red blood cell (RBC) membrane–coated nanoparticle system, where intact RBC membrane was

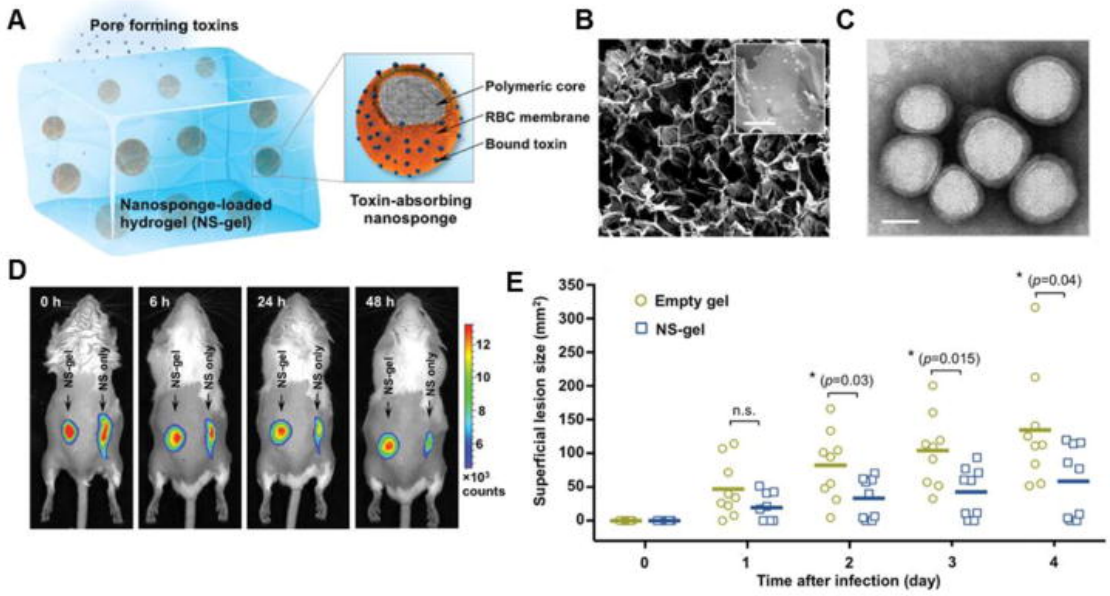

Figure 1.6: Nanosponge-hydrogel for localized detoxification. (A) Schematic illustration of a hydrogel retaining toxin-absorbing nanosponges (NS-gel) for local treatment of MRSA infection. The nanosponge was constructed with a polymeric core wrapped in natural RBC bilayer membrane and was subsequently embedded into an acrylamide-based hydrogel. (B) A scanning electron microscopy (SEM) image of the NS-gel. Scale bar, 1 μm. (C) A transmission electron microscopy (TEM) image showing the spherical core–shell structure of the nanosponges under negative staining with uranyl acetate. Scale bar, 50 nm. (D) In vivo nanosponge retention by hydrogel. Nanosponges labeled with DiD fluorescent dye was used to formulate NS-gel, which was then injected subcutaneously under the loose skin over the left flank of the mice. Free nanosponges (without hydrogel) were injected as a control group at the right flank of the same mice. Fluorescence images taken at different time points show the retention of the nanosponges under mouse skin. (E) In vivo treatment of MRSA infection. 1×10^9 CFU of MRSA 252 was mixed with 0.2 mL of 2 mg/mL NS-gel or empty gels, followed by subcutaneous injection to the backs of the mice (n = 9). Skin lesions were monitored and photographed on day 1–4 after the injections and the lesion sizes were measured. Bars represent median values. * $P < 0.05$, n.s.: not significant. Reproduced with permission from reference. [98].

wrapped onto polymeric nanoparticles (denoted as "nanosponges"), has been demonstrated as a robust toxin decoys for broad detoxification applications.[19] The ability of the nanosponges to neutralize pore-forming toxins indicated their application potential for the treatment of methicillin-resistant *Staphylococcus aureus* (MRSA)

infection.[17,18] Notably, MRSA infection commonly localizes to skin and soft tissues.[95] In the infection, a critical element of virulence results from a diverse arsenal of pore-forming toxins secreted by the bacteria, which attack the host cells.[96,97] These distinctive features of MRSA infection recently motivated the development of a nanosponge–hydrogel hybrid formulation capable of localizing nanosponges at the infection site for localized anti-virulence treatment of MRSA infection (Figure 1.6).[98]

In this NP-gel system, a 0.6% (w/w) PEGDMA crosslinker concentration was determined as it effectively retained nanosponges (with a diameter of 88.4 ± 0.3 nm, a surface zeta potential of −13.9 ± 0.9 mV, and a concentration of 2 mg/mL) within its matrix without compromising toxin transport for neutralization. Following subcutaneous injection to mice, nanosponges were effectively retained at the injection sites. In an MRSA subcutaneous mouse model, mice treated with the nanosponge–hydrogel hybrid showed markedly reduced MRSA skin lesion development. These results collectively indicate that the nanosponge–hydrogel hybrid formulation represents a new and effective detoxification strategy for the treatment of localized bacterial infection. Given the critical roles played by pore-forming toxins in pathogenesis of a wide range of bacteria, the nanosponge–hydrogel formulation holds significant potential to treat infectious diseases caused by various types of bacteria. More importantly, no antibiotics are involved in this new treatment, which is therefore unlikely to be affected by the existing bacterial antibiotic resistance mechanisms and will not exert selective pressure to bacteria for developing new resistance.

NP-gels offer additional advantages for detoxification applications. For example, confining detoxification nanoparticles within hydrogel network can potentially improve treatment safety. Particularly, for systemic detoxification, the conventional intravenous administration of nanoparticles for detoxification often leads to nanoparticle accumulation in the liver, posing a risk of secondary poisoning especially in liver-failure patients. [99,100] NP-gel formulation becomes attractive as the particle entrapment prevents their accumulation in liver. In addition, NP-gels can be easily removed from the body, a feature useful to limit the interaction of toxin-bound nanoparticles with the body to further enhance detoxification efficiency and safety. Furthermore, NP-gels can be molded to various shapes to recapitulate organ-specific detoxification mechanisms. For example, by using an advanced 3D printing technology, PEG hydrogels loaded with detoxification nanoparticles were molded to liver-mimetic structures with modified liver lobule configuration aimed to recapitulating the fast substances' exchange between blood stream and hepatic cells.[101] The resulting NP-gel system had higher surface area than the original liver lobule and allowed toxins to enter the PEG matrix more effectively for neutralization.

For enzyme-based detoxification, hydrogel can encapsulate enzyme nanocomplexes and provide a confined environment similar to that of subcellular compartments for effective chemical transformation, molecule transport, and elimination of toxic metabolic wastes.[102,103] For example, invertase, glucose oxidase, and horseradish peroxidase with complementary functions were assembled and encapsulated within a thin layer of acrylamide gel to form enzyme nanocomplexes

with a diameter approximately 30 ± 7 nm.[104] These nanocomplexes exhibited improved catalytic efficiency and enhanced stability when compared with free enzymes. Furthermore, the co-localized enzymes displayed complementary functions, whereby toxic intermediates generated by one enzyme could be promptly eliminated by another enzyme. In the study, nanocomplexes containing alcohol oxidase and catalase could reduce blood alcohol levels in intoxicated mice, offering an alternative antidote and prophylactic for alcohol intoxication.[104]

1.6. Summary

The innovative combination of nanoparticles and hydrogels, two entirely different types of biomaterials, has generated novel NP-gels with increased structural diversity and enhanced drug delivery properties. These hybrid biomaterials have shown superior capabilities in modulating drug release kinetics, releasing drugs in a remotely controlled and "on-demand" fashion, assisting site-specific drug targeting, and facilitating nanoparticle-based detoxification. These applications, collectively, have demonstrated NP-gels as a new and robust class of biomaterials with significant potential to improve drug delivery efficiency. Together with the development of NP-gels, nanoparticles have also been combined with other biomaterial platforms and devices, such as nanofibers, [105-107] microneedle patches[108,109] and nanomotors,[110,111] leading to more sophisticated drug delivery systems.

While the significant progress is made in improving on the properties of NP-gel formulations, challenges remain to improve their clinical applicability for drug delivery.[112] Especially for in vivo applications, one challenge is the foreign-body reactions, which frequently cause collagenous capsule formation and can potentially limit the performance of implantable NP-gels.[113,114] To address this challenge, novel material designs are emerging with superior capability of preventing capsule formation. Especially, the ultra-low-fouling zwitterionic hydrogels were recently developed to resist the formation of a capsule for at least 3 months after subcutaneous implantation in mice.[115] These hydrogels also promote angiogenesis in surrounding tissue, with anti-inflammatory and pro-healing functions. Another set of major challenges is to improve the ease of clinical usage of NP-gel formulation. In this respect, mechanisms that promote gelation at lower polymer concentrations and narrower gelation temperatures would reduce the risk of premature gelation inside the needle upon injection.[116] Similarly, for covalently cross-linked hydrogels, triggered gelation in situ may reduce the risk of syringe clogging. Novel cross-linkers or initiators can reduce potential *in vivo* toxicity and enable the use of single syringe as opposed to double-barreled syringes.[117] With continual efforts, we expect NP-gel hybrid approaches to generate new designs of biomaterials and to facilitate the development of novel therapeutic and diagnostic tools in medicine.

1.7. References

[1] Davis, M. E., Chen, Z., Shin, D. M. Nanoparticle therapeutics: An emerging treatment modality for cancer. *Nat. Rev. Drug Discov.* 7: 771-782, 2008.

[2] Petros, R. A., DeSimone, J. M. Strategies in the design of nanoparticles for therapeutic applications. *Nat. Rev. Drug Discov.* 9: 615-627, 2010.

[3] Wang, A. Z., Langer, R., Farokhzad, O. C. Nanoparticle delivery of cancer drugs. *Annu. Rev. Med.* 63: 185-198, 2012.

[4] Blanco, E., Shen, H., Ferrari, M. Principles of nanoparticle design for overcoming biological barriers to drug delivery. *Nat. Biotechnol.* 33: 941-951, 2015.

[5] Shi, J., Votruba, A. R., Farokhzad, O. C., Langer, R. Nanotechnology in drug delivery and tissue engineering: From discovery to applications. *Nano Lett.* 10: 3223-3230, 2010.

[6] Shi, J., Xiao, Z., Kamaly, N., Farokhzad, O. C. Self-assembled targeted nanoparticles: Evolution of technologies and bench to bedside translation. *Acc. Chem. Res.* 44: 1123-1134, 2011.

[7] Lobatto, M. E., Fuster, V., Fayad, Z. A., Mulder, W. J. M. Perspectives and opportunities for nanomedicine in the management of atherosclerosis. *Nat. Rev. Drug Discov.* 10: 835-852, 2011.

[8] Farokhzad, O. C., Langer, R. Impact of nanotechnology on drug delivery. *ACS Nano* 3: 16-20, 2009.

[9] Timko, B. P., Whitehead, K., Gao, W., Kohane, D. S., Farokhzad, O., Anderson, D., Langer, R. Advances in drug delivery. *Annu. Rev. Mater. Res.* 41: 1-20, 2011.

[10] Kolishetti, N., Dhar, S., Valencia, P. M., Lin, L. Q., Karnik, R., Lippard, S. J., Langer, R., Farokhzad, O. C. Engineering of self-assembled nanoparticle platform for precisely controlled combination drug therapy. *Proc. Natl. Acad. Sci. U. S. A.* 107: 17939-17944, 2010.

[11] Aryal, S., Hu, C.-M. J., Zhang, L. Polymeric nanoparticles with precise ratiometric control over drug loading for combination therapy. *Mol. Pharm.* 8: 1401-1407, 2011.

[12] Ma, L., Kohli, M., Smith, A. Nanoparticles for combination drug therapy. *ACS Nano* 7: 9518-9525, 2013.

[13] Morton, S. W., Lee, M. J., Deng, Z. J., Dreaden, E. C., Siouve, E., Shopsowitz, K. E., Shah, N. J., Yaffe, M. B., Hammond, P. T. A nanoparticle-based combination chemotherapy delivery system for enhanced tumor killing by dynamic rewiring of signaling pathways. *Sci. Signal.* 7: ra44, 2014.

[14] Fang, R. H., Zhang, L. Combinatorial nanotherapeutics: Rewiring, then killing, cancer cells. *Sci. Signal.* 7: pe13, 2014.

[15] Gao, W., Chan, J. M., Farokhzad, O. C. pH-responsive nanoparticles for drug delivery. *Mol. Pharm.* 7: 1913-1920, 2010.

[16] Gao, W., Thamphiwatana, S., Angsantikul, P., Zhang, L. Nanoparticle approaches against bacterial infections. *Wiley Interdiscip. Rev. Nanomed. Nanobiotechnol.* 6: 532-547, 2014.

[17] Hu, C.-M. J., Fang, R. H., Copp, J., Luk, B. T., Zhang, L. A biomimetic nanosponge that absorbs pore-forming toxins. *Nat. Nanotech.* 8: 336-340, 2013.

[18] Hu, C.-M. J., Fang, R. H., Luk, B. T., Zhang, L. Nanoparticle-detained toxins for safe and effective vaccination. *Nat. Nanotech.* 8: 933-938, 2013.

[19] Hu, C.-M. J., Zhang, L., Aryal, S., Cheung, C., Fang, R. H., Zhang, L. Erythrocyte membrane-camouflaged polymeric nanoparticles as a biomimetic delivery platform. *Proc. Natl. Acad. Sci. U. S. A.* 108: 10980-10985, 2011.

[20] Hu, C.-M. J., Fang, R. H., Wang, K.-C., Luk, B. T., Thamphiwatana, S., Dehaini, D., Phu, N., Angsantikul, P., Wen, C. H., Kroll, A. V., Carpenter, C., Ramesh, M., Qu, V., Patel, S. H., Zhu, J., Shi, W., Hofman, F. M., Chen, T. C., Gao, W., Zhang, K., Chien, S., Zhang, L. Nanoparticle biointerfacing by platelet membrane cloaking. *Nature* 526: 118-121, 2015.

[21] Huebsch, N., Mooney, D. J. Inspiration and application in the evolution of biomaterials. *Nature* 462: 426-432, 2009.

[22] Place, E. S., Evans, N. D., Stevens, M. M. Complexity in biomaterials for tissue engineering. *Nat. Mater.* 8: 457-470, 2009.

[23] Dvir, T., Timko, B. P., Kohane, D. S., Langer, R. Nanotechnological strategies for engineering complex tissues. *Nat. Nanotech.* 6: 13-22, 2011.

[24] Roux, R., Ladaviere, C., Montembault, A., Delair, T. Particle assemblies: Toward new tools for regenerative medicine. *Mater. Sci. Eng. C Mater. Biol. Appl.* 33: 997-1007, 2013.

[25] Merino, S., Martin, C., Kostarelos, K., Prato, M., Vazquez, E. Nanocomposite hydrogels: 3D polymer-nanoparticle synergies for on-demand drug delivery. *ACS Nano* 9: 4686-4697, 2015.

[26] Schexnailder, P., Schmidt, G. Nanocomposite polymer hydrogels. *Colloid. Polym. Sci.* 287: 1-11, 2009.

[27] Peppas, N. A., Hilt, J. Z., Khademhosseini, A., Langer, R. Hydrogels in biology and medicine: From molecular principles to bionanotechnology. *Adv. Mater.* 18: 1345-1360, 2006.

[28] Gao, W., Vecchio, D., Li, J., Zhu, J., Zhang, Q., Fu, V., Li, J., Thamphiwatana, S., Lu, D., Zhang, L. Hydrogel containing nanoparticle-stabilized liposomes for topical antimicrobial delivery. *ACS Nano* 8: 2900-2907, 2014.

[29] Thomas, V., Yallapu, M. M., Sreedhar, B., Bajpai, S. K. Breathing-in/breathing-out approach to preparing nanosilver-loaded hydrogels: Highly efficient antibacterial nanocomposites. *J. Appl. Polym. Sci.* 111: 934-944, 2009.

[30] Mohan, Y. M., Lee, K., Premkumar, T., Geckeler, K. E. Hydrogel networks as nanoreactors: A novel approach to silver nanoparticles for antibacterial applications. *Polymer* 48: 158-164, 2007.

[31] Grzelczak, M., Vermant, J., Furst, E. M., Liz-Marzan, L. M. Directed self-assembly of nanoparticles. *ACS Nano* 4: 3591-3605, 2010.

[32] Zhang, J., Li, Y., Zhang, X., Yang, B. Colloidal self-assembly meets nanofabrication: From two-dimensional colloidal crystals to nanostructure arrays. *Adv. Mater.* 22: 4249-4269, 2010.

[33] Li, F., Josephson, D. P., Stein, A. Colloidal assembly: The road from particles to colloidal molecules and crystals. *Angew. Chem. Int. Ed.* 50: 360-388, 2011.

[34] Wang, Q., Wang, L., Detamore, M. S., Berkland, C. Biodegradable colloidal gels as moldable tissue engineering scaffolds. *Adv. Mater.* 20: 236–239, 2008.

[35] Fuhrer, R., Athanassiou, E. K., Luechinger, N. A., Stark, W. J. Crosslinking metal nanoparticles into the polymer backbone of hydrogels enables preparation of soft, magnetic field-driven actuators with muscle-like flexibility. *Small* 5: 383-388, 2009.

[36] Yoon, Y. M., Lewis, J. S., Carstens, M. R., Campbell-Thompson, M., Wasserfall, C. H., Atkinson, M. A., Keselowsky, B. G. A combination hydrogel microparticle-based vaccine prevents type 1 diabetes in non-obese diabetic mice. *Sci. Rep.* 5, 2015.

[37] Fang, Y., Wang, C.-F., Zhang, Z.-H., Shao, H., Chen, S. Robust self-healing hydrogels assisted by cross-linked nanofiber networks. *Sci. Rep.* 3, 2013.

[38] Lin, C.-C., Metters, A. T. Hydrogels in controlled release formulations: Network design and mathematical modeling. *Adv. Drug Del. Rev.* 58: 1379-1408, 2006.

[39] Sethi, M., Sukumar, R., Karve, S., Werner, M. E., Wang, E. C., Moore, D. T., Kowalczyk, S. R., Zhang, L., Wang, A. Z. Effect of drug release kinetics on nanoparticle therapeutic efficacy and toxicity. *Nanoscale* 6: 2321-2327, 2014.

[40] Dang, T. T., Thai, A. V., Cohen, J., Slosberg, J. E., Siniakowicz, K., Doloff, J. C., Ma, M., Hollister-Lock, J., Tang, K. M., Gu, Z., Cheng, H., Weir, G. C., Langer, R., Anderson, D. G. Enhanced function of immuno-isolated islets in diabetes therapy by co-encapsulation with an anti-inflammatory drug. *Biomaterials* 34: 5792-5801, 2013.

[41] Chvatal, S. A., Kim, Y.-T., Bratt-Leal, A. M., Lee, H., Bellamkonda, R. V. Spatial distribution and acute anti-inflammatory effects of methylprednisolone after sustained local delivery to the contused spinal cord. *Biomaterials* 29: 1967-1975, 2008.

[42] Baumann, M. D., Kang, C. E., Tator, C. H., Shoichet, M. S. Intrathecal delivery of a polymeric nanocomposite hydrogel after spinal cord injury. *Biomaterials* 31: 7631-7639, 2010.

[43] Gulsen, D., Li, C. C., Chauhan, A. Dispersion of DMPC liposomes in contact lenses for ophthalmic drug delivery. *Curr. Eye Res.* 30: 1071-1080, 2005.

[44] Kapoor, Y., Chauhan, A. Drug and surfactant transport in Cyclosporine A and Brij 98 laden p-HEMA hydrogels. *J. Colloid Interface Sci.* 322: 624-633, 2008.

[45] Jung, H. J., Abou-Jaoude, M., Carbia, B. E., Plummer, C., Chauhan, A. Glaucoma therapy by extended release of timolol from nanoparticle loaded silicone-hydrogel contact lenses. *J. Control. Release* 165: 82-89, 2013.

[46] Rattanaruengsrikul, V., Pimpha, N., Supaphol, P. In vitro efficacy and toxicology evaluation of silver nanoparticle-loaded gelatin hydrogel pads as antibacterial wound dressings. *J. Appl. Polym. Sci.* 124: 1668-1682, 2012.

[47] Cometa, S., Iatta, R., Ricci, M. A., Ferretti, C., De Giglio, E. Analytical characterization and antimicrobial properties of novel copper nanoparticle-loaded electrosynthesized hydrogel coatings. *J. Bioact. Compatible Polym.* 28: 508-522, 2013.

[48] Caccavo, D., Cascone, S., Lamberti, G., Barba, A. A. Modeling the drug release from hydrogel-based matrices. *Mol. Pharm.* 12: 474-483, 2015.

[49] Siepmann, J., Peppas, N. A. Modeling of drug release from delivery systems based on hydroxypropyl methylcellulose (HPMC). *Adv. Drug Del. Rev.* 48: 139-157, 2001.

[50] Higuchi, T. Rate of release of medicaments from ointment bases containing drugs in suspension. *J. Pharm. Sci.* 50: 874-875, 1961.

[51] Siepmann, J., Peppas, N. A. Higuchi equation: Derivation, applications, use and misuse. *Int. J. Pharm.* 418: 6-12, 2011.

[52] Schmid-Wendtner, M. H., Korting, H. C. The pH of the skin surface and its impact on the barrier function. *Skin Pharmacol. Physiol.* 19: 296-302, 2006.

[53] Schaefer-Korting, M., Mehnert, W., Korting, H.-C. Lipid nanoparticles for improved topical application of drugs for skin diseases. *Adv. Drug Del. Rev.* 59: 427-443, 2007.

[54] Zhu, W., Li, Y., Liu, L., Chen, Y., Wang, C., Xi, F. Supramolecular hydrogels from cisplatin-loaded block copolymer nanoparticles and alpha-cyclodextrins with a stepwise delivery property. *Biomacromolecules* 11: 3086-3092, 2010.

[55] Ramer, L. M., Ramer, M. S., Steeves, J. D. Setting the stage for functional repair of spinal cord injuries: A cast of thousands. *Spinal Cord* 43: 134-161, 2005.

[56] Romero, M. I., Rangappa, N., Garry, M. G., Smith, G. M. Functional regeneration of chronically injured sensory afferents into adult spinal cord after neurotrophin gene therapy. *J. Neurosci.* 21: 8408-8416, 2001.

[57] Baumann, M. D., Kang, C. E., Stanwick, J. C., Wang, Y., Kim, H., Lapitsky, Y., Shoichet, M. S. An injectable drug delivery platform for sustained combination therapy. *J. Control. Release* 138: 205-213, 2009.

[58] Sekine, Y., Moritani, Y., Ikeda-Fukazawa, T., Sasaki, Y., Akiyoshi, K. A hybrid hydrogel biomaterial by nanogel engineering: Bottom-up design with nanogel and liposome building blocks to develop a multidrug delivery system. *Adv. Healthc. Mater.* 1: 722-728, 2012.

[59] Qiu, Y., Park, K. Environment-sensitive hydrogels for drug delivery. *Adv. Drug Del. Rev.* 53: 321-339, 2001.

[60] Gupta, P., Vermani, K., Garg, S. Hydrogels: From controlled release to pH-responsive drug delivery. *Drug Discov. Today* 7: 569-579, 2002.

[61] Schmaljohann, D. Thermo- and pH-responsive polymers in drug delivery. *Adv. Drug Del. Rev.* 58: 1655-1670, 2006.

[62] Zhao, X., Kim, J., Cezar, C. A., Huebsch, N., Lee, K., Bouhadir, K., Mooney, D. J. Active scaffolds for on-demand drug and cell delivery. *Proc. Natl. Acad. Sci. U. S. A.* 108: 67-72, 2011.

[63] Ninh, C., Cramer, M., Bettinger, C. J. Photoresponsive hydrogel networks using melanin nanoparticle photothermal sensitizers. *Biomater. Sci.* 2: 766-774, 2014.

[64] Gobin, A. M., Lee, M. H., Halas, N. J., James, W. D., Drezek, R. A., West, J. L. Near-infrared resonant nanoshells for combined optical imaging and photothermal cancer therapy. *Nano Lett.* 7: 1929-1934, 2007.

[65] Qu, Y., Chu, B. Y., Peng, J. R., Liao, J. F., Qi, T. T., Shi, K., Zhang, X. N., Wei, Y. Q., Qian, Z. Y. A biodegradable thermo-responsive hybrid hydrogel: Therapeutic applications in preventing the post-operative recurrence of breast cancer. *NPG Asia Materials* 7: e207, 2015.

[66] Zhang, X., Pint, C. L., Lee, M. H., Schubert, B. E., Jamshidi, A., Takei, K., Ko, H., Gillies, A., Bardhan, R., Urban, J. J., Wu, M., Fearing, R., Javey, A. Optically- and thermally-responsive programmable materials based on carbon nanotube-hydrogel polymer composites. *Nano Lett.* 11: 3239-3244, 2011.

[67] Zhu, C.-H., Lu, Y., Peng, J., Chen, J.-F., Yu, S.-H. Photothermally sensitive poly(n-isopropylacrylamide)/graphene oxide nanocomposite hydrogels as remote light-controlled liquid microvalves. *Adv. Funct. Mater.* 22: 4017-4022, 2012.

[68] Yan, B., Boyer, J.-C., Habault, D., Branda, N. R., Zhao, Y. Near infrared light triggered release of biomacromolecules from hydrogels loaded with upconversion nanoparticles. *J. Am. Chem. Soc.* 134: 16558-16561, 2012.

[69] Liu, T.-Y., Hu, S.-H., Liu, K.-H., Liu, D.-M., Chen, S.-Y. Study on controlled drug permeation of magnetic-sensitive ferrogels: Effect of Fe3O4 and PVA. *J. Control. Release* 126: 228-236, 2008.

[70] Ke, H., Jianfei, S., Zhaobin, G., Peng, W., Qiang, C., Ming, M., Ning, G. A novel magnetic hydrogel with aligned magnetic colloidal assemblies showing controllable enhancement of magnetothermal effect in the presence of alternating magnetic field. *Adv. Mater.* 27: 2507-2514, 2015.

[71] Satarkar, N. S., Hilt, J. Z. Magnetic hydrogel nanocomposites for remote controlled pulsatile drug release. *J. Control. Release* 130: 246-251, 2008.

[72] Wang, Y., Li, B., Zhou, Y., Han, Z., Feng, Y., Wei, D. A facile concentric-layered magnetic chitosan hydrogel with magnetic field remote stimulated drug release. *J. Control. Release* 172: E90, 2013.

[73] Xiang, Y., Chen, D. Preparation of a novel pH-responsive silver nanoparticle/poly (HEMA-PEGMA-MAA) composite hydrogel. *Eur. Polym. J.* 43: 4178-4187, 2007.

[74] Ilg, P. Stimuli-responsive hydrogels cross-linked by magnetic nanoparticles. *Soft Matter* 9: 3465-3468, 2013.

[75] Xia, L.-W., Xie, R., Ju, X.-J., Wang, W., Chen, Q., Chu, L.-Y. Nano-structured smart hydrogels with rapid response and high elasticity. *Nat. Commun.* 4: article number 2226, 2013.

[76] Zhao, X. L., Ding, X. B., Deng, Z. H., Zheng, Z. H., Peng, Y. X., Tian, C. R., Long, X. P. A kind of smart gold nanoparticle-hydrogel composite with tunable thermo-switchable electrical properties. *New J. Chem.* 30: 915-920, 2006.

[77] Cho, E. C., Kim, J.-W., Fernandez-Nieves, A., Weitz, D. A. Highly responsive hydrogel scaffolds formed by three-dimensional organization of microgel nanoparticles. *Nano Lett.* 8: 168-172, 2008.

[78] Messing, R., Frickel, N., Belkoura, L., Strey, R., Rahn, H., Odenbach, S., Schmidt, A. M. Cobalt ferrite nanoparticles as multifunctional cross-linkers in paam ferrohydrogels. *Macromolecules* 44: 2990-2999, 2011.

[79] Bishop, K. J. M., Wilmer, C. E., Soh, S., Grzybowski, B. A. Nanoscale forces and their uses in self-assembly. *Small* 5: 1600-1630, 2009.

[80] Wang, Q., Gu, Z., Jamal, S., Detamore, M. S., Berkland, C. Hybrid hydroxyapatite nanoparticle colloidal gels are injectable fillers for bone tissue engineering. *Tissue Eng. Part A* 19: 2586-2593, 2013.

[81] Wang, H., Hansen, M. B., Loewik, D. W. P. M., van Hest, J. C. M., Li, Y., Jansen, J. A., Leeuwenburgh, S. C. G. Oppositely charged gelatin nanospheres as building blocks for injectable and biodegradable gels. *Adv. Mater.* 23: H119-H124, 2011.

[82] Wang, Q., Jamal, S., Detamore, M. S., Berkland, C. PLGA-chitosan/PLGA-alginate nanoparticle blends as biodegradable colloidal gels for seeding human umbilical cord mesenchymal stem cells. *J. Biomed. Mater. Res. A* 96A: 520-527, 2011.

[83] Gu, Z., Aimetti, A. A., Wang, Q., Dang, T. T., Zhang, Y., Veiseh, O., Cheng, H., Langer, R. S., Anderson, D. G. Injectable nano-network for glucose-mediated insulin delivery. *ACS Nano* 7: 4194-4201, 2013.

[84] Al Ghanami, R. C., Saunders, B. R., Bosquillon, C., Shakesheff, K. M., Alexander, C. Responsive particulate dispersions for reversible building and deconstruction of 3D cell environments. *Soft Matter* 6: 5037-5044, 2010.

[85] Fraylich, M. R., Liu, R., Richardson, S. M., Baird, P., Hoyland, J., Freemont, A. J., Alexander, C., Shakesheff, K., Cellesi, F., Saunders, B. R. Thermally-triggered gelation of PLGA dispersions: Towards an injectable colloidal cell delivery system. *J. Colloid Interface Sci.* 344: 61-69, 2010.

[86] Laroui, H., Dalmasso, G., Nguyen, H. T. T., Yan, Y., Sitaraman, S. V., Merlin, D. Drug-loaded nanoparticles targeted to the colon with polysaccharide hydrogel reduce colitis in a mouse model. *Gastroenterology* 138: 843-853, 2010.

[87] Fullenkamp, D. E., Rivera, J. G., Gong, Y.-k., Lau, K. H. A., He, L., Varshney, R., Messersmith, P. B. Mussel-inspired silver-releasing antibacterial hydrogels. *Biomaterials* 33: 3783-3791, 2012.

[88] Li, L., Smitthipong, W., Zeng, H. Mussel-inspired hydrogels for biomedical and environmental applications. *Polym. Chem.* 6: 353-358, 2015.

[89] Kastrup, C. J., Nahrendorf, M., Figueiredo, J. L., Lee, H., Kambhampati, S., Lee, T., Cho, S.-W., Gorbatov, R., Iwamoto, Y., Dang, T. T., Dutta, P., Yeon, J. H., Cheng, H., Pritchard, C. D., Vegas, A. J., Siegel, C. D., MacDougall, S., Okonkwo, M., Anh, T., Stone, J. R., Coury, A. J., Weissleder, R., Langer, R., Anderson, D. G. Painting blood vessels and atherosclerotic plaques with an adhesive drug depot. *Proc. Natl. Acad. Sci. U. S. A.* 109: 21444-21449, 2012.

[90] Lang, N., Pereira, M. J., Lee, Y., Friehs, I., Vasilyev, N. V., Feins, E. N., Ablasser, K., O'Cearbhaill, E. D., Xu, C., Fabozzo, A., Padera, R., Wasserman, S., Freudenthal, F., Ferreira, L. S., Langer, R., Karp, J. M., del Nido, P. J. A blood-resistant surgical glue for minimally invasive repair of vessels and heart defects. *Sci. Transl. Med.* 6: 218ra216, 2014.

[91] Park, C. G., Shasteen, C., Amoozgar, Z., Park, J., Kim, S.-N., Lee, J. E., Lee, M. J., Suh, Y., Seok, H. K., Yeo, Y., Choy, Y. B. Photo-crosslinkable chitosan hydrogel as a bioadhesive for esophageal stents. *Macromol. Res.* 23: 882-884, 2015.

[92] Patel, R. G., Purwada, A., Cerchietti, L., Inghirami, G., Melnick, A., Gaharwar, A. K., Singh, A. Microscale bioadhesive hydrogel arrays for cell engineering applications. *Cell. Mol. Bioeng.* 7: 394-408, 2014.

[93] Fang, R. H., Luk, B. T., Hu, C.-M. J., Zhang, L. Engineered nanoparticles mimicking cell membranes for toxin neutralization. *Adv. Drug Del. Rev.* 90: 69-80, 2015.

[94] Zhang, L., Leroux, J.-C. Current and forthcoming approaches for systemic detoxification preface. *Adv. Drug Del. Rev.* 90: 1-2, 2015.

[95] Gordon, R. J., Lowy, F. D. Pathogenesis of methicillin-resistant staphylococcus aureus infection. *Clin. Infect. Dis.* 46: S350-S359, 2008.

[96] Gorwitz, R. J. Understanding the success of methicillin-resistant staphylococcus aureus strains causing epidemic disease in the community. *J. Infect. Dis.* 197: 179-182, 2008.

[97] Singer, A. J., Talan, D. A. Management of skin abscesses in the era of methicillin-resistant staphylococcus aureus. *New Engl. J. Med.* 370: 1039-1047, 2014.

[98] Wang, F., Gao, W., Thamphiwatana, S., Luk, B. T., Angsantikul, P., Zhang, Q., Hu, C.-M. J., Fang, R. H., Copp, J. A., Pornpattananangkul, D., Lu, W., Zhang, L. Hydrogel retaining toxin-absorbing nanosponges for local treatment of methicillin-resistant staphylococcus aureus infection. *Adv. Mater.* 27: 3437-3443, 2015.

[99] Nel, A., Xia, T., Madler, L., Li, N. Toxic potential of materials at the nanolevel. *Science* 311: 622-627, 2006.

[100] Hoshino, Y., Koide, H., Furuya, K., Haberaecker, W. W., III, Lee, S.-H., Kodama, T., Kanazawa, H., Oku, N., Shea, K. J. The rational design of a synthetic polymer nanoparticle that neutralizes a toxic peptide in vivo. *Proc. Natl. Acad. Sci. U. S. A.* 109: 33-38, 2012.

[101] Gou, M., Qu, X., Zhu, W., Xiang, M., Yang, J., Zhang, K., Wei, Y., Chen, S. Bio-inspired detoxification using 3D-printed hydrogel nanocomposites. *Nat. Commun.* 5: article number 3774, 2014.

[102] Schoffelen, S., van Hest, J. C. M. Multi-enzyme systems: Bringing enzymes together in vitro. *Soft Matter* 8: 1736-1746, 2012.

[103] Conrado, R. J., Varner, J. D., DeLisa, M. P. Engineering the spatial organization of metabolic enzymes: Mimicking nature's synergy. *Curr. Opin. Biotechnol.* 19: 492-499, 2008.

[104] Liu, Y., Du, J., Yan, M., Lau, M. Y., Hu, J., Han, H., Yang, O. O., Liang, S., Wei, W., Wang, H., Li, J., Zhu, X., Shi, L., Chen, W., Ji, C., Lu, Y. Biomimetic enzyme nanocomplexes and their use as antidotes and preventive measures for alcohol intoxication. *Nat. Nanotech.* 8: 187-192, 2013.

[105] Saquing, C. D., Manasco, J. L., Khan, S. A. Electrospun nanoparticle-nanofiber composites via a one-step synthesis. *Small* 5: 944-951, 2009.

[106] Chen, M., Gao, S., Dong, M., Song, J., Yang, C., Howard, K. A., Kjems, J., Besenbacher, F. Chitosan/siRNA nanoparticles encapsulated in PLGA nanofibers for sirna delivery. *ACS Nano* 6: 4835-4844, 2012.

[107] Wang, S., Zhao, Y., Shen, M., Shi, X. Electrospun hybrid nanofibers doped with nanoparticles or nanotubes for biomedical applications. *Ther. Deliv.* 3: 1155-1169, 2012.

[108] DeMuth, P. C., Su, X., Samuel, R. E., Hammond, P. T., Irvine, D. J. Nano-layered microneedles for transcutaneous delivery of polymer nanoparticles and plasmid DNA. *Adv. Mater.* 22: 4851-4856, 2010.

[109] DeMuth, P. C., Moon, J. J., Suh, H., Hammond, P. T., Irvine, D. J. Releasable layer-by-layer assembly of stabilized lipid nanocapsules on microneedles for enhanced transcutaneous vaccine delivery. *ACS Nano* 6: 8041-8051, 2012.

[110] Sattayasamitsathit, S., Kou, H., Gao, W., Thavarajah, W., Kaufmann, K., Zhang, L., Wang, J. Fully loaded micromotors for combinatorial delivery and autonomous release of cargoes. *Small* 10: 2830-2833, 2014.

[111] Wu, Z., de Avila, B. E.-F., Martin, A., Christianson, C., Gao, W., Thamphiwatana, S. K., Escarpa, A., He, Q., Zhang, L., Wang, J. Rbc micromotors carrying multiple cargos towards potential theranostic applications. *Nanoscale* 7: 13680-13686, 2015.

[112] Hoare, T. R., Kohane, D. S. Hydrogels in drug delivery: Progress and challenges. *Polymer* 49: 1993-2007, 2008.

[113] Ratner, B. D. Reducing capsular thickness and enhancing angiogenesis around implant drug release systems. *J. Control. Release* 78: 211-218, 2002.

[114] Langer, R. Perspectives and challenges in tissue engineering and regenerative medicine. *Adv. Mater.* 21: 3235-3236, 2009.

[115] Zhang, L., Cao, Z., Bai, T., Carr, L., Ella-Menye, J.-R., Irvin, C., Ratner, B. D., Jiang, S. Zwitterionic hydrogels implanted in mice resist the foreign-body reaction. *Nat. Biotechnol.* 31: 553-556, 2013.

[116] Yu, L., Ding, J. Injectable hydrogels as unique biomedical materials. *Chem. Soc. Rev.* 37: 1473-1481, 2008.

[117] Fairbanks, B. D., Schwartz, M. P., Bowman, C. N., Anseth, K. S. Photoinitiated polymerization of peg-diacrylate with lithium phenyl-2,4,6-trimethylbenzoylphosphinate: Polymerization rate and cytocompatibility. *Biomaterials* 30: 6702-6707, 2009.

Chapter 1, in full, is a reprint of the material as it appears in Annals of Biomedical Engineering, 2016, Weiwei Gao, Yue Zhang, Qiangzhe Zhang and Liangfang Zhang. The dissertation author was a major contributor and co-author of this paper.

Chapter 2

Biomimetic Nanosponges Against Bacterial Infection

2.1. Erythrocyte membrane-coated nanogel for combinatorial anti-virulence and responsive antimicrobial delivery against *Staphylococcus Aureus* infection

2.1.1. Introduction

Staphylococcus aureus (*S. aureus*) is a prominent Gram-positive bacterium responsible for a wide range of human skin and wound infections [1, 2]. With the widespread use of antibiotics during the past a few decades, *S. aureus* bacteria have experienced several waves of antibiotic resistance and now display broad resistance to the entire *β*-lactam class of antibiotics, including penicillins, cephalosporins, and carbapenems [3-5]. To keep up with the pace of antibiotic resistance development, alternative antibiotics including vancomycin, linezolid, tedezolid, daptomycin, ceftaroline, and tigecycliine have been introduced to the market in recent years [6-9]. However, the emergence of antibiotic-resistant *S. aureus* strains, especially toward vancomycin resistance, has greatly increased [10, 11]. Currently, virulent strains of methicillin-resistant *S. aureus* (MRSA) have become increasingly prevalent, imposing a major clinical challenge that threatens public health [12, 13]. Clearly, all these facts underscore an undisputed and urgent need to develop novel and effective therapeutic strategies for MRSA treatment.

To address antibiotic resistance, targeting and neutralizing virulence factors such as bacterial toxins offer an attractive alternative that is likely to lower the selective pressure on the bacterial pathogens [14]. Notably, MRSA infection features a critical

element of virulence resulting from a diverse arsenal of pore-forming toxins (PFTs) secreted by the bacteria [15]. In this perspective, coating red blood cell (RBC) membrane onto synthetic nanoparticles for broad spectrum neutralization of PFTs has recently gained much attention [16, 17]. These RBC membrane-coated nanoparticles (denoted 'nanosponges') target the membrane-disrupting mechanism shared by all PFTs regardless of their molecular structures and sources, thereby offering a non-specific and all-purpose toxin decoy strategy. For example, in a subcutaneous MRSA infection mouse model, the nanosponges alone when applied at the infection site effectively neutralized tissue-damaging α-toxin and markedly reduced the lesion development caused by MRSA infection [18].

In addition to the antibiotic resistance development, *S. aureus* bacteria are also known to invade and survive inside phagocytic cells such as macrophages, further diminishing the efficacy of existing antibiotics [19, 20]. Incomplete clearance of intracellular MRSA infection facilitates their dissemination and subsequent invasion of various non-phagocytic cell types [21]. As a result, intracellular MRSA infection is often associated with a number of chronic or recurrent infections including recurrent rhinosinusitis, pulmonary infections, osteomyelitis and endocarditis [22]. To address the challenges, nanoparticle delivery systems have attracted much attention. These nanomedicines are designed to preferentially deliver antibiotics into the host cells to inhibit residue MRSA bacteria. For example, synthetic nanoparticles made from cationic polymers such as chitosan and polyhexamethylene biguanide exploit strong charge interactions to enhance uptake by the host cells [23, 24]. Modifying

nanoparticles with targeting ligands including wheat germ agglutinin and mannose represents another effective approach to improving phagocytic uptake of antibiotic payloads and enhancing MRSA inhibition [25, 26]. Moreover, nanoparticles responsive to intracellular cues for on-demand antibiotic release have also gained much interest for targeting intracellular MRSA bacteria. In this perspective, nanoparticles capable of drug release in response to MRSA-associated enzymes such as penicillin Gamidase, β-lactamase, phosphatase, and phospholipase have been investigated for controlled release of antibiotics within the host cells [25].

Inspired by the unique toxin neutralization property of the 'nanosponges' and the 'on-demand' drug release capability of various anti-MRSA nanomedicines against intracellular infection, herein, we combined the two features into one nanoparticle system and engineered a redox-responsive RBC membrane-coated nanogel (denoted 'RBC-nanogel') platform, which consists of a responsive hydrogel core and an RBC membrane shell (Figure. 2.1A). The hydrogel core is used for redox-responsive antimicrobial delivery and release, while the RBC membrane shell is used for absorbing and neutralizing PFTs secreted bacteria. In the study, a cell membrane-templated polymerization method was utilized to prepare such RBC-nanogels [27]. Compared to the prior strategy of wrapping cell membranes onto pre-formed nanoparticle substrates, this approach forms cell membrane-derived vesicles first, followed by polymerizing hydrogel cores inside the vesicles. To make a redox-responsive hydrogel core, we synthesized a crosslinker with a disulfide bond, which is readily cleaved inside an endosome following nanoparticle phagocytosis [28]. As

shown in Figure. 2.1B, in the extracellular environment, the RBC-nanogels can absorb and neutralize PFTs secreted by MRSA bacteria. Toxin neutralization counteracts the bacterial virulence and facilitates bacterial uptake by phagocytic cells. Once inside the cells, the RBC-nanogels respond to the reducing environment and rapidly release antibiotic payloads for the inhibition of intracellular MRSA bacteria.

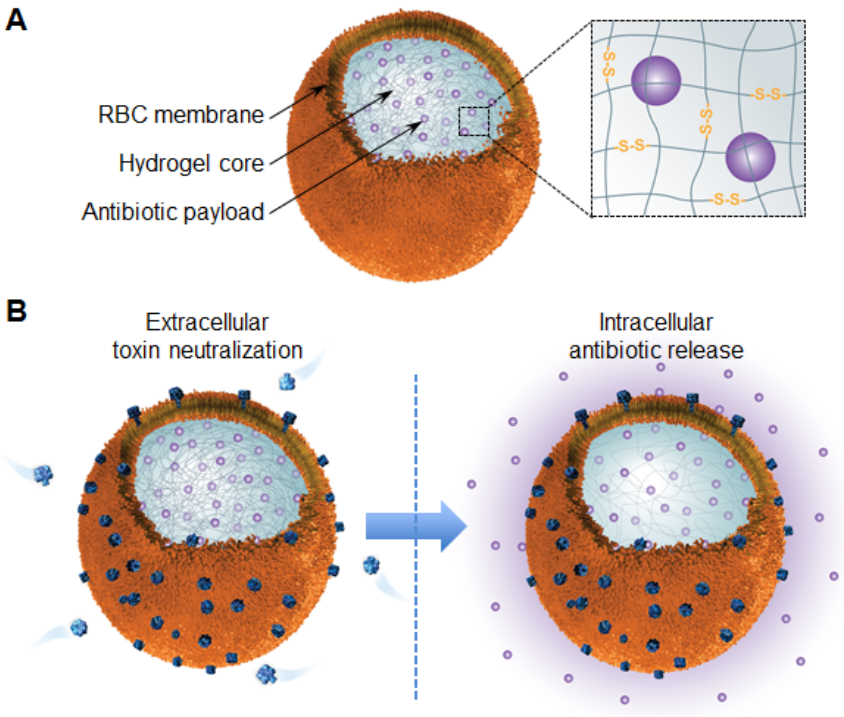

Figure 2.1: Schematic illustrations of a red blood cell (RBC) membrane-coated nanogel (RBC-nanogel) system for combinatorial extracellular toxin neutralization and intracellular redox-responsive antibiotic release. (A) The RBC-nanogel is constructed with a natural RBC membrane shell and a hydrogel core containing antibiotic payload. The hydrogel core is cross-linked with disulfide bonds, cleavable in reducing environment. (B) In extracellular environment, the RBC-nanogel absorbs and neutralizes pore-forming toxins (PFT) secreted by bacteria. Such toxin sequestration facilities the intracellular uptake of the toxin-secreting bacteria and the RBC-nanogel. Once inside the cell, the RBC-nanogel rapidly releases its encapsulated antibiotic payload triggered by a redox reaction.

2.1.2 Experimental Methods

Materials

Reagents including L-cystine, methacrylic anhydride (MA), hydrochloride acid, Triethanolamine (TEA), *N, N*'-methylene bis-acrylamide (non-responsive crosslinker), acrylamide (monomer), tris(2-carboxyethyl) phosphine (TCEP), and Triton X-100 were purchased from Sigma-Aldrich (St. Louis, USA) and used as received unless otherwise stated. Acetonitrile (ACN, HPLC grade) were purchased from EMD Chemicals (Gibbstown, USA). Succinimidyl succinate-poly (ethylene glycol)-succinimidyl succinate (NHS-PEG-NHS, average molecular weight = 3400 g/mol) was purchased from Laysan Bio, Inc. (Alabama, USA). The macromolecular inhibitor TEMPO-PEG-TEMPO was synthesized by conjugating HNS-PEG-NHS and 4-amino-2,2,6,6-tetramethylpiperidine-1-oxyl (4-aimno-TEMPO) in tetrahydrofuran (THF) with the presence of triethylamine (TEA) following a published protocol [27]. The photoinitiator lithium phenyl-2,4,6-trimethylbenzoylphosphinate (LAP) was synthesized following a published protocol [29, 30].

Synthesis and characterization of redox-responsive crosslinker.

To synthesize cystine dimethacrylate (CDA), a redox-responsive crosslinker, L-cystine (0.48 g, 2 mmol) was dissolved with 5 mL DI water and 1 mL TEA was added to the solution. After complete dissolution of L-cystine, 2 mL MA was added dropwise into the solution. The mixture was then stirred vigorously, and the reaction was allowed for 48 h at room temperature. Following the reaction, TEA and unreacted

MA were extracted with diethyl ether. Then the pH value of the resulted solution was adjusted to 2 with hydrochloric acid. The sample was then lyophilized, and the final product was obtained as an off-white powder. Its molecular structure was confirmed by ^{1}HNMR (Varian Inova-500M, Varian Inc., Palo Alto, USA) with $CO(CD_3)_2$ (d-Acetone) as the solvent and tetramethylsilane (TMS) as the internal standard. Its molecular weight was confirmed by matrix-assisted laser desorption/ionization time-of-flight (MALDI-TOF, Bruker Biflex IV MALDI-TOFMS) mass spectrometry.

Preparation and characterization of RBC membrane-coated nanogels (RBC-nanogels).

RBC membranes were derived by following a previously published protocol [31]. Briefly, the whole blood withdrawn from male ICR mice (Charles River Laboratories, Wilmington, MA) was centrifuged (×800 g for 5 min at 4°C) to remove the plasma and the buffy coat. The resulting packed RBCs were washed and the RBC ghosts were prepared through a hypotonic treatment. To prepare RBC-nanogels, the collected RBC ghosts were mixed with acrylamide as monomer (0.71 mmol), CDA as redox-responsive crosslinker (0.03 mmol), and LAP (5 μmol) in PBS containing 1 mM Mg^{2+} and 1 mM Ca^{2+}. Then the mixture was sonicated for 5 min using a bath sonicator (FS30D, Fisher Scientific) at a frequency of 42 kHz and power of 100 W. The mixture was then extruded serially through 400 nm and then 100 nm polycarbonate porous membranes with an Avanti mini extruder (Avanti Polar Lipids). Following the extrusion, macromolecular inhibitor, TEMPO-PEG-TEMPO (7 nmol),

was added into the solution. For gelation, the solution was degassed by blowing nitrogen and then irradiated with ultraviolet (UV) light for 5 min (Black Ray® Lamp, 365 nm, model UVL-56, Upland, USA). To synthesize non-responsive RBC-nanogels (control nanogels), CDA was replaced with *N, N*'-methylene bis-acrylamide (0.03 mmol) as a non-responsive crosslinker. For filtration study, rhodamine B (0.3 mg/mL) was included into the reactant mixture for encapsulation. Following the nanogel synthesis, samples were added with 0.25 mL 5% w/v Triton X-100 and 20 μg proteinase K (New England Biolabs, Inc., Beverly, USA) to dissolve RBC membranes. To dissolve hydrogel core, 10 μL TCEP (300 mM) was added to the solution with a final concentration of 10 mM. Samples were filtered through an Amicon ultra filter with a molecular weight cut-off of 100 kDa. The released rhodamine B from both samples was then quantified by a UV spectrophotometer (Lambda 850 spectrophotometer, Perkin Elmer Inc., Waltham, MA, USA). Further characterizations with dynamic light scattering (DLS) were carried on a Zetasizer Nano ZS (Malvern Instruments). The nanogel concentrations of all samples were quantified by using a Pierce™ BCA Protein Assay Kit (Thermo Fisher Scientific) and following the manufacturer's protocol.

In vitro toxin neutralization with RBC-nanogels.

Alpha toxin neutralization with RBC-nanogels was examined by first mixing a fixed amount of RBC-nanogels (3 μL, 0.8 μg/μL protein) with various amount of α-toxins, followed by incubating the mixture at 37°C for 30 min. After the incubation,

500 μL 5% purified mouse RBCs was added and the samples were incubated for another 30 min. The released haemoglobin was then quantified by UV-vis spectrometer at 576 nm to determine the percentage of RBCs being lysed.

Bacterial culture

MRSA USA300 bacteria were cultured on tryptic soy broth (TSB) agar overnight at 37°C. Then a single colony was inoculated in TSB medium and the medium was cultured in a rotary shaker at 37°C. Overnight culture was refreshed in TSB medium at 1:100 dilution and under shaking for another 3 h until the OD_{600} of the culture medium reached approximately 1.0 (logarithmic growth phase). The bacteria were then harvested by centrifugation at 5000 ×g for 10 min, and then washed with sterile PBS twice. After the removal of PBS by centrifugation, the obtained bacteria pallet was suspended in an appropriate amount of sterile PBS for future use.

Cellular uptake of MRSA bacteria

MRSA USA300 bacteria were labelled by mixing 10 μl calcein-AM (1 mg/mL, excitation/emission = 495/516 nm) with 0.5 mL bacterial suspension (1.5×10^9 CFU/mL). The mixture was incubated at 37°C for 30 min. The free Calcein-AM was removed by washing the bacteria with PBS solution twice. THP-1 cells were cultured in RPMI1640 medium (Gibco Life technologies) supplemented with 2 mM L-glutamine, 1% penicillin, 1% streptomycin and 10% fetal bovine serum (HyClone Laboratories). THP-1 cells were differentiated with phorbol 12-myristate 13-acetate (PMA, Sigma-Aldrich, St. Louis, MO, USA) at the concentration of 100 ng/mL in

RPMI1640 medium with all the aforementioned supplement for 4 days. For uptake study, 8×10^5 differentiated THP-1 cells were seeded to each well of a 12-well plate. After cell adhesion, different concentrations of free α-toxin or α-toxin mixed with RBC-nanogels were added. To each well, 8×10^7 Calcein-AM labelled USA300 bacteria were added. The plate was cultured for 2 h with gentle shaking. Following the incubation, cells were washed, detached, and fixed with 10% formalin for intracellular bacterial quantification using flow cytometry (BD FACSCanto-II).

Vancomycin loading and release study

Vancomycin was encapsulated into the RBC-nanogels by mixing 5 mg/mL drug solution with the reactant mixture during the nanogel synthesis process described above. Nanogels were lyophilized and weighed for total mass. To quantify encapsulated vancomycin, nanogels were resuspended with DI water and the suspension was stirred for 24 h to allow for equilibrium. Vancomycin concentration was quantified with high-performance liquid chromatography (HPLC, Perkin Elmer Flexar series 200, Waltham, MA, USA) equipped with a Brownlee SPP C18 column (100 mm × 4.6 mm and 2.7 μm beads). The mobile phase contained 25 mM KH_2PO_4 solution and ACN (9:1, volume ratio) with a flow rate of 1.0 mL/min. The detection wavelength was set at 230 nm. The loading efficiency was calculated as the percentage of encapsulated vancomycin to initial vancomycin input. The loading yield was calculated as the weight percentage of vancomycin to total nanogels. Vancomycin release was measured by loading 1 mL RBC-nanogel suspension into a dialyzer

(Harvard Apparatus, Holliston, USA). Dialysis membranes with pores of 50 nm in diameter (Isopore membrane filters, Merck Millipore Ltd. Billerica, USA) were used. The dialyzer was immersed into 1000 mL PBS, PBS with Triton X-100 (5% w/v), or PBS with Triton X-100 (5% w/v) and TCEP (10 mM) at 37°C under agitation. The released vancomycin at pre-determined time intervals was quantified with the same HPLC method.

In vitro MRSA inhibition activity of vancomycin-loaded RBC-nanogels

Bacterial suspensions (1 mL) containing 1×10^8 CFU/mL (OD_{600} = 0.1) MRSA USA300 bacteria in TSB were added to UV-transparent cuvettes. To each cuvette, 100 μL TECP (10 mM) and 2 μL Triton X-100 (5% w/v) were added, followed by the addition of vancomycin-loaded RBC-nanogels, vancomycin-loaded control nanogels, or free vancomycin at various pre-determined concentrations. The cuvettes were incubated at 37°C for 24 h and then the values of OD600 were measured.

Vancomycin-loaded RBC-nanogels against intracellular MRSA infection

THP-1-derived macrophages were seeded onto 6-well plates at a density of 2×10^6 cells/well. The cells were allowed to adhere for overnight. To infect the cells, 2×10^7 bacteria (100 μL at a concentration of 2×10^8 CFU/mL) were added to each well

and the plates were incubated at 37°C for 2 h. Following the incubation, the cells were gently washed with warm PBS and then medium containing 100 µg/mL gentamicin was added. The plates were incubated for another 3 h to eliminate any extracellular bacteria. After establishing the intracellular infection, PBS, empty RBC-nanogels, control-nanogels, vancomycin-loaded RBC-nanogels, vancomycin-loaded control-nanogels, and free vancomycin (with an equivalent vancomycin concentration of 5 µg/mL) were added to the wells. The plates were incubated for 6 h followed by macrophage disruption and bacterial enumeration. The viable intracellular bacteria were quantified by first erupting the macrophages with hypotonic treatment. Then a series of 10-fold dilution from the suspension was inoculated to TSB agar plate. The agar plate was cultured at 37°C for 24 h and the colony formation was counted.

2.1.3. Results and Discussion

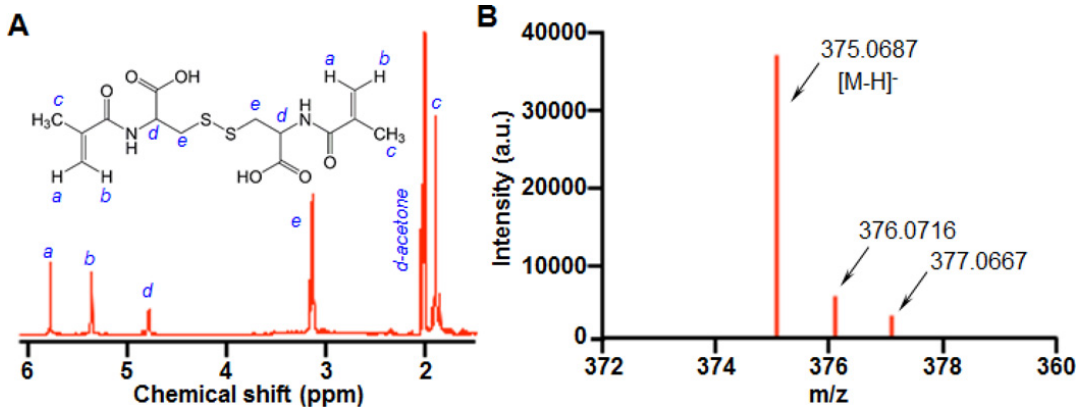

Figure 2.2: Characterization of cystine dimethacrylate (CDA), a redox-responsive crosslinker. (A) ^{1}H-NMR spectrum and (B) MALDI-TOF spectrum of CDA.

In the study, we first synthesized cystine dimethacrylate (CDA) as a redox-responsive crosslinker through a reaction between methacrylic anhydride (MA) and L-cystine in tetrahydrofuran (THF) with the presence of triethylamine (TEA). The product was purified by repeated extraction with ethyl acetate followed by evaporating the solvent. The molecular structure of the product was first analyzed with ^{1}H NMR (Figure. 2.2A). The spectrum shows the characteristic resonance signals of vinyl hydrogens adjacent to the C=C double bond (*a* and *b*), methyl (*c*), methine (*d*, hydrogens adjacent to the -COOH carboxyl bond), and methylene (*e*, hydrogens adjacent to the S-S disulfide bond). The matrix-assisted laser desorption and ionization time-of-flight mass spectrometry (MALDI-TOF MS) was used to further confirm the conjugation reaction and analyze the purity of the product (Figure. 2.2B). The mass spectrum of CDA was dominated by the deprotonated ions $[M-H]^-$ at m/z 375.0687 and exhibited negligible fragmentation. In addition, the mass spectrum also shows other ions of lower intensity (m/z 376.0716 and m/z 377.0667 ions), attributable to the presence of the ^{13}C isotopic analog of the peak of m/z 375.0687. The close match between the measured and the theoretical values of CDA confirms the successful synthesis of the crosslinker.

Following the synthesis of the crosslinker, we proceeded to prepare RBC-nanogels by using RBC membrane-derived vesicles (RBC-vesicles) as templates for *in situ* polymerization [27]. Herein, the RBC vesicles were used not only as nanoreactors to encapsulate the reactants including monomers, crosslinkers, initiators, and drug payloads, but also as a template to control the final nanogel size. After forming

vesicles of approximately 100 nm in diameter using an extrusion method, we added a water-soluble macromolecular inhibitor, TEMPO-PEG-TEMPO, to the mixture. As the inhibitor is membrane impermeable, it selectively inhibits the polymerization reaction outside of the vesicles while keeping the reaction inside alive. To confirm the nanogel formation, we loaded rhodamine B to the precursor solution. Following the synthesis, the samples were treated with Triton X-100 and proteinase K, followed by filtration through Amicon ultra filters with a molecular weight cutoff of 100 kDa.

Triton X-100 was shown to disrupt the RBC membrane coating on the nanogels; however, samples treated with Triton X-100 did not release rhodamine B into the solution, suggesting the hydrogel cores were formed and entrapped the dye (Figure. 2.3A). When a reducing agent, TCEP, was added to the solution, it effectively cleaved the disulfide bonds, resulting in quick release of the encapsulated rhodamine B. This result indicates the potential of redox-responsive drug release from the RBC-nanogels. The resulting RBC-nanogels were also stained with uranyl acetate and visualized with transmission electron microscopy (TEM). As shown in Figure 2.3B, the nanogels exhibited an inner core region enclosed by a thin shell of approximately 10∼15 nm in diameter. Such morphology is consistent with the core-shell structure of the nanogels.

To further confirm the RBC-nanogel formation, we examined nanogel size with dynamic light scattering (DLS). Prior to the UV irradiation, the RBC-vesicles showed a hydrodynamic size of 100.8 ± 0.3 nm in diameter with a unimodal size distribution (Figure 2.3B). When added with Triton-X and proteinase K, the measured

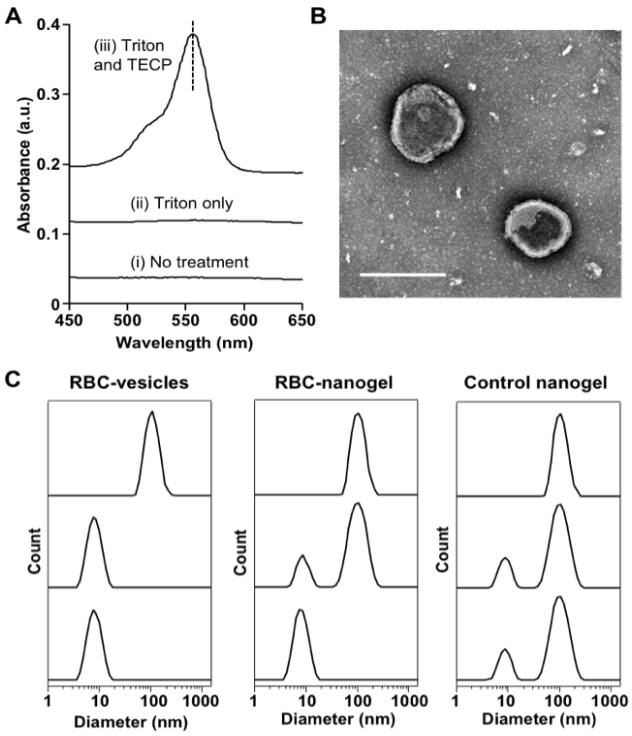

Figure 2.3: The formulation and characterization of RBC-nanogels. (A) RBC-nanogels loaded with rhodamine B were formulated and subjected to (i) no treatment, (ii) treated with Triton X-100 and proteinase K, or (iii) Triton X-100 and proteinase K followed by tris(2-carboxyethyl) phosphine (TCEP). The RBC-nanogels were then filtered to collect the released dye, which was further measured by a UV-vis spectrophotometer. (B) A representative TEM image of RBC-nanogels (scale bar = 100 nm). (C) Dynamic light scattering (DLS) measurements of the size and size distribution of RBC-vesicles, RBC-nanogels, and non-responsive RBC nanogels (Control nanogels) subjected to the same treatment as in (A).

size of the vesicles decreased to 10.2 ± 0.5 nm in diameter. This peak was likely attributed to small lipid micelles because of the surfactants solubilizing the phospholipid bilayers. The RBC-nanogels showed a diameter of 104 ± 0.4 nm after UV irradiation. However, when Triton-X and proteinase K were added to the solution, two particle peaks were observed: a small micelle peak at 10.7 ± 0.1 nm and a large

particle peak at 93.2 ± 0.6 nm. The presence of the large peak suggests the formation of crosslinked hydrogel cores within the RBC membrane coating as the crosslinked cores remained insoluble in the surfactant. The diameter of the insoluble hydrogel cores was approximate 12 nm smaller as compared to the RBC-nanogels; the diameter decrease was consistent with the dissolution of the RBC membrane bilayer. Notably, the observed large peak disappeared after the addition of TCEP, a reducing agent that can break the disulfide bonds and thus cause core dissolution. To confirm the role played by the disulfide bonds, we also synthesized a non-responsive RBC-nanogels (control nanogels) by replacing CDA with methacrylic anhydride (MA). Following the synthesis, we added Triton-X and proteinase K and observed a small micelle peak at 10.1 ± 0.2 nm and a large particle peak at 93.7 ± 0.4 nm. However, the large peak remained after adding TCEP, indicating the non-responsive nature of the control nanogels. Together, these results confirm the successful formation of the RBC-nanogels with a redox-responsive property.

Following the synthesis, we examined the bioactivity of RBC-nanogels in neutralizing α-toxin, a major hemolytic virulence factor released by MRSA bacteria. In the study, α-toxins with amounts ranging from 0.3 to 3.6 μg were either directly added to 5% purified mouse RBCs or first incubated with 2.4 μg (protein amount) of RBC-nanogels, followed by the addition to the RBCs. RBC hemolysis was quantified by measuring the released hemoglobin percentage. As shown in Figure 2.4A, free α-toxin exhibited a concentration-dependent hemolytic activity and the hemolysis reached maximum at 3.6 μg of α-toxin. On the other hand, RBC-nanogels were able to

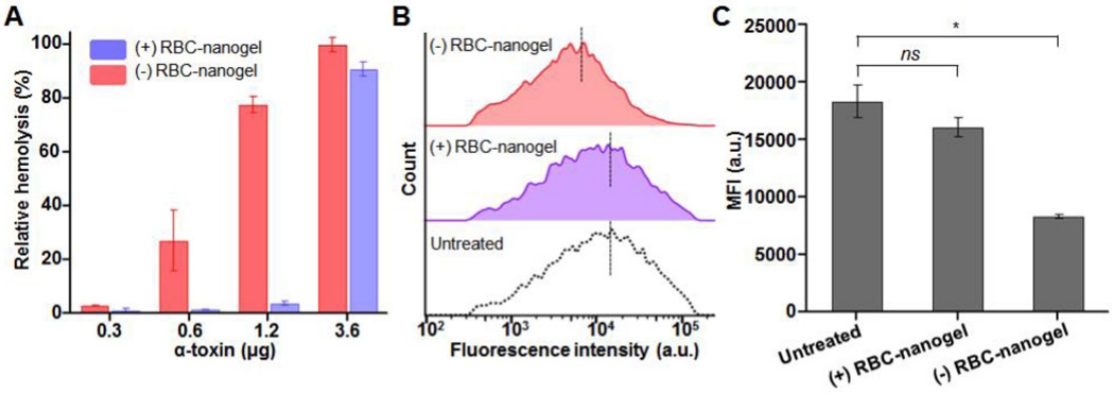

Figure 2.4: Toxin neutralization by RBC-nanogels promotes intracellular uptake of MRSA USA300 bacteria by THP-1 derived macrophages. (A) The relative hemolysis activity of α-toxin in the presence or absence of 2.4 μg (protein amount) of RBC-nanogels is quantified by measuring the absorption of released hemoglobin in the supernatant. (B) Representative flow cytometry analyses of bacterial uptake by macrophages. The bacteria were labeled with calcein-AM and exposed to macrophages after treated with 20 μg free α-toxin or 20 μg α-toxin mixed with 50 μg RBC-nanogels (protein amount). Untreated sample served as a control group. (C) Quantification of the mean fluorescence intensity values based on the histograms in (B). Data are shown in mean ± SEM (*$p < 0.5$). Three independent experiments were carried out.

completely inhibit the hemolytic activity of up to 1.2 μg of α-toxin. Above this concentration, hemolysis was observed, indicating the presence of excessive free α-toxin. Based on these results, 1 μg (protein amount) of RBC-nanogels was able to neutralize about 0.5 μg of α-toxin.

Neutralization of toxins, especially α-toxin, has been shown to increase proinflammatory cytokine production and enhance bacterial clearance [32, 33]. Therefore, by neutralizing toxins, RBC-nanogels may facilitate bacterial uptake by the immune cells. To test this hypothesis, we used THP-1 derived macrophages as a model cell line and compared their ability to take up MRSA USA300 bacteria with or without the presence of RBC-nanogels. In the study, we first added 20 μg free α-toxins or the mixture of 20 μg α-toxins with 50 μg RBC-nanogels to macrophages. Then to

the cell culture, calcein-labeled MRSA bacteria were added. The bacterial uptake by the cells was quantified by measuring the fluorescence intensity from the phagocytosed MRSA USA300 in each cell using flow cytometry. As shown in Figure 2.4B, macrophages treated with α-toxin showed a decreased bacterial uptake when compared to the untreated macrophages. In contrast, macrophages treated with the mixture of α-toxin and RBC-nanogels demonstrated a similar uptake level to that of

A

	Vancomycin loading efficiency (%)	Vancomycin loading yield (%)
RBC-nanogel	1.08 ± 0.04	2.59 ± 0.09
Control-nanogel	1.10 ± 0.06	2.41 ± 0.07

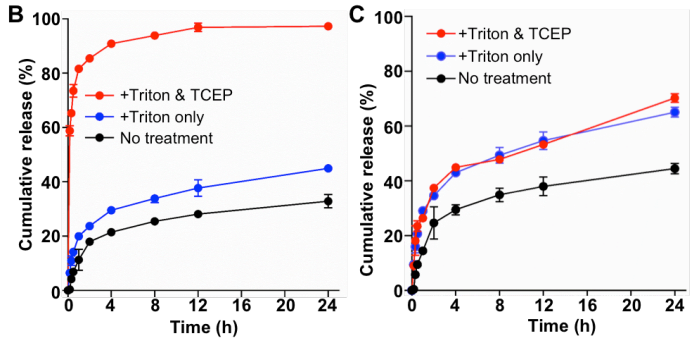

Figure 2.5: Vancomycin loading and release studies. (A) Quantification of vacomycin loading efficiency and loading yield in both RBC-nanogels and control nanogles. The cumulative release profiles of vancomycin from (A) RBC-nanogels and (B) non-responsive RBC-nanogels (Control nanogels). The nanogels were treated with Triton X-100, treated with Triton X-100 followed by TCEP, or not treated by anything.

the untreated macrophages. The mean fluorescence intensity based on the histograms was further quantified (Figure 2.4C). The comparison showed that macrophages treated with the mixture of α-toxin and RBC-nanogels had taken up significantly more bacteria compared to those treated with α-toxin alone. These results indicate that the RBC-nanogels can neutralize α-toxin and promote bacterial uptake by the immune cells.

To demonstrate a redox-responsive drug release property, we first encapsulated vancomycin into RBC-nanogels and control nanogels, respectively, and characterized

their loading efficiency (the percentage of encapsulated vancomycin to initial vancomycin input) and loading yield (the weight percentage of vancomycin to total nanogels). Both formulations show comparable vancomycin loading efficiency and loading yield (Figure. 2.5 A). We then compared their drug release profiles under various conditions (Figure 2.5B and C). In PBS (no treatment), RBC-nanogels and control nanogels released approximately 30% and 40% of the total encapsulated vancomycin in 24 h, respectively. To simulate the degradation condition in endosome, we first added Triton X-100 to the nanogel suspensions. RBC membrane coating was shown to act as a diffusion barrier to hinder drug release. With the presence of Triton X-100, vancomycin release increased in both groups: RBC-nanogels and control nanogels released approximately 40% and 50% of the total encapsulated vancomycin in 24 h, respectively. Next, we added both Triton X-100 and TCEP to the nanogel suspensions. In this case, vancomycin release from RBC-nanogels was significantly accelerated, reaching a cumulative release of approximately 65% of the total encapsulated drug in 0.5 h and 95% in 24 h, indicating a clear responsiveness to the reducing environment. However, such responsive release of vancomycin was not observed for the control nanogel sample. In fact, similar vancomycin release profiles were observed from the control nanogels in the absence or presence of TCEP. Such responsive antibiotic release is expected to benefit MRSA treatment. Most of the loaded vancomycin will remain in the RBC-nanogels for a considerable time when the nanogels stay in the extracellular space under normal

physiological conditions. However, the drug will be quickly released when the RBC-nanogels are taken up by the infected macrophages.

After having confirmed the redox-responsive vancomycin release from RBC-nanogels, we proceeded to evaluate their anti-MRSA efficacy. We first incubated MRSA USA300 (1×10^6 CFU/mL) with free vancomycin, vancomycin-loaded RBC-nanogels, and vancomycin-loaded control nanogels with vancomycin concentrations ranging from 0.3 to 20 μg/mL. Bacterial culture was supplemented with TCEP and Triton X-100 to mimic reducing environment inside the mammalian cells and cultured for 24 h at 37°C [28]. Following the incubation, vancomycin-loaded RBC-nanogels exhibited an anti-MRSA efficacy comparable to that of free vancomycin, with a minimum inhibition concentration (MIC) of 2.5 μg/mL for both groups (Figure 2.6A). In contrast, vancomycin-loaded control nanogels showed a reduced anti-MRSA efficacy with an MIC value of 5 μg/mL. Since Triton and TCEP were added to all samples, a higher MIC value of control nanogels compared to RBC-nanogels was attributable to the slow release of vancomycin from non-responsive nanogel formulation. These results imply that rapid release of vancomycin after RBC-nanogels are taken up by macrophages will be beneficial for treating intracellular bacterial infection.

Lastly, we tested the anti-MRSA efficacy of vancomycin-loaded RBC-nanogels on an in vitro intracellular infection model by using THP-1 derived macrophages as the cellular reservoir for MRSA USA300. In the study, we incubated macrophages with MRSA bacteria at a ratio of 1:10 and used gentamicin to eradicate

extracellular bacteria. Under the condition, the ratio of macrophages to the intracellular bacteria was determined to be ~20:1. Next, the infected macrophages were treated with PBS, empty RBC-nanogels, empty control nanogels, vancomycin-loaded RBC-nanogels, vancomycin-loaded control nanogels and free vancomycin. After culturing the cells for 6 h, macrophages were lysed and the intracellular MRSA bacteria were quantified. Cells treated with PBS and vehicle controls (empty RBC-nanogels and empty control nanogels) showed a significant increase of intracellular bacterial burden to more than 15 CFU/100 macrophages. In comparison, cells treated with free vancomycin and vancomycin-loaded control nanogels only showed a moderate increase of bacterial burdens to 6 and 7 CFU/100 macrophages, respectively. Among all the groups, only vancomycin-loaded RBC-nanogels demonstrated an inhibition of intracellular MRSA bacteria (Figure 2.6B).

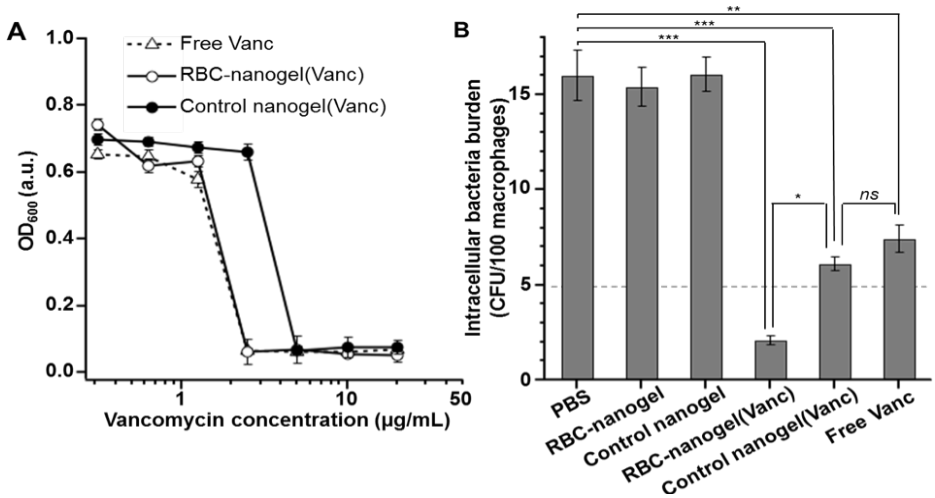

Figure 2.6: Antimicrobial efficacy of vancomycin-loaded RBC-nanogels against intracellular MRSA USA300 bacteria. (A) In vitro antibacterial activity of free vancomycin (Free Vanc), vancomycin-loaded RBC-nanogels (RBC-nanogels(Vanc)), and vancomycin-loaded control nanogels (control nanogel(Vanc)) at different vancomycin concentrations. (B) Quantification of bacterial burden inside macrophages treated with PBS, empty RBC-nanogels, empty control nanogels, RBC-nanogels(Vanc), control nanogel(Vanc) and free Vanc, respectively. For treatment groups, vancomycin concentration was 5 μg/mL. The dash line marks initial intracellular bacterial burden. The viable bacteria of each group were enumerated 6 h after the treatment. The statistical significance was assessed with student *t* test: *ns*, no significant difference, **p* < 0.5, ***p* < 0.01, ****p* < 0.001.

2.1.4. Conclusion

In summary, we synthesized a cell membrane-coated nanogel system consisting of a redox-responsive hydrogel core and an RBC membrane shell. The RBC membrane coating is for spontaneously absorbing and neutralizing virulence factors secreted by MRSA bacteria. The antibiotics-loaded hydrogel core is crosslinked with disulfide bonds responsive to intracellular reducing environment for 'on-demand' drug release specifically targeting intracellular MRSA bacteria. We demonstrated that in extracellular environment the RBC-nanogels effectively neutralized MRSA-associated

toxins, which promoted bacterial uptake by macrophages. Once inside the cells, the RBC-nanogels rapidly released their carried antibiotics and showed remarkable antibacterial activity as compared to free antibiotics and non-responsive control nanogels. It is well documented that bacteria-secreting toxins play a critical role in bacterial pathogenesis [34]. Therefore, antivirulence treatment by the RBC-nanogels can be potentially applied to a variety of different bacteria that are associated with hemolytic toxins. Meanwhile, although we chose vancomycin as a model anti-MRSA antibiotic in the study, cell membrane-templated nanogel synthesis can be applied to load other water-soluble antibiotics; membranes of other cells, especially those that target MRSA bacteria such as platelets, can be also used to template nanogel synthesis [35, 36]. Moreover, with the advancement of hydrogel technology, other responsive mechanisms, especially those responsive to bacterium-specific enzymes, can be incorporated into the hydrogel cores to further improve the controlled release and tempospatial resolution during the treatment [37]. These features together make the RBC-nanogels a promising system for the treatment of various types of bacteria.

2.1.5. Reference

[1] T.J. Foster, J.A. Geoghegan, V.K. Ganesh, M. Hook, Adhesion, invasion and evasion: The many functions of the surface proteins of *Staphylococcus aureus*, *Nat. Rev. Microbiol*. 12: 49-62, 2014.

[2] A. Pantosti, Methicillin-resistant *Staphylococcus aureus* associated with animals and its relevance to human health, *Front. Microbiol*. 3: 127, 2012.

[3] H.F. Chambers, F.R. Deleo, Waves of resistance: *Staphylococcus aureus* in the antibiotic era, *Nat. Rev. Microbiol*. 7: 629-641, 2009.

[4] P. Yoong, G.B. Pier, Antibody-mediated enhancement of community-acquired methicillin-resistant *Staphylococcus aureus* infection, *Proc. Natl. Acad. Sci. U. S. A*. 107: 2241-2246, 2010.

[5] B. Edwards, R. Andini, S. Esposito, P. Grossi, D. Lew, T. Mazzei, A. Novelli, A. Soriano, I.M. Gould, Treatment options for methicillin-resistant *Staphylococcus aureus* (MRSA) infection: Where are we now? *J. Glob. Antimicrob. Resist*. 2: 133-140,2014.

[6] C. Vuong, A.J. Yeh, G.Y.C. Cheung, M. Otto, Investigational drugs to treat methicillin-resistant *Staphylococcus aureus*, *Expert Opin. Investig. Drugs*. 25, 73-93, 2016.

[7] T. Tirilomis, Daptomycin and its immunomodulatory effect consequences for antibiotic treatment of methicillin-resistant *Staphylococcus aureus* wound infections after heart surgery, *Front. Immunol*. 5: 97, 2014.

[8] S.L. Burke, W.E. Rose, New pharmacological treatments for methicillin-resistant *Staphylococcus aureus* infections, *Expert Opin. Pharmacother*. 15: 483-491, 2014.

[9] K. Kumar, S. Chopra, New drugs for methicillin-resistant *Staphylococcus aureus*: An update, *J. Antimicrob. Chemother*. 68, 1465-1470, 2013.

[10] S. Gardete, A. Tomasz, Mechanisms of vancomycin resistance in *Staphylococcus aureus*, *J. Clin. Invest*. 124: 2836-2840, 2014.

[11] S.J. Peacock, G.K. Paterson, Mechanisms of methicillin resistance in *Staphylococcus aureus*, Annu. Rev. Biochem. 84: 577-601, 2015.

[12] A.J. Singer, D.A. Talan, Management of skin abscesses in the era of methicillin-resistant *Staphylococcus aureus*, *New Engl. J. Med*. 370: 1039-1047, 2014.

[13] A. Brauner, O. Fridman, O. Gefen, N.Q. Balaban, Distinguishing between resistance, tolerance and persistence to antibiotic treatment, *Nat. Rev. Microbiol*. 14: 320-330, 2016.

[14] C.M.J. Hu, L.F. Zhang, Nanotoxoid vaccines, *Nano Today* 9: 401-404, 2014.

[15] M. Greenlee-Wacker, F.R. DeLeo, W.M. Nauseef, How methicillin-resistant *Staphylococcus aureus* evade neutrophil killing, *Curr. Opin. Hematol*. 22: 30-35, 2015.

[16] C.M.J. Hu, R.H. Fang, J. Copp, B.T. Luk, L.F. Zhang, A biomimetic nanosponge that absorbs pore-forming toxins, *Nat. Nanotechnol*. 8: 336-340, 2013.

[17] C.M.J. Hu, R.H. Fang, B.T. Luk, L.F. Zhang, Nanoparticle-detained toxins for safe and effective vaccination, *Nat. Nanotechnol*. 8: 933-938, 2013.

[18] F. Wang, W. Gao, S. Thamphiwatana, B.T. Luk, P. Angsantikul, Q.Z. Zhang, C.M.J. Hu, R.H. Fang, J.A. Copp, D. Pornpattananangkul, W.Y. Lu, L.F. Zhang, Hydrogel retaining toxin-absorbing nanosponges for local treatment of methicillin-resistant *Staphylococcus aureus* infection, *Adv. Mater*. 27: 3437-3443, 2015.

[19] T.J. Foster, Immune evasion by staphylococci, *Nat. Rev. Microbiol*. 3: 948-958, 2015.

[20] S.M. Lehar, T. Pillow, M. Xu, L. Staben, K.K. Kajihara, R.V. Andlen, L. DePalatis, H. Raab, W.L. Hazenbos, J.H. Morisaki, J. Kim, S. Park, M. Darwish, B.C. Lee, H. Hernandez, K.M. Loyet, P. Lupardus, R.N. Fong, D.H. Yan, C.C. Halouni, E. Luis, Y. Khalfin, E. Plise, J.C. Heong, J.P. Lyssikatos, M. Strandh, K. Koefoed, P.S. Andersen, J.A. Flygare, M.W. Tan, E.J. Brown, S.M. Ariathasan, Novel antibody-antibiotic conjugate eliminates intracellular *S. Aureus*, *Nature* 527: 323-328, 2015.

[21] M. Kubica, K. Guzik, J. Koziel, M. Zarebski, W. Richter, B. Gajkowska, A. Golda, A. Maciag-Gudowska, K. Brix, L. Shaw, T. Foster, J. Potempa, A potential new pathway for staphylococcus aureus dissemination: The silent

survival of s. Aureus phagocytosed by human monocyte-derived macrophages, *PLoS One* 3: e1409, 2018.

[22] H.K. Kim, V. Thammavongsa, O. Schneewind, D. Missiakas, Recurrent infections and immune evasion strategies of staphylococcus aureus, *Curr. Opin. Microbiol*. 15: 92-99, 2012.

[23] S. Maya, S. Indulekha, V. Sukhithasri, K.T. Smitha, S.V. Nair, R. Jayakumar, R. Biswas, Efficacy of tetracycline encapsulated o-carboxymethyl chitosan nanoparticles against intracellular infections of staphylococcus aureus, *Int. J. Biol. Macromol*. 51: 392-399, 2012.

[24] N.F. Kamaruzzaman, R. Firdessa, L. Good, Bactericidal effects of polyhexamethylene biguanide against intracellular *staphylococcus aureus* EMRSA-15 and USA 300, *J. Antimicrob. Chemother*. 71: 1252-1259, 2012.

[25] M.H. Xiong, Y.J. Li, Y. Bao, X.Z. Yang, B. Hu, J. Wang, Bacteria-responsive multifunctional nanogel for targeted antibiotic delivery, *Adv. Mater*. 24: 6175-6180, 2012.

[26] Y.S. Meng, X.C. Hou, J.X. Lei, M.M. Chen, S.C. Cong, Y.Y. Zhang, W.M. Ding, G.L. Li, X.R. Li, Multi-functional liposomes enhancing target and antibacterial immunity for antimicrobial and anti-biofilm against methicillin-resistant *Staphylococcus aureus*, *Pharm. Res*. 33: 763-775, 2016.

[27] J.H. Zhang, W.W. Gao, R.H. Fang, A.J. Dong, L.F. Zhang, Synthesis of nanogels via cell membrane-templated polymerization, *Small* 11; 4309-4313, 2015.

[28] W. Gao, R. Langer, O.C. Farokhzad, Poly(ethylene glycol) with observable shedding, *Angew. Chem. Int. Ed*. 49: 6567-6571, 2010.

[29] B.D. Fairbanks, M.P. Schwartz, C.N. Bowman, K.S. Anseth, Photoinitiated polymerization of PEG-diacrylate with lithium phenyl-2,4,6-trimethylbenzoylphosphinate: Polymerization rate and cytocompatibility, *Biomaterials* 30: 6702-6707, 2009.

[30] Y.J. Ma, J. Thiele, L. Abdelmohsen, J.G. Xu, W.T.S. Huck, Biocompatible macro-initiators controlling radical retention in microfluidic on-chip photopolymerization of water-in-oil emulsions, *Chem. Commun*. 50: 112-114, 2014.

[31] C.M.J. Hu, L. Zhang, S. Aryal, C. Cheung, R.H. Fang, L.F. Zhang, Erythrocyte membrane-camouflaged polymeric nanoparticles as a biomimetic delivery platform, *Proc. Natl. Acad. Sci. U. S. A*. 108: 10980-10985, 2011.

[32] M.P. McGee, A. Kreger, E.S. Leake, S. Harshman, Toxicity of staphylococcal alpha-toxin for rabbit alveolar macrophages, *Infect. Immun*. 39: 439-444, 1983.

[33] B.J. Berube, J.B. Wardenburg, *Staphylococcus aureus* alpha-toxin: Nearly a century of intrigue, *Toxins (Basel)* 5: 1140-1166, 2013.

[34] K. Ray, B. Marteyn, P.J. Sansonetti, C.M. Tang, Life on the inside: The intracellular lifestyle of cytosolic bacteria, *Nat. Rev. Microbiol*. 7: 333-340, 2009.

[35] C.M.J. Hu, R.H. Fang, K.C. Wang, B.T. Luk, S. Thamphiwatana, D. Dehaini, P. Nguyen, P. Angsantikul, C.H. Wen, A.V. Kroll, C. Carpenter, M. Ramesh, V. Qu, S.H. Patel, J. Zhu, W. Shi, F.M. Hofman, T.C. Chen, W.W. Gao, K. Zhang, S. Chien, L.F. Zhang, Nanoparticle biointerfacing by platelet membrane cloaking, *Nature* 526: 118-121, 2015.

[36] Q.Y. Hu, W.J. Sun, C.G. Qian, C. Wang, H.N. Bomba, Z. Gu, Anticancer platelet-mimicking nanovehicles, *Adv. Mater*. 27: 7043-7050, 2015.

[37] Y.M. Li, G.H. Liu, X.R. Wang, J.M. Hu, S.Y. Liu, Enzyme-responsive polymeric vesicles for bacterial-strain-selective delivery of antimicrobial agents, *Angew. Chem. Int. Ed*. 55: 1760-1764, 2016.

2.2. Inhibition of bacterial adhesion by bacterial outer membrane-coated nanoparticles

2.2.1. Introduction

Most infectious diseases are initiated by adhesion of pathogenic bacteria to the host cells and tissues.[1, 2] As a result, therapies aimed at disrupting the ability of the bacteria to adhere have become attractive against infections.[3, 4] These anti-adhesion therapies are considered less likely to propagate resistance when compared with conventional antibiotics, as they do not directly interfere with bacterial cycles for killing.[5] In addition, weakening bacterial adhesion also facilitates the host immune system to eliminate the pathogen.[6] Furthermore, anti-adhesion therapies combined with additional antibiotics have shown to generate synergistic antimicrobial activities, resulting in more efficacious bacterial inhibition.[7] These advantages together have led to the development of various anti-adhesion compounds. Some target specific adhesins on the pathogen for anti-adhesion activity.[7, 8] Alternatively, some act as analogs of bacterial adhesins, competing with the bacteria to reduce their binding to the host.[9] To improve the potency, conjugating many copies of anti-adhesion molecules onto nanoparticles has become a popular approach to develop multivalent adhesion inhibitors.[10]

Toward effective anti-microbial treatments, recently, cell membrane-coated nanoparticles have emerged as a unique anti-virulence approach against infectious

diseases.[11] These nanoparticles are generally made by wrapping the plasma membrane of natural cells onto synthetic cores.[12] Such biomimicry allows them to act as decoys of the source cells and intercept virulence factors for neutralization. The use of natural cell membrane bypasses the need to identify, synthesize, and conjugate anti-adhesion molecules in conventional development. In addition, cell membrane-coated nanoparticles harness the function of the host cells rather than the structural or molecular characteristics of the toxins for neutralization, making them a broad-spectrum anti-virulence platform.[13] For example, nanoparticles coated with red blood cell (RBC) membranes have demonstrated robust capability of neutralizing bacterial pore-forming toxins and therefore inhibiting infections caused by bacteria such as methicillin-resistant *Staphylococcus aureus* (MRSA) and Group A Streptococcus.[13, 14] Nanoparticles coated with the membrane of macrophages were able to neutralize endotoxins and proinflammatory cytokines, which together reduced lethality of sepsis in mice.[15] Recently, nanoparticles coated with membranes from T cells inherited T cell surface antigens critical for human immunodeficiency virus (HIV) binding.[16] They acted as decoys of the host T cells for viral attack and reduced overall infectivity of HIV.

Inspired by the unique anti-virulence ability of cell membrane-coated nanoparticles, in current study, we coated bacterial outer membrane onto synthetic polymeric cores and made nanoparticle decoys of the pathogenic bacteria (denoted 'OM-NP'). We hypothesize that by inheriting natural adhesins, OM-NP compete with the source bacteria for binding and therefore reduce natural bacterial adherence to the

host. In the study, we chose *Helicobacter pylori* (*H. pylori*) as a model pathogen to study the anti-adhesion effect of OM-NP (Figure 2.7A). *H. pylori* are considered an etiologic agent in the development of gastritis ulcers and gastric cancer.[17] They infect more than half of the world population and the treatment has been increasingly challenged by the rapid development of antibiotic resistance.[18, 19] The adherence of *H. pylori* shows a high degree of species-specific tissue tropism, suggesting the potential of anti-adhesion therapy against their colonization.[20, 21] Although a plethora of adhesins on *H. pylori* have been identified, their highly dynamic and complex biofunctions have made effective anti-adhesion strategy elusive.[22, 23] Herein, we show that OM-NP inherit the surface antigens from the source *H. pylori* and therefore are capable of binding with AGS cells, a human gastric epithelial cancer cell line. Treatment of AGS with OM-NP reduces subsequent *H. pylori* adhesion. The presence of OM-NP also promotes the detachment of *H. pylori* pre-bound to epithelial monolayers. In addition, on mouse stomach, OM-NP significantly reduced *H. pylori* adherence. Overall, the results demonstrate that OM-NP confer an anti-adhesion property and show promise as an effective anti-adhesion approach against bacterial infections.

2.2.2. Experimental Methods

Bacteria culture

H. pylori Sydney strain 1 (SS1) from frozen stock was inoculated and maintained on Columbia agar supplemented with 5 v/v % horse blood (Hardy

Diagnostic) and 1 v/v % 250 μg/mL Amphotericin B (Gibco) at 37°C under microaerobic condition (10% CO2, 85% N2 and 5% O2). A single colony was inoculated to Brain Hear Infusion (BHI) broth containing 10 v/v % heat-inactivated fetal bovine serum (FBS, Hyclone) and cultured overnight under microaerobic conditions with moderate reciprocal shaking. Following the culture, bacteria were then harvested by centrifugation at 5000 ×g for 20 min, washed with sterile 1× PBS twice, and suspended to a concentration of 1×10^8 CFU/mL (optical density or OD600 = 1.0) in PBS.

Derivation of *H. pylori* outer membrane vesicles (OMVs)

To collect OMVs, *H. pylori*, culture was centrifuged at 5000 ×g for 20 mins to remove the bacteria. Then the supernatant was filtered with a 0.45 μm filter unit (Millipore Stericup, Millipore) before concentrated 10 times with a tangential flow filtration system (TFF, Spectrum) equipped with a column of 30 kDa molecular weight cutoff. Finally, OMVs in the concentrated supernatant was collected by ultracentrifugation (Beckmann, Optima XPN-80 ultracentrifuge, SW32 Ti) at 150,000 ×g and 4°C for 2 h. OMVs were collected as an off-white pellet and resuspended in DI water. OMV suspensions were aliquoted and stored at -80 °C for subsequent experiments.

Preparation of OM-NP

First, PLGA cores were prepared with a nanoprecipitation method. Briefly, 1

mL PLGA in acetone (5 mg/mL) was quickly added to 2 mL DI water. The solution was stirred under vacuum for 2 h to evaporate acetone. Then OMV collected above were mixed with PLGA cores at a protein-to-polymer ratio of 3:1. The mixture was sonicated (FS60, 100W, and Fisher Scientific) for 2 min. Following the sonication, the mixture was centrifuged at 16100 ×g and 4°C for 15 min to precipitate the nanoparticles. The supernatant was removed, and the nanoparticles were suspended in DI water at desired concentrations for subsequent use. To prepare fluorescently labeled OM-NP, PLGA was mixed with DiD dye in acetone (polymer-to-dye weight ratio=10000:1) before the nanoprecipitation.

Characterization of OM-NP

The hydrodynamic size and zeta-potential of PLGA core, OMV, and OM-NP were measured with dynamic light scattering (ZEN 3600 Zetasizer, Malvern). All measurements were carried out in triplicate at room temperature. To examine the nanoparticle microscopic morphology, OM-NP were visualized with transmission electron microscopy (TEM, Tecnai G2 Sphera FEI 200 kV). Briefly, OM-NP samples (1 mg/mL, protein concentration) were dropped onto carbon-coated copper grid and left for 1 min, and then washed off with DI water. The sample was then stained with 1 wt% uranyl acetate (Sigma-Aldrich) before imaging. The total protein content on the OM-NP was quantified with a BCA assay (Thermo Scientific). For dot blot analysis, the proteins on PLGA, OMV and OM-NP were denatured with 4× detergent solution made with 37% glycerol (Fisher Chemical), 55% 1 M Tris-HCl pH 8 (Mediatech), and

8% Triton X-100 (EMD Millipore) at 70°C for 30 mins. Then 5 μL of denatured PLGA, OMV, and OM-NP (2 mg/mL) were blotted onto nitrocellulose membrane (Pierce). The membrane was left under vacuum to dry. Afterward, bovine serum albumins (BSA, 5 wt% in PBST) was used to block the membrane for 1 h. Blots were then probed with anti-*H. pylori* antibody (Biolegend) followed by donkey anti-rabbit IgG-horseradish peroxidase (HRP)-conjugates (Biolegend). The membrane was then incubated with enhanced chemiluminescence western blotting substrate (Pierce). The color was developed with Mini-Medical/90 Developer (ImageWorks). The image was analyzed with Image J.

AGS cell culture

AGS cell line (human gastric adenocarcinoma, ATCC CRL-1739) was purchased from the American Type Culture Collection (ATCC) and maintained in Ham F-12K Medium (Invitrogen) supplemented with 10% fetal bovine serum (FBS, Hyclone) and 1% penicillin-streptomycin (100 U/mL penicillium and 100 μg/mL streptomycin, Invitrogen) at 37°C in a humidified atmosphere containing 5% CO2. To prepare the cell monolayer, 2×10^4 AGS cells were seeded into per well on a 96-well plate and cultured overnight until the cell density reached 80% confluency. The cells were fixed with 4% paraformaldehyde (affymetrix) and kept at 4°C for subsequent studies. The nuclei were stained with 50 μL 0.001 v/v% Hoechst 33342 (Invitrogen) before the experiments.

OM-NP binding study

To study the binding of OM-NP to AGS cells, DiD-labeled OM-NP (2 mL, 0.5 mg/mL to each well) were incubated with AGS monolayers at 37°C for 1.5 h. After removing the nanoparticle suspension, 2 mL PBS was refilled to wash off any unbound OM-NP. This step was repeated three times. AGS cell monolayer was imaged with a confocal fluorescence microscope (Olympus FV1000). The fluorescence intensity from cell-bound nanoparticles was measured with a microplate reader (BioTek Synergy Mx) and the values were normalized to the maximum intensity. To study binding specificity, OM-NP were first blocked with anti-*H. pylori* antibody (Biolegend) at 37°C for 1 h and then added to AGS.

H. pylori adhesion to AGS cell monolayer:

H. pylori were first labeled with fluorescein isothiocyanate (FITC, Thermo Fisher) followed a published protocol. Briefly, 1 μL 10 μg/ μL FITC in anhydrous DMSO was incubated with 1mL 1× 108 CFU/mL *H. pylori* at 37°C for 2 h. Unbound FITC was removed from FITC-*H. pylori* with centrifugation (5000 ×g for 5 min). This step was repeated 8 times until no FITC signal was detected in the supernatant ((BioTek Synergy Mx microplate reader). To study how pre-treating AGS with OM-NP would affect *H. pylori* adhesion (pre-incubation regimen), AGS cells were added with 50 μL PBS or DiD-labeled OM-NPs for 1.5 h at 37°C. Then 10 μL of *H. pylori* (4×108 CFU/mL) was added later and incubate for another 1.5 h prior to fluorescence imaging. To study the effect of mixing OM-NP and *H. pylori* on bacterial binding (co-

incubation regimen), 50 μL DiD-labelled OM-NPs and 10 μL *H. pylori* were pre-mixed and then added to AGS cells. The 100% control was the AGS cells incubated with *H. pylori* only. To study the effect of OM-NP on *H. pylori* dissociation, AGS cells were incubated with 50 μL FITC-labeled H. pylori (5×107 CFU/mL) at 37°C for 1.5 h. After the unbound bacteria were removed, OM-NP were added at various concentrations (0, 10, 20, 30, and 40 mg/mL) and incubated with the cells for 1, 3, 6, and 22 h. Following the incubation, samples were washed with 1× PBS. The fluorescence images were captured with EVOS inverted fluorescence microscope. The remaining *H. pylori* on AGS cells was quantified by measuring FITC intensity (BioTek Synergy Mx microplate reader) and the values were normalized to the maximum intensity (e.g. the saturation coverage of *H. pylori* on AGS cells). The group without adding OM-NP was used as the control.

H. pylori adhesion to mouse stomach:

Male C57BL/6 mice of 6~10-week old were purchased from Envigo Harlan. Mice were housed in the Animal Facility at the University of California San Diego under federal, state, local, and National Institutes of Health guidelines for animal care. To collect the stomach, mouse was sacrificed, and the stomach was removed from the abdominal cavity. The stomach was cut open along the greater curvature and rinsed with clean PBS to gently remove the content. The stomach was then kept in 1× PBS at 4°C for the subsequent experiments. The freshly dissected stomach tissue was submerged in 500 μL 1× PBS or 500 μL 1× PBS containing 40 mg/mL OM-NP.

Samples were incubated at 37°C for 1.5 h. Then the stomach was transferred to 500 μL *H. pylori* suspensions (5×107 CFU/mL). The mixture was incubated at 37°C for an additional 1.5 h. After the incubation, the stomach was rinsed with 5 mL PBS for three times and then placed on a glass slide for imaging (Olympus MVX10). The fluorescence intensity of *H. pylori* was quantified in Image J. To normalize the fluorescence intensity, PBS group was used as 100%.

2.2.3. Results and discussion

To synthesize OM-NP, we chose outer membrane vesicles (OMV) of *H. pylori* as the membrane source. These vesicles are known to contain virulence factors similar to those of the intact bacteria, including adhesins critical for attachment and pathogenesis.[24] In the study, OMV were collected from the bacterial culture based on a published protocol.[25] Meanwhile, polymeric cores were made from poly(lactic-co-glycolic acid) (PLGA) with a nanoprecipitation method.[12] Lastly, OMV were allowed to fuse onto the PLGA core through sonication.[26] To remove the excess vesicles and soluble proteins, samples were washed through repeated centrifugation. Following the synthesis, the measurement of OM-NP with dynamic light scattering showed a hydrodynamic diameter of 105.7 ± 3.1 nm (Figure 2.7B). The diameter increased approximately 16 nm compared to that of the bare PLGA cores, consistent with the addition of a thin lipid bilayer on the nanoparticle surface. Meanwhile, zeta potential of the nanoparticles changed from -40.6 ± 5.3 mV of PLGA cores to -28.8 ± 1.9 mV of OM-NP, indicating the charge screening effect conferred by the coated

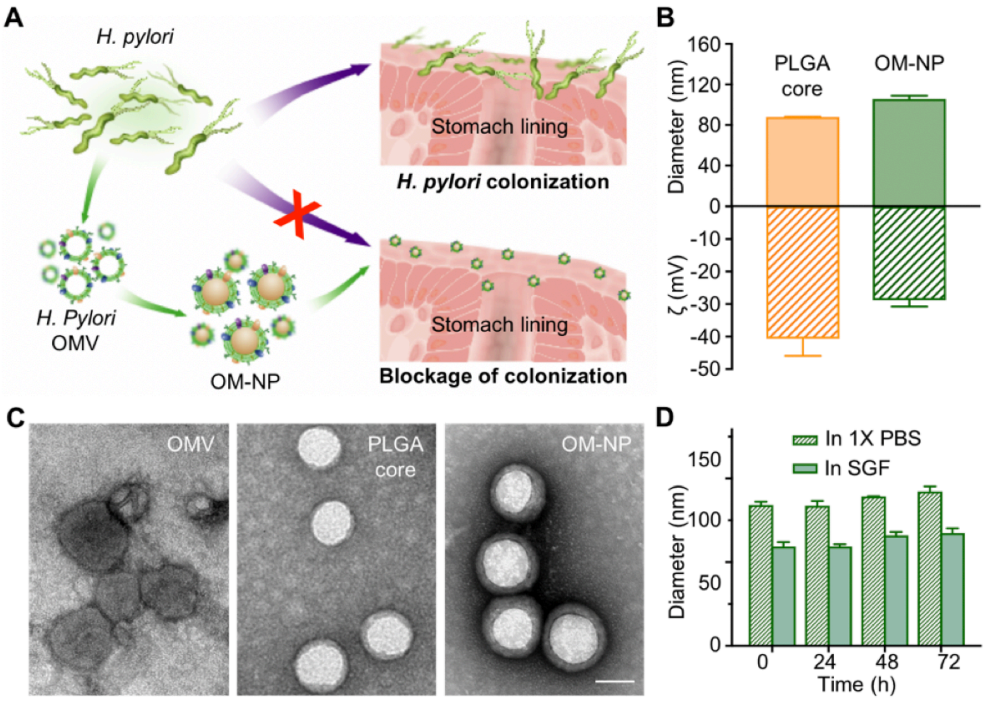

Figure 2.7. Preparation and characterization of *Helicobacter pylori* (*H. pylori*) outer membrane-coated nanoparticles (OM-NP). (A) Schematic representation of using OM-NP to inhibit *H. pylori* adhesion on stomach lining. OM-NP were prepared by coating polymeric cores made from poly(lactic-*co*-glycolic acid) (PLGA) with *H. pylori* outer membranes containing adhesins critical for bacterial colonization. By mimicking the adhesion of *H. pylori* onto gastric epithelium, OM-NP occupy the binding sites and hence inhibit the colonization of the bacteria. (B) Measurements of hydrodynamic size (diameter, nm) and zeta-potential (ζ, mV) of PLGA cores and OM-NPs, respectively. Error bars represent standard deviations (n = 3) (C) Transmission electron microscopy images of OMV (left), PLGA core (middle), and OM-NP (right). Samples were negatively stained with uranyl acetate before imaging. Scale bar = 50 nm. (D) Stability of OM-NP in 1×PBS or simulated gastric fluid (SGF), determined by monitoring nanoparticle size (diameter, nm) over 72 h. Error bars represent standard deviations (n = 3).

membrane. To verify the membrane coating, OM-NP were examined with transmission electron microscopy (TEM) for morphology (Figure 2.7C). Under the microscope, OM-NP maintained the spherical shape of the polymeric cores with a thin shell on the outer surface, consistent with previously reported core-shell structure of the unilamellar membrane coating on PLGA cores.[12, 27] When OM-NP samples

were suspended in 1× PBS or simulated gastric fluid (SGF), their size remained stable for at least 72 h, demonstrating a high colloidal stability conferred by membrane coating (Figure 2.7D).[28] Overall, these results demonstrate successful coating of *H. pylori* outer membrane onto PLGA cores.

Following the nanoparticle formulation, we next characterized the protein and binding properties of OM-NP. First, the membrane protein content on OM-NP was quantified with a protein bicinchoninic acid (BCA) assay. While no protein content was detected from bare PLGA cores, measurements of OM-NP showed a clear presence of protein indicated by an absorption at 562 nm. Further quantification indicated a protein loading yield, defined as the weight ratio between the immobilized proteins and PLGA cores, of approximately 24.3 ± 3.3 wt % (Figure 2.8A). In a dot blot assay, where polyclonal anti-*H. pylori* antibody was used as the primary immunostain, PLGA core did not react with the antibody (Figure 2.8B). In contrast, OM-NP showed significant binding with the antibody and the intensity of staining was comparable to that of the OMV, suggesting that the proteins on OM-NP were *H. pylori*-specific. We hypothesize that the inheritance of *H. pylori*-specific antigens would confer OM-NP the adhesion to AGS cells. To test this hypothesis, we labeled OM-NP with fluorescence dye and added them onto AGS cell monolayer. Following the incubation and washing, fluorescence microscopy showed retention of nanoparticles by the cell monolayer, indicating nanoparticle-cell adhesion (Figure 2.8C). In the control group, where OM-NP were incubated with anti-*H. pylori*

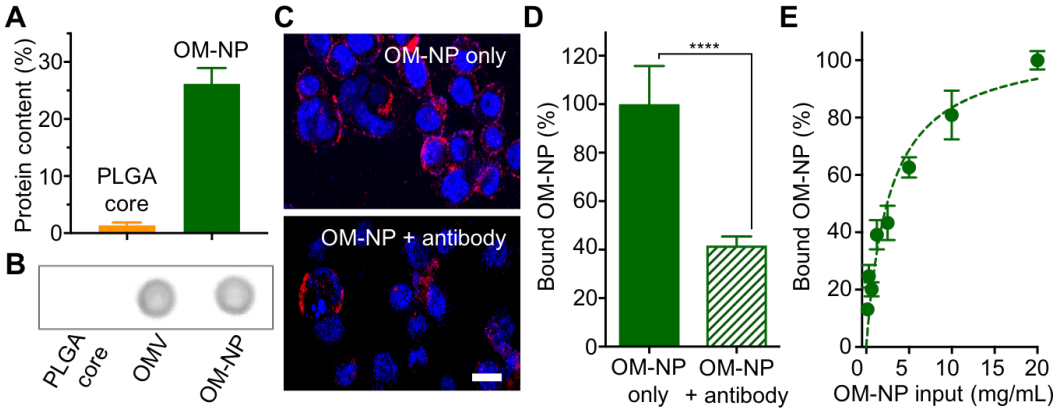

Figure 2.8. Characterization of OM-NP adhesion to gastric epithelial cells (AGS). (A) Quantification of protein content on OM-NP. Error bars represent standard deviations (n = 3). (B) Dot blot analysis of PLGA core, OMV, and OM-NP using polyclonal anti-*H.pylori* antibodies as the primary immunostain. (C) Fluorescence images of AGS after incubation with OM-NP (top) and OM-NP blocked with anti-*H. pylori* antibodies (bottom). OM-NP were labeled with DiD dye (red) and nuclei of AGS with DAPI (blue). Scale bar = 25 µm. (D) Quantification of the nanoparticle fluorescence intensity in (C). Error bars represent standard deviations (n=6). Statistical analysis was performed using unpaired two-tailed *t*-test (****$P \leq 0.0001$). (E) Quantification of OM-NP bound to AGS cells at different input concentrations. Error bars represent standard deviations (n=3). Data were fitted with a non-linear binding model in GraphPad Prism.

antibody prior to the addition to AGS monolayer, the fluorescence intensity from OM-NP was lower. Further quantification of the fluorescence intensity showed a significant decrease of retained OM-NP when treated with the antibody (Figure 2D). The decrease of OM-NP binding with AGS cells following the treatment of antibody indicates that the binding is indeed medicated by *H. pylori*-specific antigens. We further examined the correlation between OM-NP concentration and binding with AGS cells. It was observed that the fluorescence intensity measured from the captured OM-NP increased gradually as OM-NP input concentration increased till it reached a plateau at an OM-NP concentration of 20 mg/mL or higher (Figure 2.8E). Such two-stage concentration dependence is consistent with previous studies of binding affinity

and kinetics of targeted-nanoparticles to ligand-modified 2D surfaces.[29] A Langmuir binary interaction model was used to fit the data curves, leading to an equilibrium binding constant of 2.7 ± 0.5 mg/mL.

After having characterized the binding of OM-NP with AGS cells, we next studied the inhibition of *H. pylori* adhesion with OM-NP. First, we labeled *H. pylori* with green dye and added them to AGS monolayer. After removing the unbound bacteria in the solution, samples were examined with fluorescence microscopy. As shown in Figure 2.9A, *H. pylori* bound to the cell monolayer following the incubation and the number increased when the input of *H. pylori* was increased. In parallel, we added OM-NP to AGS monolayer and then *H. pylori*. Samples at all tested input concentrations emitted much weaker fluorescence, indicating an anti-adhesion effect from OM-NP. For a quantitative analysis, we varied *H. pylori* input from 0.03 to 4 × 10^8 CFU/mL and compared fluorescence intensity from AGS with or without OMV-NP treatment (Figure 2.9B). In both groups, the amount of bound *H. pylori* increased initially as the bacterial input was increased and then plateaued. However, on AGS cells treated with OM-NP, less *H. pylori* were detected, confirming the anti-adhesion property of OM-NP. Based on the Hill equation, an *H. pylori* bacterial input of 8.2 × 10^7 CFU/mL resulted in 50% of saturation coverage (EC50). However, with the same bacterial input concentration, only approximately 10% of the saturation coverage was reached. Overall, this study shows that pre-treatment of AGS with OM-NP is effective in reducing *H. pylori* adhesion.

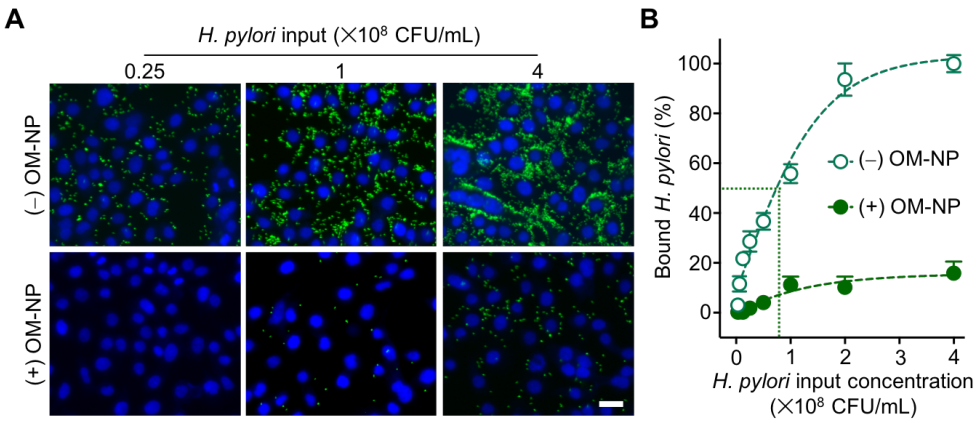

Figure 2.9. Pre-treatment of AGS with OM-NP reduces subsequent *H. pylori* adhesion. (A) Fluorescence images of AGS monolayers without treatment (top row) or treated with OM-NP (bottom row), followed by incubation with *H. pylori* at various concentrations (from left to right: 0.25, 1, and 4 × 10^8 CFU/mL). In the images, green represents FITC-labeled *H. pylori* and blue represents nuclei of AGS. Scale bar = 25 μm. (B) Mean fluorescence intensity (MFI) of *H. pylori* bound with AGS cells pre-treated with OM-NP. The input concentration of *H. pylori* varied from 0 to 4 × 10^8 CFU/mL. Error bars represent standard deviations (n = 3). Data were fitted with a non-linear binding model in GraphPad Prism.

To gain further understandings on the anti-adhesion of OM-NP, we then examined how the dosage of OM-NP and the dosing sequence relative to that of *H. pylori* would affect *H. pylori* adhesion. In a pre-incubation regimen, we added OM-NP of various concentrations to the AGS monolayer first, followed by adding a fixed concentration of *H. pylori* for binding. The amount of *H. pylori* bound onto AGS were measured with fluorescence microscopy. As shown in Figure 2.10A, when OM-NP concentration was increased, *H. pylori* binding decreased accordingly. We also tested the binding in a competitive regimen, where *H. pylori* bacteria were mixed with OM-NP first followed by the addition of their mixture to AGS for binding. In this regimen, *H. pylori* binding also decreased while OM-NP concentration was increased. However, more *H. pylori* were found to bind with AGS monolayers than those in the

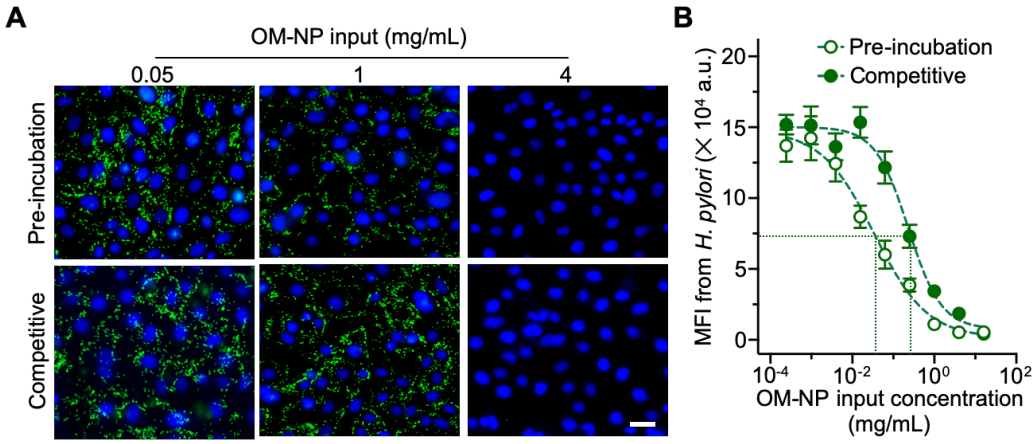

Figure 2.10. Effects of OM-NP dosage and dosing sequence on *H. pylori* adhesion to AGS. (A) Fluorescence images of *H. pylori* bound with AGS after incubating OM-NP with AGS first followed by adding H. pylori (top row, pre-incubation regimen) or adding both concurrently to the AGS (bottom row, competitive regimen). In the study, *H. pylori* concentration was kept at 5×10^7 CFU/mL and OM-NP concentrations of 0.06, 1, and 16 mg/mL were used. In the images, green represents FITC-labeled *H. pylori* and blue represents nuclei of AGS. Scale bar = 25 µm. (B) MFI from *H. pylori* bound with AGS cells with the presence of OM-NP in either pre-incubation or competitive dosing regimens. In the study, *H. pylori* concentration was kept at 5×10^7 CFU/mL and concentrations of OM-NP varied. Error bars represent standard deviations. (n = 3) The data was fitted with a variable slope model in GraphPad Prism.

pre-incubation regimen, suggesting a lower anti-adhesion efficacy in the competitive regimen. To quantitatively analyze the effects of OM-NP dosage and dosing sequence, fluorescence intensity measured from the bound *H. pylori* was plotted against OM-NP concentration (Figure 2.10B). The dose response of both regimens follows a typical sigmoid curve, but at the same input concentration, OM-NP inhibited more *H. pylori* in pre-incubation regimen compared to that in competitive regimen. Under our experimental conditions, the half maximal inhibitory concentration (IC50) of OM-NP in the pre-incubation regimen was found to be 0.034 mg/mL. In the competitive regimen, the IC50 values increased to 0.23 mg/mL.

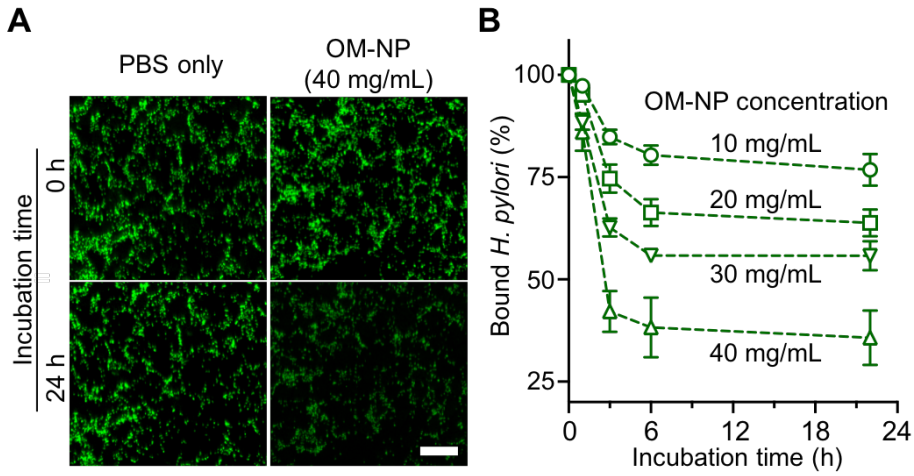

Figure 2.11. OM-NP promote *H. pylori* dissociation from AGS. (A) Fluorescence images of *H. pylori* on AGS before and after 22 h of incubation with PBS only or OM-NP (40 mg/mL). Green represents FITC-labeled *H. pylori*. Scale bar = 25 μm. (B) Remaining *H. pylori* on AGS when incubated with OM-NP (10, 20, 30, and 40 mg/mL) at various time points. At each time point, fluorescence intensity of *H. pylori* measured from samples with PBS only was defined as 100%. Error bars represent standard deviations (n = 3).

It is known that antibodies against *H. pylori* adhesins were able to detach the bacteria pre-bound to gastric cells. [30, 31] Therefore, we hypothesize that OM-NP may also facilitate *H. pylori* dissociation after the bacteria adhere to AGS cells. To test this hypothesis, *H. pylori* were first allowed to bind with AGS monolayer. After removing the unbound bacteria, 40 mg/mL of OM-NP were added to the cells. Control samples were added with PBS only without OM-NP. Samples were incubated for 22 h and then washed prior to fluorescence microscopic study. Under the microscope, samples incubated with PBS only showed little change in overall fluorescence, indicating the retention of *H. pylori* on AGS monolayer (Figure 2.11A). In contrast, images taken from samples added with OMV-NP showed observable decrease of overall fluorescence, implying a higher level of *H. pylori* dissociation. Following this

observation, we further tested the effects of OM-NP concentration and incubation time on bacterial dissociation. As shown in Figure 2.11B, when OM-NP concentration was increased from 10 to 40 mg/mL, the percentage of remaining *H. pylori* on AGS monolayer decreased accordingly. After 22 h of incubation, approximately 76.8, 63.8, 55.8, and 35.7% of H. pylori remained with the presence of 10, 20, 30, and 40 mg/mL of OM-NP, respectively. When the dissociation curves were fitted with a one-phase exponential decay model, values of the dissociation half-life (t1/2) were estimated to be 2.1, 1.8, 1.4, and 1.3 h with the addition of 10, 20, 30, and 40 mg/mL of OM-NP, respectively.

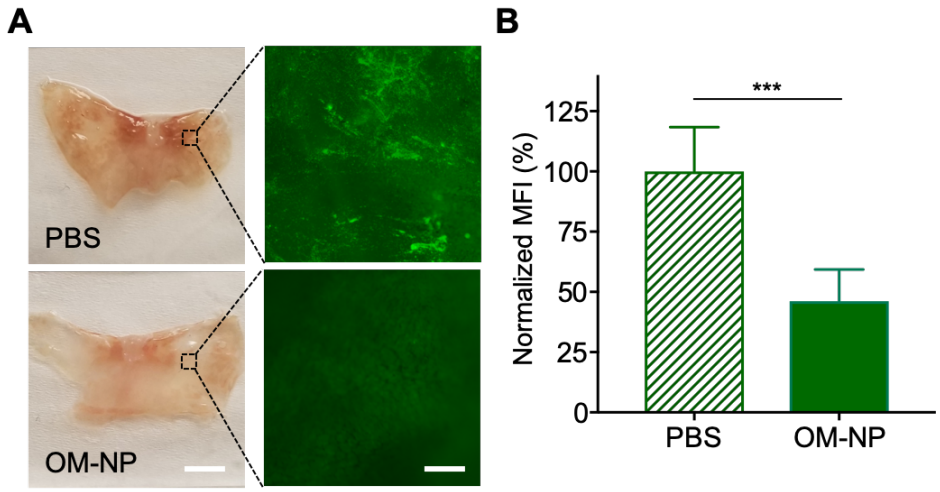

Figure 2.12. OM-NP reduce *H. pylori* colonization on the mouse stomach. (A) Freshly dissected mouse stomach tissues were incubated with 1× PBS or OM-NP (40 mg/mL) for 1.5 hours before *H. pylori* (5×10^7 CFU/mL) were added. Scale bar = 5 mm. Left: brightfield images of the stomachs. Right: fluorescence images showing the colonization of *H. pylori.* Green represents FITC-labeled *H. pylori*. Scale bar = 1 mm. (B) Quantification of *H. pylori* measured from the stomach tissues incubated with 1× PBS or OM-NP prior to *H. pylori* colonization. Error bars represent standard deviations (n = 6). The statistical analysis was calculated with non-paired *t*-test, ***$P \leq 0.001$.

After demonstrating the anti-adhesion effect of OM-NP, lastly, we examined whether the nanoparticles would inhibit the attachment of H. pylori on stomach tissue. In the study, mouse stomachs were excised, and the luminal lining was cut open. Then the samples of stomach tissue were incubated with suspensions of FITC-labeled H. pylori. Following the incubation, the samples were gently rinsed and examined with fluorescence microscopy. Under the microscope, the stomach tissue showed strong fluorescence, indicating the attachment of *H. pylori* bacteria to the stomach lining (Figure 2.12A). However, when the stomach tissues were first incubated with OM-NP and then with *H. pylori*, the fluorescence intensity clearly decreased, indicating the inhibition of bacterial attachment with OM-NP. Further quantification reveals that the fluorescence intensity from stomach tissues treated with OM-NP before *H. pylori* exposure is only 46.2 ± 13.1% of that measured from stomach tissues treated with PBS only (Figure 2.12B). The significant reduction of *H. pylori* attached on stomach tissues further confirms the anti-adhesion effect of OM-NP.

2.2.4. Conclusion

In conclusion, herein, we report on the development of biomimetic OM-NP by coating polymeric cores with bacterial outer membranes. These nanoparticles carry adhesins similar to the source bacteria and therefore adhere to the epithelial cells of the host. The adherence allows OM-NP to occupy binding sites on the host and in turn reduce the adherence of the bacteria. Such anti-adhesion property is dependent on OM-NP dosage and dosing sequence relative to bacterial binding. It is also

demonstrated that OM-NP facilitate the detachment of *H. pylori* bacteria pre-bound to epithelial monolayers. On mouse stomach, *H. pylori* mixed with OM-NP show significantly reduced adherence when compared to *H. pylori* alone. These results demonstrate a clear anti-adhesion effect from OM-NP. A distinct advantage of using OM-NP is to bypass the identification of key adhesins or host receptors otherwise needed for structure-based design of anti-adhesion agents. Toward future development, the anti-adhesion efficacy of OM-NP can be further optimized. One potential approach is to modulate adhesin expression on the outer membrane through genetic modification.[32] Another approach is to optimize OM-NP sizes by changing the size of the nanoparticle cores. Meanwhile, the anti-adhesion approach with OM-NP is expected to be applicable with nanoparticles coated with membranes of the host cells. In this case, nanoparticles compete with host cells to bind with the bacteria for the anti-adhesion effect. In fact, nanoparticles coated with membranes from AGS cells were able to bind specifically with *H. pylori* for targeted antibiotic delivery.[33] Overall, OM-NP present an attractive nanomedicine design promising for effective anti-adhesion intervention against bacterial infections.

2.2.5. Reference

[1] . J. Pizarro-Cerda, P. Cossart, Bacterial adhesion and entry into host cells. Cell 2006, 124, 715.

[2] . C. Berne, C. K. Ellison, A. Ducret, Y. V. Brun, Bacterial adhesion at the single-cell level. Nat. Rev. Microbiol. 2018, 16, 616.

[3] . D. A. Rasko, V. Sperandio, Anti-virulence strategies to combat bacteria-mediated disease. Nat. Rev. Drug Discov. 2010, 9, 117.

[4] . Asadi, S. Razavi, M. Talebi, M. Gholami, A review on anti-adhesion therapies of bacterial diseases. Infection 2019, 47, 13.

[5] . Ofek, D. L. Hasy, N. Sharon, Anti-adhesion therapy of bacterial diseases: prospects and problems. FEMS Immunol. Med. Microbiol. 2003, 38, 181.

[6] . M. R. Knowles, R. C. Boucher, Mucus clearance as a primary innate defense mechanism for mammalian airways. J. Clin. Invest. 2002, 109, 571.

[7] . C. K. Cusumano, J. S. Pinkner, Z. F. Han, S. E. Greene, B. A. Ford, J. R. Crowley, J. P. Henderson, J. W. Janetka, S. J. Hultgren, Treatment and prevention of urinary tract infection with orally active FimH inhibitors. Sci. Transl. Med. 2011, 3.

[8] . Denis, M. Le Bris, L. Le Guennec, J.-P. Barnier, C. Faure, A. Gouge, H. Bouzinba-Ségard, A. Jamet, D. Euphrasie, B. Durel, N. Barois, P. Pelissier, P. C. Morand, M. Coureuil, F. Lafont, O. Join-Lambert, X. Nassif, S. Bourdoulous, Targeting Type IV pili as an antivirulence strategy against invasive meningococcal disease. Nat. Microbiol. 2019.

[9] . N. Sharon, Carbohydrates as future anti-adhesion drugs for infectious diseases. Biochim. Biophys. Acta 2006, 1760, 527.

[10] . A. Bernardi, J. Jimenez-Barbero, A. Casnati, C. De Castro, T. Darbre, F. Fieschi, J. Finne, H. Funken, K. E. Jaeger, M. Lahmann, T. K. Lindhorst, M. Marradi, P. Messner, A. Molinaro, P. V. Murphy, C. Nativi, S. Oscarson, S. Penades, F. Peri, R. J. Pieters, O. Renaudet, J. L. Reymond, B. Richichi, J. Rojo, F. Sansone, C. Schaffer, W. B. Turnbull, T. Velasco-Torrijos, S. Vidal, S. Vincent, T. Wennekes, H. Zuilhof, A. Imberty, Multivalent glycoconjugates as anti-pathogenic agents. Chem. Soc. Rev. 2013, 42, 4709.

[11] . R. H. Fang, A. V. Kroll, W. Gao, L. Zhang, Cell Membrane Coating Nanotechnology. Adv. Mater. 2018, 30.

[12] . C. M. J. Hu, L. Zhang, S. Aryal, C. Cheung, R. H. Fang, L. Zhang, Erythrocyte membrane-camouflaged polymeric nanoparticles as a biomimetic delivery platform. Proc. Natl. Acad. Sci. U. S. A. 2011, 108, 10980.

[13] . C. M. J. Hu, R. H. Fang, J. Copp, B. T. Luk, L. Zhang, A biomimetic nanosponge that absorbs pore-forming toxins. Nat. Nanotechnol. 2013, 8, 336.

[14] . Y. J. Chen, M. C. Chen, Y. Zhang, J. H. Lee, T. Escajadillo, H. Gong, R. H. Fang, W. Gao, V. Nizet, L. Zhang, Broad-Spectrum Neutralization of Pore-Forming Toxins with Human Erythrocyte Membrane-Coated Nanosponges. Adv. Healthc. Mater. 2018, 7.

[15] . S. Thamphiwatana, P. Angsantikul, T. Escajadillo, Q. Z. Zhang, J. Olson, B. T. Luk, S. Zhang, R. H. Fang, W. Gao, V. Nizet, L. Zhang, Macrophage-like nanoparticles concurrently absorbing endotoxins and proinflammatory cytokines for sepsis management. Proc. Natl. Acad. Sci. U. S. A. 2017, 114, 11488.

[16] . X. L. Wei, G. Zhang, D. N. Ran, N. Krishnan, R. H. Fang, W. Gao, S. A. Spector, L. Zhang, T-Cell-Mimicking Nanoparticles Can Neutralize HIV Infectivity. Adv. Mater. 2018, 30.

[17] . O'Connor, C. A. O'Morain, A. C. Ford, Population screening and treatment of Helicobacter pylori infection. Nat. Rev. Gastroenterol. Hepatol. 2017, 14, 230.

[18] . Thung, H. Aramin, V. Vavinskaya, S. Gupta, J. Y. Park, S. E. Crowe, M. A. Valasek, Aliment. Review article: the global emergence of Helicobacter pylori antibiotic resistance. Pharmacol. Ther. 2016, 43, 514.

[19] . Y. Hu, M. Zhang, B. Lu, J. Dai, Helicobacter pylori and Antibiotic Resistance, A Continuing and Intractable Problem. Helicobacter 2016, 21, 349.

[20] . N. R. Salama, M. L. Hartung, A. Muller, Life in the human stomach: persistence strategies of the bacterial pathogen Helicobacter pylori. Nat. Rev. Microbiol. 2013, 11, 385.

[21] . Y. Yamaoka, Mechanisms of disease: Helicobacter pylori virulence factors. Nat. Rev. Gastroenterol. Hepatol. 2010, 7, 629.

[22] . G. Ayala, W. I. Escobedo-Hinojosa, C. F. de la Cruz-Herrera, I. Romero, Exploring alternative treatments for Helicobacter pylori infection. World J. Gastroenterol. 2014, 20, 1450.

[23] . C. Y. Kao, B. S. Sheu, J. J. Wu, Helicobacter pylori infection: An overview of bacterial virulence factors and pathogenesis. Biomedical Journal 2016, 39, 14.

[24] . E. Mullaney, P. A. Brown, S. M. Smith, C. H. Botting, Y. Y. Yamaoka, A. M. Terres, D. P. Kelleher, H. J. Windle, Proteomic and functional characterization of the outer membrane vesicles from the gastric pathogen Helicobacter pylori. Proteomics Clin. Appl. 2009, 3, 785.

[25] . H. Parker, K. Chitcholtan, M. B. Hampton, J. I. Keenan, Uptake of Helicobacter pylori outer membrane vesicles by gastric epithelial cells. Infect. Immun. 2010, 78, 5054.

[26] . W. Gao, R. H. Fang, S. Thamphiwatana, B. T. Luk, J. M. Li, P. Angsantikul, Q. Z. Zhang, C. M. J. Hu, L. Zhang, Modulating antibacterial immunity via bacterial membrane-coated nanoparticles. Nano Lett. 2015, 15, 1403.

[27] . W. Gao, C. M. J. Hu, R. H. Fang, B. T. Luk, J. Su, L. Zhang, Surface functionalization of gold nanoparticles with red blood cell membranes. Adv. Mater. 2013, 25, 3549.

[28] . B. T. Luk, C. M. J. Hu, R. N. H. Fang, D. Dehaini, C. Carpenter, W. Gao, L. Zhang, Interfacial interactions between natural RBC membranes and synthetic polymeric nanoparticles. Nanoscale 2014, 6, 2730.

[29] . C. Tassa, J. L. Duffner, T. A. Lewis, R. Weissleder, S. L. Schreiber, A. N. Koehler, S. Y. Shaw, Binding affinity and kinetic analysis of targeted small molecule-modified nanoparticles. Bioconj. Chem. 2010, 21, 14.

[30] . M. A. Guzman-Murillo, E. Ruiz-Bustos, B. Ho, F. Ascencio, Involvement of the heparan sulphate-binding proteins of Helicobacter pylori in its adherence to HeLa S3 and Kato III cell lines. J. Med. Microbiol. 2001, 50, 320.

[31] . Younson, R. O'Mahony, H. Liu, S. Grant, C. Campion, L. Jennings, D. Vaira, C. G. Kelly, I. M. Roitt, J. Holton, A human domain antibody and Lewis b glycoconjugate that inhibit binding of Helicobacter pylori to Lewis b receptor and adhesion to human gastric epithelium. J. Infect. Dis. 2009, 200, 1574.

[32] . Turner, J. Praszkier, M. L. Hutton, D. Steer, G. Ramm, M. Kaparakis-Liaskos, R. L. Ferrero, Increased Outer Membrane Vesicle Formation in a Helicobacter pylori tolB Mutant. Helicobacter 2015, 20, 269.

[33] . P. Angsantikul, S. Thamphiwatana, Q. Zhang, K. Spiekermann, J. Zhuang, R. H. Fang, W. Gao, M. Obonyo, L. Zhang, Coating nanoparticles with gastric epithelial cell membrane for targeted antibiotic delivery against Helicobacter pylori infection. Adv. Ther. 2018, 1, article number 1800016.

The first portion of chapter 2 contains the material as it appears in Journal of Controlled Release. Yue Zhang, Jihua Zhang, Wansong Chen, Pavimol Angsantikul, Kevin, Spiekermann, Ronnie, Fang, Weiwei Gao and Liangfang Zhang. The dissertation author was the primary investigator and author of this material.

The second portion of chapter 2 is the reprint of the material being submitted. Yue Zhang; Yijie Chen; Christopher Lo; Jia Zhuang; Pavimol Angsantikul; Qiangzhe Zhang; Xiaoli Wei; Zhidong Zhou; Marygorret Obonyo; Ronnie Fang; Weiwei Gao; Liangfang Zhang. The dissertation author is the primary investigator and author of this material.

Chapter 3

Nanosponge Composite Against Bacterial Infection

3.1. Introduction

Colloidal gels comprise a continuous network of particles assembled through strong, yet transient and reversible, electrostatic charge interactions. [1,2] With compelling shear thinning and self-healing characteristics, they are becoming an important class of biomaterials with broad applications.[1-3] Recently, the use of therapeutic nanoparticles as building blocks to formulate colloidal gels is gaining attention in drug delivery and tissue engineering applications.[4,5] Polymeric nanoparticles have distinct engineering flexibility for tailored physicochemical properties such as size, charge, and surface chemistry; therefore, they offer a simple route to assemble highly tunable gel-like materials while avoiding complex molecular design and synthesis.[6,7] The resulting nanoparticle colloidal gels confer two levels of structural hierarchy, namely the polymer chain network within each nanoparticle and the cross-linked nanoparticle assembly, which together provide advanced control over drug release kinetics.[8] Compared to bulk hydrogel systems, nanoparticle colloidal gels can effectively alleviate mass transport barriers within the gel network without compromising bulk mechanical strength. As a result, these advanced biomaterials exhibit a fast response to local chemical cues for triggered drug release.[9] In addition, colloidal gels made with high concentrations of nanoparticles exhibit pseudoplastic behavior desirable for fabricating moldable and shape-specific materials.[10] Notably, when constructed of biocompatible and biodegradable materials, these colloidal gels have high potential for tissue regeneration.[11] Together, these multiple advantages make nanoparticle-based colloidal gels a

promising class of biomaterials.

Multi-functional nanoparticle design for therapeutic applications has made considerable progress in recent years. [12,13] One emerging approach is the use of natural cell membranes to coat synthetic nanoparticles for bio-functionalization.[14-16] In this approach, intact plasma membranes are collected from natural cells and then wrapped onto nanoparticle surfaces. The resulting cell membrane-coated nanoparticles inherit and display natural surface antigens and associated functions while preserving the highly tunable physicochemical properties of synthetic nanomaterials. [17] This 'top-down' fabrication makes it possible to replicate complex biological interfaces present in nature to confer sophisticated nanoparticle functionality without exposure to foreign materials or unfavorable chemical reactions. Following this approach, nanoparticles have been coated with membranes derived from various cell types including red blood cells (RBCs), platelets, cancer cells, leukocytes, and bacteria. [14,16,18-20] These biomimetic nanoparticles have inspired a wide range of innovations in areas such as detoxification, drug delivery, and vaccine nanotechnology.[21-23] Interestingly, regardless of their diverse biological identity and functionality, cell membrane-coated nanoparticles in general carry a net negative surface charge inherited from their source membranes. Therefore, they may spontaneously engage in electrostatic charge interactions with cationic materials without the need for further modification. [17,24] This feature motivated us to hypothesize that cell membrane-coated nanoparticles could be used as building blocks to construct colloidal gels. If so, this conceptual framework could allow creation of

novel colloidal gels that combine biomimetic functionalities with cohesive network properties.

To test our hypothesis, we first fabricated RBC membrane-coated nanoparticles (also referred to as 'nanosponges', here denoted 'RBC-NPs') by coating RBC membranes onto polymeric cores made from poly (lactic-co-glycolic acid) (PLGA) (Figure 3.1A). At the same time, we prepared companion chitosan-functionalized PLGA nanoparticles that possessed a similar size but opposite surface charge (denoted 'Chi-NPs'). Upon mixing, these two oppositely charged nanoparticles self-assembled, forming a cohesive 3D network or 'nanosponge colloidal gel' (denoted 'NC-gel'). When applied with an external shear force, the NC-gel demonstrated shear-thinning behavior; however, upon removal of the external force, its strong cohesive properties recovered. Such reversible network stability is attributable to the transient disruption of inter-particle interactions, indicating a successful colloidal gel formation.

Notably, prior work with RBC-NPs harnessed their capability to absorb and neutralize structurally diverse bacterial pore-forming toxins for therapeutic administration as antivirulence agents.[15,23,25] When embedded into covalently cross-linked hydrogels for injection, the RBC-NPs effectively neutralized secreted bacterial toxins to impede the development of local infection.[26] In the present study, we fabricate a NC-gel pairing RBC-NPs and Chi-NPs and achieve significantly prolonged retention of RBC-NPs in both biological buffers and mouse subcutaneous tissues without the need for chemical conjugation. In vitro, the NC-gel retained the full

capacity to inhibit toxin-induced hemolysis seen with RBC-NPs alone, indicating that the gel formulation preserves the critical biological functionality of the RBC-NPs. In a mouse model of subcutaneous infection with the toxin-producing human bacterial pathogen group A *Streptococcus* (GAS), the NC-gel showed significant therapeutic efficacy, as evidenced by markedly diminished bacterial skin lesion development. Overall, we have successfully used cell membrane-coated nanoparticles as building blocks to formulate a novel NC-gel entirely based on material self-assembly without chemical cross-linking. The new colloidal gel system demonstrated significant potential as an injectable formulation for medical applications including anti-virulence therapy against localized bacterial infection.

3.2. Experimental Methods

Materials.

Chemicals including chitosan oligosaccharide lactate (Mw = 5000), dithiothreitol (DTT), and acetone were purchased from Sigma-Aldrich. Fluorophores including 1,1'-dioctadecyl-3,3,3',3'-tetramethylindodicarbocyanine, 4-chlorobenzenesulfonate salt (DiD, excitation/emission = 644/665 nm) and 3,3'-dioctadecyloxacarbocyanine perchlorates (DiO, excitation/emission = 484/501 nm) were purchased from ThermoFisher Scientific. Poly (lactic-*co*-glycolic) acid (PLGA, 50:50, 0.67 dL/g) was purchased from LACTEL Absorbable Polymers. Packed human red blood cells (RBCs) were purchased from ZenBio, Inc., from which cell membrane was derived according to a previously published protocol.[14]

Preparation of RBC membrane-coated nanosponge colloidal gel (NC-gel):

RBC-NPs were synthesized by coating bare PLGA cores with RBC membrane.[27] Briefly, to prepare bare PLGA cores, 10 mL of PLGA (20 mg/mL in acetone) was added to 20 mL of Tris-HCl buffer (10 mM, pH = 8). The solution was stirred and allowed to evaporate for 2 h. For membrane coating, purified RBC membrane was first mixed with PLGA core at a protein-to-polymer weight ratio of 1:4, followed by bath sonication for 10 min. To prepare chitosan nanoparticles (Chi-NPs), 50 mL of PLGA (4 mg/mL in acetone) was added to 100 mL chitosan solution (1 mg/mL in water) under continuous stirring, followed by evaporation for 10 h.[28] For fluorescence labeling, DiD or DiO was mixed with PLGA polymer (dye-to-polymer weight ratio = 1:40,000) in acetone followed by nanoparticle preparation. RBC-NPs or Chi-NPs were collected with centrifugation (19,000 ×g for 20 min). The pellets were washed with DI water three times to remove excess membrane or chitosan and re-dispersed in deionized water to a concentration of 20% w/v. The colloidal gel was prepared by mixing the two nanoparticle suspensions at desired ratios followed by a brief bath sonication of 3 min. The resulting NC-gel was stored at 4°C for further usage.

Characterization of NC-gel.

The rheological analysis was carried out at 25 ± 0.1°C on a strain-controlled AR-G2 rheometer with a 20 mm-diameter parallel-plate geometry (TA Instruments

Inc., New Castle, DE). The 500 μm gap was filled with the 200 μL gel samples. A solvent trap was placed around the geometry to prevent liquid evaporation during the measurements. Oscillatory rheological measurements were performed in the linear viscoelastic region. The strain was kept at 0.03% and a dynamic frequency sweep from 0.1 to 10 rad/s was conducted to measure the storage modulus G' and loss modulus G''. The viscosity was monitored while the stress was increased (frequency = 1 Hz). Measurements were performed in triplicate with 10 min between cycles. The gel recoverability was assessed using no time break between cycles. For fluorescence imaging, 10 μL NC-gel was dropped onto the glass slide followed by covering it with a cover slip. The slide was then blocked with nail polish. The sample was imaged on Olympus FV1000 confocal microscope. To study hydrogel morphology, NC-gel was lyophilized and the flake of the gel was placed on a silicon wafer. The sample was coated with iridium and then examined with SEM (FEI XL30 SFEG).

RBC-NP retention study

To study retention of RBC-NPs within the NC-gel, the RBC-NPs were labeled with a florescent dye DiD. The resulting NC-gel (500 μL) was loaded into a micro equilibrium dialyzer (Harvard Apparatus) and membrane filters (Whatman, nuclepore track-etch membrane) with the pore size of 1 μm in diameter were used for dialysis against 1 L water. At pre-determined time points, 250 μL of water outside of the chamber was taken and the fluorescence intensity was measured. RBC-NP suspension (10% w/v, 500 μL) without Chi-NPs were used as a control. RBC-NP retention was

also studied in vivo. Specifically, prior to the study, the back of the mice (six week old male ICR mice from Envigo, n = 3) was carefully shaved. Then 50 μL DiD-labeled NC-gel was injected subcutaneously to the left flanks of the mice. As a control, RBC-NP suspension (10% w/v, 50 μL) without Chi-NPs was used and injected subcutaneously to the right flanks of the same mice. For live whole-body imaging, mice were anesthetized with isoflurane at designated time points (day 0, 1, 2, and 3) and imaged with a Xenogen IVIS 200 system. Fluorescence intensities were quantified and normalized across the time points. Heat maps were overlaid on bright field images. All animal experiments followed protocols that were reviewed, approved and performed under the regulatory supervision of the University of California, San Diego's institutional biosafety program and the Institutional Animal Care and Use Committee (IACUC).

Expression and purification of recombinant streptolysin O (SLO)

The *slo* gene was cloned into vector pET15b and transformed into BL21 DE3 *Escherichia coli*. Bacteria expressing SLO were cultured in 1 L of Luria-Bertani broth (LB) and incubated at 37°C with shaking. Expression was induced in cultures at 0.7 A_{600} with 0.5 mm isopropyl 1-thio-β-*D*-galactopyranoside (Bio-Vectra) and maintained at 30°C for 4 h. Bacterial pellets were disrupted by sonication, and soluble 6× histidine-tagged SLO was purified using nickel-nitrilotriacetic acid-agarose (Invitrogen). Fractions corresponding to the full-length SLO were pooled and further purification was achieved using Amicon Ultra centrifugal filters (Millipore Sigma).

Protein was monitored by SDS-PAGE and quantitated by A_{280} and frozen in aliquots at –80 °C. Assays were performed in the presence of 10 mm dithiothreitol (DTT) for reducing conditions.

Group A Streptococcus (GAS) culture.

GAS (M1 5448) bacteria were inoculated from a frozen stock to Todd-Hewitt agar plates and cultured for 12 h at 37°C. Following the culture, a single colony was selected and inoculated to 8 mL of Todd-Hewitt Broth (THB). After an overnight culture, 4 mL of the bacterial medium was reconstituted with 250 mL of fresh THB medium and the culture was continued until the optical density value at 600 nm (OD_{600}) reached 0.4, corresponding to 0.8×10^8 CFU/mL. The bacteria were then collected with centrifugation (4000 ×*g* for 5 min) and wash twice with PBS.

SLO neutralization study.

SLO hemolytic activity was first studied. 60 μL SLO (containing 10 mM DTT) with varied concentration was incubated with 0.1 mL 5% purified human RBCs at 37°C for 30 min. The concentration of SLO to induce 100% hemolysis were determined when the percentage of the released hemoglobin reached the same level as the lysate from the same amount of RBCs. To evaluate SLO neutralization by the NC-gel in vitro, 1.6 μL of SLO solution (0.1 mg/mL containing 10 mM of DTT) was mixed with 59 μL NC-gel, free RBC-NPs, and PBS, respectively. Then 0.1 mL of 5% purified human RBCs was added to each sample, followed by incubation at 37°C for

30 min. The samples were carefully centrifuged and the extent of RBC lysis was quantified by measuring the absorption of the supernatants at 540 nm. All experiments were performed in triplicate. To study neutralization of SLO by the NC-gel in vivo, 100 μL of SLO solution (0.6 mg/mL, containing 10 mM of DTT) was mixed with 100 μL of NC-gel and the mixture was injected subcutaneously into the flank region of 6 week-old male ICR mice (Envigo, n = 3). Three other groups, including SLO mixed with free RBC-NPs, SLO toxin alone, and PBS, were used as controls. After 72 h the lesion was photographed. Then the mice were sacrificed and the skin and muscle samples were removed. The tissues were frozen, cut, and stained with hematoxylin and eosin (H&E) for histological analysis (Hamamatsu Nanozoomer).

Antivirulence efficacy against localized GAS subcutaneous infection:

Prior to the study, the flanks of 18 ICR mice (6-week-old male, Envigo) were carefully shaved. Then a challenge dose of 2×10^9 CFU of GAS M1 5448 suspended in 100 μL PBS was injected subcutaneously into the flank region. Then the mice were randomly divided into three groups (n = 6 per group). For the treatment group, 0.1 mL NC-gel was injected into the infection region. For the control groups, free RBC-NPs or PBS were injected. The progression of infection in each mouse was carefully monitored and measured for 3 days, with serial photographic image capture and lesion size measurement using Image J software.

3.3. Results and discussion

In the study, RBC-NPs (nanosponges) were prepared by coating membranes derived from human RBCs onto PLGA polymeric cores through a sonication process.[27] The resulting RBC-NPs exhibited a hydrodynamic diameter of 150.9 ± 0.8 nm and a surface zeta potential of -22.3 ± 1.7 mV. Meanwhile, to prepare Chi-NPs, an acetone solution containing PLGA was added dropwise into an aqueous solution of chitosan.[28] The subsequent acetone evaporation led to the formation of Chi-NPs with a diameter of 194.3 ± 1.8 nm and a surface charge of 34.2 ± 0.4 mV. Following the preparations, we directly mixed the two oppositely charged nanoparticles at a fixed mass concentration (20 wt%, PLGA polymer content), but varied the mass ratios of the nanoparticle components. Each formulation was examined for its rheological characteristics. In steady flow measurements, nanoparticle suspensions containing RBC-NP or Chi-NP alone showed low viscosity with minimum shear-thinning behavior (Figure 3.1B). In contrast, a significant increase in viscosity was observed when two nanoparticles were mixed, revealing the occurrence of strong electrostatic charge interactions between the two colloids. Notably, viscosity values measured from the sample with an equal mass ratio of the colloids (50 wt% of RBC-NP and 50 wt% of Chi-NPs) were slightly lower than that calculated for the sample with a RBC-NP concentration of 30 wt%. This likely reflects the smaller absolute value of zeta potential of negatively-charged RBC-NPs compared to Chi-NPs, which means that a more equivalent overall charge balance is achieved when theChi-NPs are provided in excess.[10]

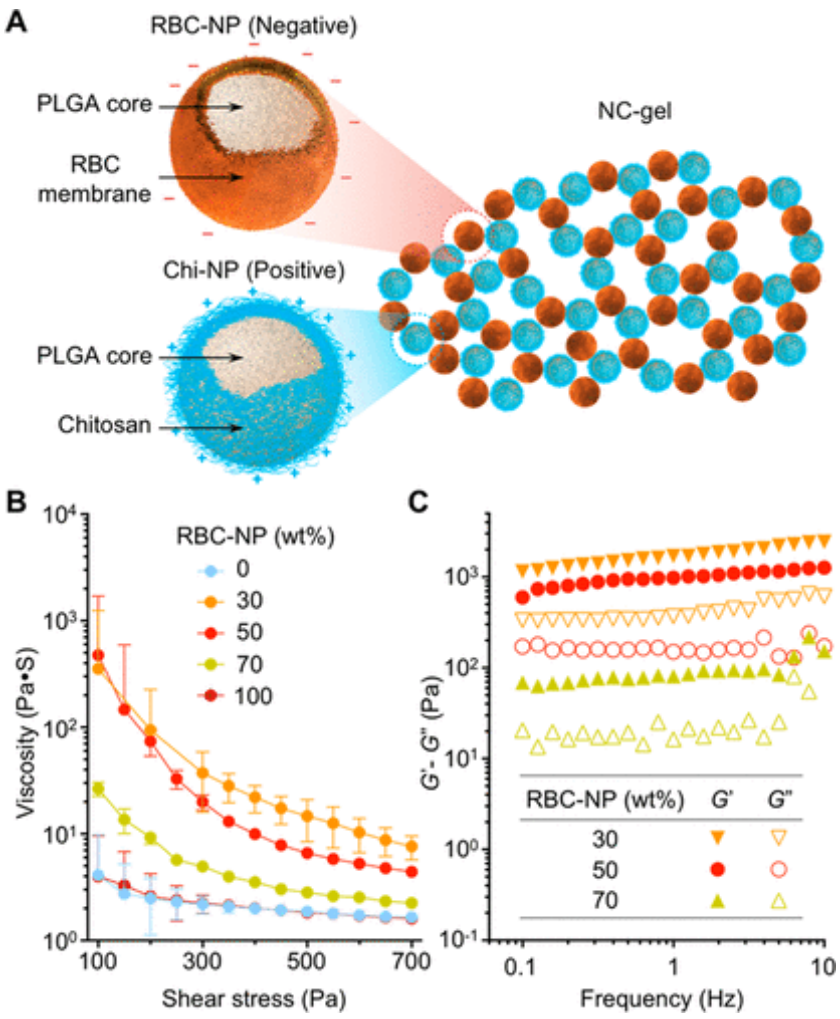

Figure 3.1: Preparation of nanosponge colloidal gel (denoted 'NC-gel'). (A) Schematic illustration of NC-gel formulation by mixing red blood cell membrane-coated nanoparticles (RBC-NPs), which possess a negative surface charge, with chitosan-modified nanoparticles (Chi-NPs) as positively charged nanoparticle counterparts. (B) RBC-NPs and Chi-NPs mixed at different mass ratios (0, 30, 50, 70, and 100 wt% of RBC-NP, respectively) were measured for viscosity with varying shear stress (100-700 Pa). (C) RBC-NPs and Chi-NPs mixed at different mass ratios (30, 50, and 70 wt% of RBC-NP, respectively) were measured for the storage modulus G' and loss modulus G'' against frequency (0.1-10 Hz). All rheological measurements were performed at 25°C.

Viscous mixtures were further examined with dynamic rheological measurements of the storage modulus (*G'*) and the loss modulus (*G"*) as a function of frequency (Figure 3.1C). In all three samples, *G'* exceeded the corresponding *G"* over the entire frequency range tested, and both moduli showed weak dependence on frequency, implying the dominance of a gel-like viscoelastic behavior. [29] Results from steady flow and dynamic measurements were consistent: the mixture with higher viscosity also possessed higher values for the corresponding moduli. Overall, the rheological measurements confirmed the gel formation was predominantly mediated by electrostatic charge interactions. For the subsequent studies, we specifically selected an NC-gel that contained equal masses of RBC-NPs and Chi-NPs (50 wt% of each), as this formulation showed both high viscosity and pronounced shear-thinning behavior, while containing a substantial fraction of RBC-NPs as the active component for biodetoxification.

We next characterized the NC-gel to verify its cohesive network properties. Colloidal gels consisting of oppositely charged nanoparticles are known to exhibit pseudoplastic characteristics, which facilitate the formation of materials with defined shapes under static conditions. [8,10] Indeed, the suspensions of single component RBC-NPs or Chi-NPs were fluid-like, and unable to form a defined 3D structure when placed onto a substrate (Figure 3.2A). In contrast, the NC-gel retained a freestanding 3D structure, implying a critical function of its internal charge interactions for maintaining the overall cohesive properties of the colloidal assembly. In addition, consecutive acceleration sweeping with a shear force revealed nearly identical

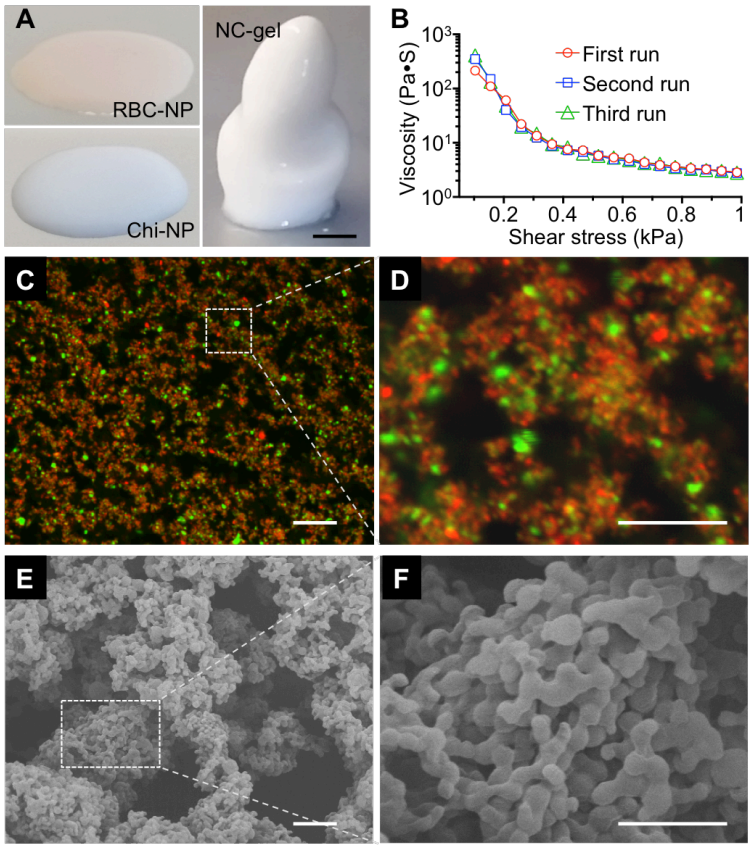

Figure 3.2. Characterization of the NC-gel. (A) Images of RBC-NPs, Chi-NPs, and NC-gel samples when they were placed onto a flat substrate. Scale bar = 5 mm. (B) Viscosity measurements were performed on the same NC-gel sample at 25°C for three consecutive runs without interval between each run. (C) A representative fluorescence image of the NC-gel, in which RBC-NPs were labeled with DiD dye (red) and Chi-NPs with DiO dye (green). Scale bar = 1 μm. (D) A zoomed-in image of the marked area in (C). Scale bar = 10 μm. (E) A representative scanning electron microscopy (SEM) image of NC-gel. Scale bar = 1 μm. (F) A zoomed-in SEM image of the marked area in (E). Scale bar = 0.5 μm.

viscosity profiles, indicating an excellent recovery of the NC-gel architecture upon the removal of the external shear force (Figure 3.2B). The NC-gel was also examined for its microscopic morphology. In the study, RBC-NPs and Chi-NPs were labeled with red (DiD) and green (DiO) fluorescent dyes, respectively, and the resulted NC-gel

sample examined by laser scanning confocal microscopy (LSCM, Figure 3.2C). In ambient conditions, the fluorescent imaging showed the two distinct nanoparticle components to be clearly distinguishable, suggesting reduced particle mobility upon the formation of colloidal assemblies. In addition, the green and red signals were evenly distributed, indicating the homogenous mixing of both nanoparticle components. The imaging also revealed long-range ring- and branch-like structures. When zoomed in, a representative fluorescence image shows that the nanoparticle agglomerates were connected to form a porous structure (Figure 3.2D). To further characterize these microscopic structures, the NC-gel sample was dried and examined under a scanning electron microscope (SEM). The ultrastructure exhibited a porous morphology with nanoparticles linked into loosely organized circular structures (Figure 3.2E). In a representative zoomed-in image, domains of more tightly packed nanoparticle agglomerates and open pores were seen **(**Figure 3.2F). The observed NC-gel morphology, which features mixed agglomerates and pores, also matches previous studies on nanoparticle colloidal gel systems, implying the cohesive nature of NC-gel as a result of the interplay between nanoparticle attraction (agglomerates) and repulsion (pores).[9,10] Overall, the structural retention under static conditions, excellent shear-thinning behavior, and microscopic characterizations collectively suggest the successful formation of colloidal gels using RBC-NPs as building blocks.

For local administration and treatment, prolonged retention of RBC-NPs by using the gel formulation is desirable. We hypothesized that the electrostatic attractions among oppositely charged nanoparticle building blocks of NC-gel would

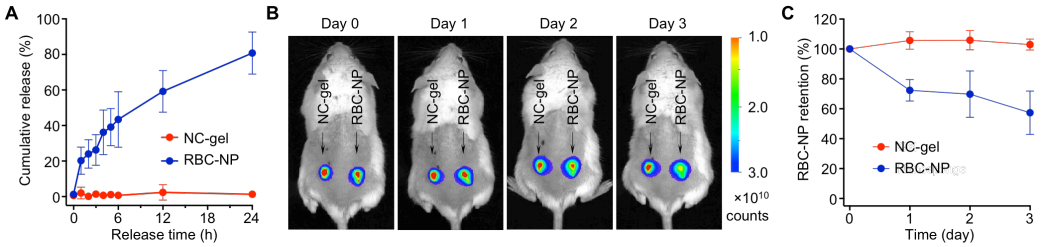

Figure 3.3: RBC-NP retention within the NC-gel. (A) The cumulative release of RBC-NPs measured from the NC-gel and RBC-NP suspension, respectively. RBC-NP was labeled with DiD dye and samples were placed in dialysis chambers equipped with filters of pore size of 1 µm. (B) Fluorescence images of mice injected with NC-gel and RBC-NP samples. NC-gel was formulated with DiD-labeled RBC-NPs. The samples were injected subcutaneously under the loose skin over the left flank of the mice. RBC-NPs alone without mixing with Chi-NPs were injected as a control over the right flank of the same mice. Fluorescence images were taken on day 0, 1, 2, and 3 after the injection. (C) Quantification of the fluorescence intensity as observed in (B). All images are representative of three mice from each group and error bars represent the standard deviation

prolong RBC-NP retention under physiological conditions and began by examining RBC-NP diffusion out of the NC-gel network *in vitro*. In this study, the NC-gel was formulated with fluorescently-labeled RBC-NPs and loaded into a dialysis chamber equipped with pores of 1 µm in diameter. The release of RBC-NPs was monitored by measuring the fluorescence intensity outside of the dialysis chamber. For comparison, RBC-NPs alone were used as a control. Within 24 h, the NC-gel released 1.3 ± 1.5% of the total RBC-NPs, a negligible amount compared to 80.8 ± 11.1% measured from the pure RBC-NP suspension control (Figure 3.3A). This sharp contrast in nanoparticle release indicates that the NC-gel can effectively immobilize and retain RBC-NPs within its network. We then investigated retention of the RBC-NPs within the gel under *in vivo* conditions. NC-gel samples containing fluorescently labeled RBC-NPs were injected subcutaneously into the left flank of mice. As a control,

samples containing the same quantity of free RBC-NPs were injected to the right flank of the same mice. Following the injection, whole body imaging of the mice revealed the confinement of fluorescence at the injection sites (Figure 3.3B). In the study, a faster decay of fluorescence intensity was observed at sites injected with free RBC-NPs compared to to sites injected with the NC-gels, indicating a more rapid loss of nanoparticles through diffusion to surrounding tissues. Quantification of the fluorescence intensity showed that nearly 30% of the free RBC-NPs diffused away from the injection site by day 2 and nearly 50% by day 3. In contrast, the NC-gel formulation showed negligible loss of RBC-NPs during the full 3-day testing period (Figure 3.3C), demonstrating the prolonged retention of RBC-NPs achieved with NC-gel formulation. Compared to previous studies that used acrylate-based hydrogels for nanoparticle encapsulation and retention, the current approach achieves enhanced nanoparticle retention relying entirely on physical self-assembly without any chemical processing. [26,29]

RBC nanosponges have shown unique capabilities to absorb and neutralize various pore-forming toxins (PFTs). In this study, we selected this property as a functional assay to test whether the NC-gel formulation retained key biological functionality of the entrapped nanosponges. To do so, we selected the well-characterized GAS toxin (SLO) as a model pore-forming toxin, and tested the ability of the NC-gel to inhibit SLO-induced hemolytic activity compared to free RBC-NPs. An SLO concentration of 1 μg/mL was utilized because at this concentration the toxin causes complete cell lysis. Recombinant SLO was mixed with serial dilutions of NC-

gel or RBC-NPs prior to mixing with freshly purified human RBCs. As shown in Figure 3.4A, in both groups, as the concentration of RBC-NP increased, the degree of RBC hemolysis was correspondingly reduced. Specifically, 50% inhibition of hemolysis was achieved with an RBC-NP concentration of approximately 0.25 mg/mL, and a nearly 100% inhibition observed with a RBC-NP concentration of 1 mg/mL. At all tested concentrations, the NC-gel sample showed an inhibition efficiency comparable to that of free RBC-NPs, suggesting that the NC-gel formulation retains the full neutralization capability of its component RBC-NPs upon gelation.

Neutralization of SLO by NC-gel was further tested *in vivo* (Figure 3.4B). In the study, SLO toxin was mixed with NC-gel and free RBC-NPs, respectively, and then injected into the loose flanks of the mice. Mice injected with SLO only and PBS, respectively, served as two control groups. At 72 h after injection, mice challenged with SLO alone developed clear skin lesion with characterized by localized edema and inflammation. In contrast, mice injected with the NC-gel and free RBC-NP preparations had healthy appearing skin at the injection site similar to a PBS control group. Skin biopsy sections were further analyzed with histological staining. Mouse skin treated with SLO alone showed intracellular edema within the stratum spinosum, alteration of vascular structure in the dermal layes, obvious erythrocyte extravasation, and keratinocyte necrosis. In contrast, skin treated with NC-gel, RBC-NPs, or PBS alone possessed normal epithelial structures in skin histology without discernible damages; all of these samples showed stratified squamous epithelium with intact

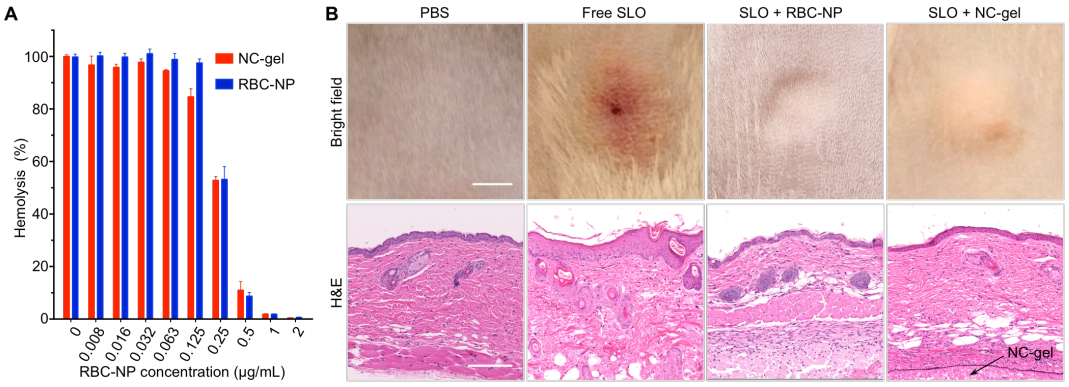

Figure 3.4: Evaluation of toxin neutralization capability of the NC-gel in vitro and in vivo. (A) In vitro neutralization of Streptolysin-O (SLO) by the NC-gel and free RBC-NPs to inhibit toxin-induced hemolysis. In all samples, SLO concentration was maintained at 1 μg/mL and the concentration of RBC-NP component was varied. (B) In vivo neutralization of SLO. Free SLO, SLO+RBC-NP, or SLO+NC-gel was injected subcutaneously into CD-1 mice. Mice injected with PBS only served as a control group. Mice injected with free SLO developed skin lesions after 3 days, but no lesions were observed for mice in other treatment groups (scale bar = 20 mm). Hematoxylin and eosin (H&E) stained histological sections revealed inflammatory infiltrate, apoptosis, necrosis, and edema in the epidermis for the SLO-treated mice. In contrast, mice in other groups showed no abnormality in the epidermis (scale bars = 0.2 mm).

fibrous structures and absence of erythrocyte extravasation. Similar complete toxin neutralization effects observed with the NC-gel compared to RBC-NP group *in vivo* further confirm that the neutralization function of RBC-NP is well preserved within the NC-gel formulation.

Finally, to demonstrate the therapeutic potential of the NC-gel, we tested their use as an antivirulence agent to protect mice from a live subcutaneous bacterial infection. GAS, which elaborates SLO and several other pore forming toxins and proteases [31,32], is a major cause of invasive to skin and soft tissue infection in humans.[30], making it a relevant model to for testing the efficacy of NC-gel in local treatment. Subcutaneous GAS infection was established by injecting 2×10^9 CFU

bacteria underneath the flank skin of ICR mice, randomized into three groups (n = 6 per group) for treatment with PBS, free RBC-NPs, and NC-gel, respectively. Therapeutic efficacy was evaluated by measurement of the GAS-induced skin lesion.[33,34] On day 1 after the bacterial challenge, all groups developed visible skin lesions of similar size (Figure 3.5A,B). However, on days 2 and 3, the mice treated with the NC-gel showed significantly smaller lesions than mice injected with the PBS control of free RBC-NPs. A partial therapeutic benefit of free RBC-NPs compared to the PBS control was seen on day 3. A superior efficacy in lesion reduction observed with the NC-gel verifies its potential as an effective local treatment agent to mitigate tissue damage produced by GAS infection.

The combination of therapeutic nanoparticles with hydrogels has emerged as a novel biomaterial formulation with intriguing and versatile therapeutic application potentials.[5] However, such combinations to date have relied largely on chemical cross-linking to embed and retain nanoparticles within the gel network. From this perspective, the NC-gel reported herein provides a straightforward and gentle approach to use nanoparticles themselves as building blocks coupled with an entirely physical gelation process. The resulting NC-gel also generates a unique synergy between cell membrane-coated nanosponges and gel-like bulk assembly: while the nanosponges offer unique biomimetic toxin absorption and neutralization, the hydrogel enhance retention of the nanosponges at the site of application (e.g. an infected tissue focus), which focuses localized bioactivity for enhanced efficacy. Nanoparticles coated with membranes of mammalian cells or bacterial cells possess a

negative surface charge; therefore, the approach of NC-gel formulation likely be extended to nanoparticles coated with many other types of cell membranes. Such cell membrane-coated nanoparticles would also be expected to interact with other cationic materials such as polymers and nanofibers for self-assembly and gelation.[6,35] This powerful platform of material diversity and formulation flexibility make the NC-gel approach broadly applicable.

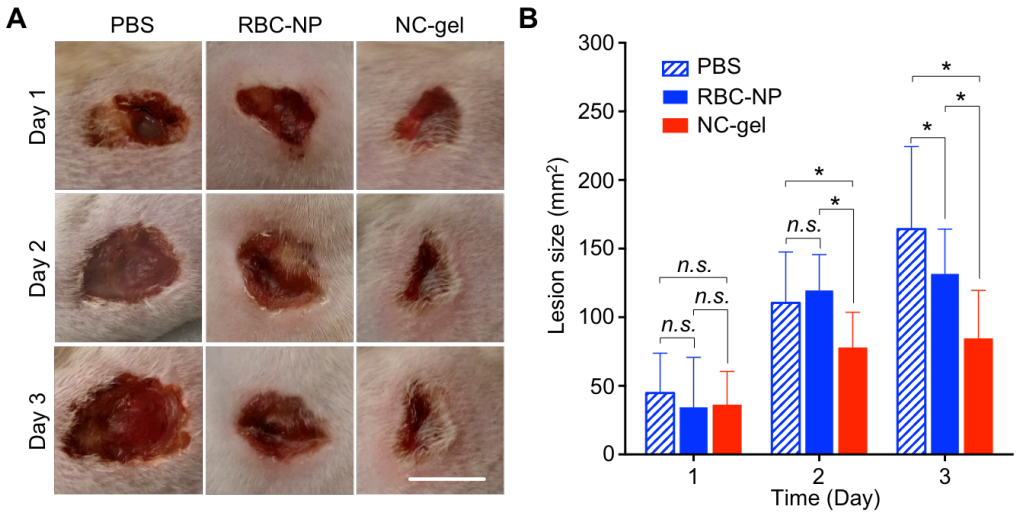

Figure 3.5: Evaluation of the NC-gel for protecting mice from group A *Streptococcus* (GAS) infection in vivo**.** To establish GAS infection, 2×10^9 CFU of GAS bacteria were injected subcutaneously under the loose skin on the back of the mice (n = 6 per group). Immediately after injection of the bacteria, PBS, RBC-NP alone, or NC-gel was injected to the infection site. (A) Skin lesions were monitored and photographed on day 1, 2, and 3 after the injection (scale bar = 1 cm). (B) The lesion sizes were measured and compared among the groups. Bars represent median values (*: $P < 0.05$, *n.s.*: not significant). Statistical analysis was performed with One-way ANOVA followed by unpaired two-tailed t test in GraphPad Prism.

3.4. Conclusion

This study introduced a framework for using cell membrane-coated nanoparticles to fabricate colloidal gels. RBC-NPs were studied as a model nanoparticle system and paired them with cationic Chi-NPs to formulate a NC-gel. This colloidal gel was optimized by varying the relative composition of the two oppositely charged nanoparticles. The resulting gel effectively retained RBC-NPs within its network without compromising their toxin neutralization capability. In a GAS subcutaneous mouse infection model, mice treated with the NC-gel showed clear reductions in skin lesion development. The reported NC-gel takes advantage of the natural surface charge of cell membranes in general, and this formulation process is expected to be applicable to nanoparticles coated with membranes of other cell types. The formulation process is physical, facile, and chemical-free, hence allowing the NC-gel to retain functionalities without affecting the original functions of the building blocks. The resulting colloidal gel combines the biomimetic functionality from the cell membrane-coated nanoparticles with the cohesive network property from the bulk gel, together opening new opportunities for advanced therapeutic applications.

3.5. References

[1] Zaccarelli, E., Colloidal gels: equilibrium and non-equilibrium routes. J. Phys.: Condens. Matter 2007, 19, article number 323101.

[2] Joshi, Y. M., Dynamics of colloidal glasses and gels. Annu. Rev. Chem. Biomol. Eng. 2014, 5, 181-202.

[3] Lu, P. J.; Weitz, D. A., Colloidal particles: crystals, glasses, and gels. Annu. Rev. Condens. Matter Phys. 2013, 4, 217-233.

[4] Kamata, H.; Li, X.; Chung, U. I.; Sakai, T., Design of hydrogels for biomedical applications. Adv. Healthc. Mater. 2015, 4, 2360-2374.

[5] Gao, W. W.; Zhang, Y.; Zhang, Q. Z.; Zhang, L. F., Nanoparticle-Hydrogel: A Hybrid Biomaterial system for localized drug delivery. Ann. Biomed. Eng. 2016, 44, 2049-2061.

[6] Appel, E. A.; Tibbitt, M. W.; Webber, M. J.; Mattix, B. A.; Veiseh, O.; Langer, R., Self-assembled hydrogels utilizing polymer-nanoparticle interactions. Nat. Commun. 2015, 6, article number 6295.

[7] Diba, M.; Wang, H. N.; Kodger, T. E.; Parsa, S.; Leeuwenburgh, S. C. G., Highly elastic and self-healing composite colloidal gels. Adv. Mater. 2017, 29, article number 1604672.

[8] Wang, Q.; Wang, J. X.; Lu, Q. H.; Detamore, M. S.; Berkland, C., Injectable PLGA-based colloidal gels for zero-order dexamethasone release in cranial defects. Biomaterials 2010, 31, 4980-4986.

[9] Gu, Z.; Aimetti, A. A.; Wang, Q.; Dang, T. T.; Zhang, Y. L.; Veiseh, O.; Cheng, H.; Langer, R. S.; Anderson, D. G., Injectable nano-network for glucose-mediated insulin delivery. ACS Nano 2013, 7, 4194-4201.

[10] Wang, Q.; Wang, L. M.; Detamore, M. S.; Berkland, C., Biodegradable colloidal gels as moldable tissue engineering scaffolds. Adv. Mater. 2008, 20, 236-239.

[11] Wang, Q.; Gu, Z.; Jamal, S.; Detamore, M. S.; Berkland, C., Hybrid hydroxyapatite nanoparticle colloidal gels are injectable fillers for bone tissue engineering. Tissue Eng. Part A 2013, 19, 2586-2593.

[12] Kim, B. Y. S.; Rutka, J. T.; Chan, W. C. W., Current concepts: nanomedicine. New Engl. J. Med. 2010, 363, 2434-2443.

[13] Bobo, D.; Robinson, K. J.; Islam, J.; Thurecht, K. J.; Corrie, S. R., Nanoparticle-based medicines: a review of FDA-approved materials and clinical trials to date. Pharm. Res. 2016, 33, 2373-2387.

[14] Hu, C. M. J.; Zhang, L.; Aryal, S.; Cheung, C.; Fang, R. H.; Zhang, L. F., Erythrocyte membrane-camouflaged polymeric nanoparticles as a biomimetic delivery platform. Proc. Natl. Acad. Sci. U. S. A. 2011, 108, 10980-10985.

[15] Hu, C. M. J.; Fang, R. H.; Copp, J.; Luk, B. T.; Zhang, L. F., A biomimetic nanosponge that absorbs pore-forming toxins. Nat. Nanotechnol. 2013, 8, 336-340.

[16] Hu, C. M. J.; Fang, R. H.; Wang, K. C.; Luk, B. T.; Thamphiwatana, S.; Dehaini, D.; Nguyen, P.; Angsantikul, P.; Wen, C. H.; Kroll, A. V.; Carpenter, C.; Ramesh, M.; Qu, V.; Patel, S. H.; Zhu, J.; Shi, W.; Hofman, F. M.; Chen, T. C.; Gao, W. W.; Zhang, K.; Chien, S.; Zhang, L. F., Nanoparticle biointerfacing by platelet membrane cloaking. Nature 2015, 526, 118-121.

[17] Luk, B. T.; Hu, C. M. J.; Fang, R. N. H.; Dehaini, D.; Carpenter, C.; Gao, W. W.; Zhang, L. F., Interfacial interactions between natural RBC membranes and synthetic polymeric nanoparticles. Nanoscale 2014, 6, 2730-2737.

[18] Fang, R. H.; Hu, C. M. J.; Luk, B. T.; Gao, W. W.; Copp, J. A.; Tai, Y. Y.; O'Connor, D. E.; Zhang, L. F., Cancer cell membrane-coated nanoparticles for anticancer vaccination and drug delivery. Nano Lett. 2014, 14, 2181-2188.

[19] Parodi, A.; Quattrocchi, N.; van de Ven, A. L.; Chiappini, C.; Evangelopoulos, M.; Martinez, J. O.; Brown, B. S.; Khaled, S. Z.; Yazdi, I. K.; Vittoria Enzo, M.; Isenhart, L.; Ferrari, M.; Tasciotti, E., Synthetic nanoparticles functionalized with biomimetic leukocyte membranes possess cell-like functions. Nat. Nanotechnol. 2013, 8, 61-68.

[20] Gao, W. W.; Fang, R. H.; Thamphiwatana, S.; Luk, B. T.; Li, J. M.; Angsantikul, P.; Zhang, Q. Z.; Hu, C. M. J.; Zhang, L. F., Modulating antibacterial immunity via bacterial membrane-coated nanoparticles. Nano Lett. 2015, 15, 1403-1409.

[21] Gao, W. W.; Zhang, L. F., Engineering Red blood cell membrane-coated nanoparticles for broad biomedical applications. AICHE J. 2015, 61, 738-746.

[22] Hu, C. M. J.; Fang, R. H.; Luk, B. T.; Zhang, L. F., Nanoparticle-detained toxins for safe and effective vaccination. Nat. Nanotechnol. 2013, 8, 933-938.

[23] Wei, X.; Gao, J.; Wang, F.; Ying, M.; Angsantikul, P.; Kroll, A. V.; Zhou, J.; Gao, W.; Lu, W.; Fang, R. H.; Zhang, L., In Situ Capture of bacterial toxins for antivirulence vaccination. Adv. Mater. 2017, 29, article number 1701644.

[24] Chen, W. S.; Zhang, Q. Z.; Luk, B. T.; Fang, R. H.; Liu, Y. N.; Gao, W. W.; Zhang, L. F., Coating nanofiber scaffolds with beta cell membrane to promote cell proliferation and function. Nanoscale 2016, 8, 10364-10370.

[25] Li, L. L.; Xu, J. H.; Qi, G. B.; Zhao, X. Z.; Yu, F. Q.; Wang, H., Core-shell supramolecular gelatin nanoparticles for adaptive and "on-demand" antibiotic delivery. ACS Nano Wang, F.; Gao, W. W.; Thamphiwatana, S.; Luk, B. T.; Angsantikul, P.; Zhang, Q. Z.; Hu, C. M. J.; Fang, R. H.; Copp, J. A.; Pornpattananangkul, D.; Lu, W. Y.; Zhang, L. F., Hydrogel retaining toxin-absorbing anosponges for local treatment of methicillin-resistant Staphylococcus aureus infection. Adv. Mater. 2015, 27, 3437-3443.

[26] Copp, J. A.; Fang, R. H.; Luk, B. T.; Hu, C. M. J.; Gao, W. W.; Zhang, K.; Zhang, L. F., Clearance of pathological antibodies using biomimetic nanoparticles. Proc. Natl. Acad. Sci. U. S. A. 2014, 111, 13481-13486.

[27] Wang, Q.; Jamal, S.; Detamore, M. S.; Berkland, C., PLGA-chitosan/PLGA-alginate nanoparticle blends as biodegradable colloidal gels for seeding human umbilical cord mesenchymal stem cells. J. Biomed. Mater. Res. A 2011, 96A, 520-527.

[28] Gao, W. W.; Vecchio, D.; Li, J. M.; Zhu, J. Y.; Zhang, Q. Z.; Fu, V.; Li, J. Y.; Thamphiwatana, S.; Lu, D. N.; Zhang, L. F., Hydrogel containing nanoparticle-stabilized liposomes for topical antimicrobial delivery. ACS Nano 2014, 8, 2900-2907.

[29] Walker, M. J.; Barnett, T. C.; McArthur, J. D.; Cole, J. N.; Gillen, C. M.; Henningham, A.; Sriprakash, K. S.; Sanderson-Smith, M. L.; Nizet, V.,

Disease manifestations and pathogenic mechanisms of group A Streptococcus. Clin. Microbiol. Rev. 2014, 27, 264-301.

[30] Buffalo, C. Z.; Bahn-Suh, A. J.; Hirakis, S. P.; Biswas, T.; Amaro, R. E.; Nizet, V.; Ghosh, P., Conserved patterns hidden within group A Streptococcus M protein hypervariability recognize human C4b-binding protein. Nat. Microbiol. 2016, 1, article number 16155.

[31] Stewart, C. M.; Buffalo, C. Z.; Valderrama, J. A.; Henningham, A.; Cole, J. N.; Nizet, V.; Ghosh, P., Coiled-coil destabilizing residues in the group A Streptococcus M1 protein are required for functional interaction. Proc. Natl. Acad. Sci. U. S. A. 2016, 113, 9515-9520.

[32] Humar, D.; Datta, V.; Bast, D. J.; Beall, B.; De Azavedo, J. C. S.; Nizet, V., Streptolysin S and necrotising infections produced by group G Streptococcus. Lancet 2002, 359, 124-129.

[33] Zhu, H.; Liu, M. Y.; Sumby, P.; Lei, B. F., The secreted esterase of group A Streptococcus is important for invasive skin infection and dissemination in mice. Infect. Immun. 2009, 77, 5225-5232.

[34] Kim, J.; Li, W. A.; Choi, Y.; Lewin, S. A.; Verbeke, C. S.; Dranoff, G.; Mooney, D. J., Injectable, spontaneously assembling, inorganic scaffolds modulate immune cells in vivo and increase vaccine efficacy. Nat. Biotechnol. 2015, 33, 64-72.

Chapter 3, in full, is a reprint of the material as it appears in ACS Nano, 2017, Yue Zhang, Weiwei Gao, Yijie Chen, Tamara Escajadillo, Jessica Ungerleider, Ronnie Fang, Karen Christman, Victor Nizet and Liangfang Zhang. The dissertation author was the primary investigator and author of this paper.

Chapter 4

Conclusion

4.1. Biomimetic nanosponges against bacterial infection

The treatment of bacterial infection is increasingly challenged by the rapid emergence of antibiotic resistance. Among various alternatives, anti-virulence therapies that interfere with the virulence mechanisms are attractive, as they avoid the direct disruption of bacterial cycles for killing and thus may alleviate resistance development. In this chapter, the anti-virulence platform was developed by wrapping cellular membrane onto synthetic nanoparticles. Two types of anti-virulence mechanisms were discussed to show the therapeutic potential of nanosponge.

In the first part, we reported an erythrocyte membrane-coated nanogel (RBC-nanogel) system with combinatorial antivirulence and responsive antibiotic delivery for the treatment of methicillin-resistant Staphylococcus aureus (MRSA) infection. RBC membrane was coated onto the nanogel via a membrane vesicle templated in situ gelation process, whereas the redox-responsiveness was achieved by using a disulfide bond-based crosslinker. We demonstrated that the RBC-nanogels effectively neutralized MRSA-associated toxins in extracellular environment and the toxin neutralization in turn promoted bacterial uptake by macrophages. In intracellular reducing environment, the RBC-nanogels showed an accelerated drug release profile, which resulted in more effective bacterial inhibition. When added to the macrophages infected with intracellular MRSA bacteria, the RBC-nanogels significantly inhibited bacterial growth compared to free antibiotics and non-responsive nanogel counterparts.

These results indicate the great potential of the RBC-nanogel system as a new and effective antimicrobial agent against MRSA infection.

In the second part, we developed an anti-adhesion nanomedicine platform which was made by wrapping synthetic polymeric cores with bacterial outer membranes. The resulting bacterium-mimicking nanoparticles (denoted 'OM-NP) inherit adhesins of the source bacteria, compete for binding sites on the host, and subsequently reduce the adhesion of the bacteria. OM-NP avoid the identification of the adhesin and bypass the design of agonists against specific adhesins. In this study, OM-NP are made with membranes of *Helicobacter pylori* (*H. pylori*) and shown to bind with gastric epithelial cells (e.g., AGS cells). Treatment of AGS cells with OM-NP reduces *H. pylori* adhesion and such anti-adhesion efficacy is dependent on OM-NP concentration as well as the dosing sequence relative to that of *H. pylori*. In addition, OM-NP displace *H. pylori* pre-bound to AGS monolayers. On mouse stomach, OM-NP reduce *H. pylori* adherence. These results together demonstrate that OM-NP confer an anti-adhesion approach against bacterial infection.

4.2. Nanosponge composite against bacterial infection

Biomaterial designs increasingly leverage colloidal gels that combine oppositely charged nanoparticles for emerging applications in drug delivery and tissue engineering. Meanwhile, cell membrane-coated nanoparticles are becoming unique biomimetic nanomedicine for a wide range of innovative therapeutics. Inspired by the remarkable potential of both material platforms, herein, we investigated the use of cell

membrane-coated nanoparticles as building blocks to form colloidal gel. Specifically, we coated nanoparticles with membrane derived from red blood cells (denoted by 'RBC-NPs') and mixed them with cationic nanoparticles of similar sizes but opposite surface charge. Upon mixing, the two colloids self-assembled, forming a gel-like and cohesive material (denoted by 'NC-gel'). When applied with an external shear force, NC-gel showed a shear-thinning behavior; however, upon removal of the external force, the cohesive property recovered. NC-gel prolonged the retention of RBC-NPs in both biological buffers and mouse subcutaneous tissues. It also preserved the toxin absorption and neutralization capability of RBC-NPs. In a mouse model of subcutaneous Group A Streptococcus infection, NC-gel showed significant anti-bacterial efficacy by markedly reducing skin lesion development. Overall, this study demonstrates the successful use of cell membrane-coated nanoparticles as building blocks to formulate colloidal gel that entirely based on material self-assembly without chemical cross-linking. The new colloidal gel system is promising as an injectable formulation for therapeutic applications including bio-detoxification against local infections.

To sum up, we covered three representative work of using cell membrane-coated nanoparticles against bacterial infection. Instead of purely relying on the traditional antibiotic treatment, we designed the nanoparticle platform to neutralize the major virulence factors (i.e. pore forming toxins and adhesins), which is thought to be a promising alternative to address the prevalent problem of antibiotic resistance. Moreover, those work highlights the engineering flexibility of cell-membrane coating

technology. We can easily incorporate multiple functionality to a tiny nanoparticle by changing the surface coating and formulation composition. For instance, by switching to macrophage membrane, we can expand neutralization ability of the nanosponge towards other virulence factors, such as bacterial cell wall components and hemolytic enzymes. We believe the cell membrane coating technology has great potential to revolutionize the landscape of the infectious disease management.